

Localization in a Distributed Software Defined Radio Framework

Von der Fakultät für Elektrotechnik und Informationstechnik
der Rheinisch-Westfälischen Technischen Hochschule Aachen
zur Erlangung des akademischen Grades eines Doktors
der Ingenieurwissenschaften genehmigte Dissertation

vorgelegt von

Diplom-Ingenieur
Johannes Schmitz

aus Krefeld

Berichter: Universitätsprofessor Dr. rer. nat. Rudolf Mathar
Professor Sivan Toledo, Ph.D.

Tag der mündlichen Prüfung: 7. November 2017

Diese Dissertation ist auf den Internetseiten
der Hochschulbibliothek online verfügbar.

Preface

Dieses Dokument ist während meiner Zeit am Institut für Theoretische Informationstechnik der RWTH Aachen entstanden. Im Zusammenhang damit gilt mein besonderer Dank meinem Betreuer Prof. Dr. Rudolf Mathar, der mich zu diesem Promotionsvorhaben ermutigt und mich dabei immer unterstützt hat. Durch das Vertrauen und die Freiheit, die ich dabei erfahren durfte, sind viele Details der Arbeit und nicht zuletzt eine starke persönliche Entwicklung erst möglich geworden.

Eine einmalige Erfahrung waren dabei auch meine beiden Forschungsaufenthalte in Kolumbien und Israel. Hierfür möchte ich neben Professor Mathar auch den gastgebenden Professoren Roberto Carlos Hincapié Reyes, Cristina Gómez Santamaría, Leonardo Betancur Agudelo sowie Sivan Toldeo herzlichst danken.

Ich danke Professor Sivan Toledo weiterhin besonders für die Durchführung des Zweitgutachtens und seine wertvollen Kommentare. Der Aufenthalt bei ihm in Tel Aviv und die daran anknüpfende Zusammenarbeit haben mich inhaltlich einen großen Schritt weiter gebracht. Im Zusammenhang damit ist auch Yotam Orchan von der Hebrew University of Jerusalem zu nennen, der sich mit viel Aufwand um die Wartung und Instandhaltung des Wildlife Tracking Systems kümmert, auf dessen Messdaten einige Ergebnisse meiner Arbeit beruhen.

Ein spezieller Dank gilt weiterhin Manuel Hernández und Felix Bartsch für die wundervolle Zusammenarbeit im Labor und ihre hilfreichen Beiträge zu meiner Arbeit. In diesem Zusammenhang möchte ich auch den Roboterclub Aachen e.V. erwähnen, der mich mehrfach durch Zugang zu seiner Werkstatt unterstützt hat. Ebenso danke ich meinen zahlreichen Kollegen für viele interessante und gewinnbringende Diskussionen, vor allem Milan Zivkovic und Saeed Shojaee, die so lange mit mir ein Büro geteilt haben. Die Arbeit in einem so internationalen Team, wie bei uns am Institut, habe ich immer als große Bereicherung angesehen.

Ein besonderes Dankeschön geht an alle Freunde und Verwandten die während der besonders anstrengenden Endphase immer ein offenes Ohr für mich hatten.

Zu guter Letzt danke ich meinen Eltern Hans Georg Schmitz und Irmgard Schmitz für die bedingungslose Unterstützung, die sie mir in meiner nun insgesamt fast 30-jährigen Ausbildungszeit entgegengebracht haben.

Aachen, November 2017

Johannes Schmitz

Contents

Preface	iii
1 Introduction	1
1.1 Outline	3
2 Technical Background of RF-Based Localization	5
2.1 Physical Principles	6
2.1.1 Uplink and Downlink Localization	6
2.1.2 Ranging	7
2.1.3 Time Difference of Arrival	8
2.1.4 Direction of Arrival	8
2.1.5 Hybrid Methods	9
2.1.6 Carrier Phase-Based Methods	10
2.1.7 Fingerprinting	10
2.1.8 Range Free Methods	12
2.1.9 Importance of Physical Layer, Protocols and Topology in Network- Based Localization	12
2.1.10 Cooperative Localization	13
2.1.11 Sensor Network Self-Localization	13
2.2 Application Examples	14
2.2.1 2G/3G/4G/5G Cellular Networks	14
2.2.2 Personal and Industrial Indoor Localization	15
2.2.3 Localization in Aviation	15
2.2.4 Maritime Localization	17
2.2.5 Spectrum Regulation and Surveillance	18
2.2.6 Search and Rescue	18
2.2.7 Wildlife Radio Tracking	19
3 Localization with TDOA	23
3.1 TDOA System Model and Geometry	23
3.2 TDOA Localization Algorithms	25
3.3 TDOA Estimation from Known and Unknown Waveforms	27
3.4 Interpolation	29
3.5 Time of Arrival Estimation using OFDM Signals	32
3.5.1 Estimation Based on Cyclic Prefix and Preamble	32

3.5.2	OTDOA in LTE Downlink	34
3.5.3	UTDOA in LTE uplink	34
3.6	Dilution of Precision and Cramér-Rao Bound	35
3.7	Kalman Filter Based Tracking	41
3.8	Cramér-Rao Bound and Synchronization in Systems with Calibration Emitter	42
3.8.1	System and Clock Model	44
3.8.2	Clock Error Correction	47
3.8.3	Cramér-Rao Bound Analysis	49
3.8.4	Results	53
4	Grid-Based Sparse TDOA Localization	59
4.1	TDOA Localization Using Spatial Sparsity	59
4.2	Location Estimation	60
4.2.1	Joint Sparsity	62
4.2.2	Compressed Sensing	62
4.2.3	Localization Algorithm	63
4.2.4	Results	64
4.2.5	Localization of Many Sources	66
4.3	Ray Tracing for Urban Scenarios	67
4.3.1	Ray Launching Based Fingerprinting	70
4.3.2	Results	72
5	Sensor Network Self-Localization using TDOA	75
5.1	Active and Passive Methods	75
5.2	Self-Localization with Classical Multidimensional Scaling	76
5.3	Procrustes Transform and Absolute Localization	76
5.4	Differential Multidimensional Scaling	77
5.4.1	Stress Criteria for Differential MDS	79
5.4.2	Iterative Displacement of Points	79
5.4.3	Convergence and Stopping Criteria	80
5.4.4	Overcoming Local Minima	81
5.4.5	Numerical Gradient Descent	81
5.5	Anchoring	82
5.6	Simultaneous Anchoring with Weighted Gradient Descend	83
5.7	Self-Localization in the Presence of Clock Offsets	84
5.8	Results	86
6	Experimental Evaluation using Software Defined Radio	87
6.1	Distributed Software Defined Radio Testbed	87
6.2	System Architecture	89
6.2.1	Hardware	89
6.2.2	Software	89
6.2.3	Coordinate Systems	92

6.3	Synchronization	93
6.3.1	Receiver Clock Characterization and Allan Deviation	93
6.3.2	Synchronization Using GPS	96
6.3.3	Hybrid Synchronization with GPS and a Reference Emitter	99
6.4	Measurement Results	102
6.4.1	Obtaining Ground Truth	102
6.4.2	Pedestrian Tracking	104
6.4.3	Sensor Self-localization	104
7	Conclusions	109
7.1	Summary	109
7.2	Outlook	111
	List of Acronyms	113
	List of Symbols and Notation	117
	Bibliography	123

1 | Introduction

Beginning in the early 20th century, mankind started to explore the possibilities of localization using man-made signals and technology. All longer range localization systems, that provide an absolute localization result¹ are based on acoustic or electromagnetic waves. The relevant spectra can be further split into audible and ultrasonic as well as radio waves and light. From systems such as the acoustic gun detection using simple microphones and manual calculation [1] to the Global Positioning System (GPS) using satellites in space [2], many of the breakthrough technologies have been driven by military purposes. Nevertheless, today, a point of broad civilian access to a large selection of localization systems, algorithms and technologies has been reached. The latest change in the mass market occurred due to the ubiquitous proliferation of smartphones all over the world. This, for the first time, brought personal navigation including localization at everyone's fingertips. Other emerging applications, that are still less proliferated as they mostly require individual fitting and customization for each use-case, are guidance systems for museums and conferences, warehouse management systems due to the ever increasing automatization and sports and wildlife tracking. Other factors driving innovation in the sector of personal electronic devices are regulatory requirements, e.g., E911 [3], a set of rules that enables localization for emergency response which has recently been updated.

With the advent of self-driving cars on the horizon, highly accurate localization in urban environments and deep urban canyons becomes very important. Due to multipath propagation current global navigation satellite systems (GNSSs) achieve insufficient accuracy in this context. First iterations of autonomous vehicles defeat the problem by using optical technologies, i.e., image recognition, light detection and ranging (LIDAR), and also active radio frequency (RF) systems, i.e., radio detection and ranging (RADAR). Due to the small wavelength, optical systems achieve high resolutions but usually involve a significant amount of signal processing and require costly hardware. In practice though, limitations of optical systems including a limited range, the inability to provide any result in non-line-of-sight (NLOS) conditions, problems in bad weather conditions and others, require autonomous vehicles to carry a suite of various sensors and localization technologies. Localization is then performed by sensor fusion algorithms. Besides GNSS, one of the candidates to improve location information in autonomous driving

¹The concept of odometry and dead reckoning may use sensors based on other physical principals but does not provide absolute location results.

is network based localization. This is also of interest to advance the fifth generation of cellular networks (5G) and beyond, which considers massive multiple input multiple output (MIMO) base stations, or for applications like cognitive radio (CR). In both cases location awareness can be crucial for the performance. Other applications require very low-power, low-cost devices and large range, an example for this is wildlife tracking. In this application, for many scenarios, only radio wave based localization is feasible. Another related problem is the localization of illegal emissions by the national spectrum agencies. This is a harder problem because it is a form of non-cooperative localization where the knowledge about the signal waveform in the sensors is limited. This thesis considers both scenarios, the case of known waveforms which enables signal parameter estimation at the sensor level and that of unknown waveforms where estimation is performed in a fusion center (FC) after collecting the baseband signal samples from several distributed sensors.

The latter two examples, wildlife tracking and spectrum surveillance are low volume applications that often require tailor-made system designs. Further, in research and development environments, it might be desirable to quickly build prototypes in order to try out the feasibility of a single new idea. Until the beginning of the 21st century, the accessibility of smaller research institutions to such projects was severely limited or completely impossible. This was mainly due to the high costs and large development time and effort involved in the experimental evaluation. A principle, that has fundamentally changed experimental research on radio wave based systems in the last decade, is the concept of software defined radio (SDR) [4], [5], the idea being that the complete physical layer signal processing stack shall be implemented in software, in order to achieve maximum flexibility. It has turned out to be highly efficient and cost-effective for research and early prototyping, where a lot of small improvement and ideas have to be tested, as it allows for very short development iterations compared to integrated circuit (IC) hardware design. Highly accessible frameworks and tools, such as GNU Radio [6], as well as the availability of suitable hardware platforms for the RF transmission, subsequently transformed SDR into a mainstream research tool for the physical layer.

Localization based on RF essentially uses the same low-level signal processing principles that are used in communication systems. Therefore, although it was initially not developed with a focus on this purpose, SDR is also highly suitable for research in this area. However, as opposed to classical communication systems², certain distributed localization schemes require extremely accurate synchronization among distributed receivers. This aspect requires special attention to detail, as absolute nanosecond level synchronization accuracy can not be achieved without taking the peculiarities of the internal clocks of the RF frontend into account, which is examined in some detail in the experimental part of this thesis.

One goal of the experimental part of this thesis is to develop a modular and extensible

²Several next generation communication schemes known as coordinated multi-point (CoMP) do have tighter synchronization requirements.

framework for accurate real-time network based localization. To this end, it identifies and addresses major challenges by extensive technical analysis and through the proposal of several new algorithms and approaches. Consequently, this thesis develops the theoretical concepts and algorithms in parallel to an experimental distributed SDR testbed. The resulting SDR implementation provides a very flexible basis for further experiments as the testbed aims to be a generic framework for the evaluation of the discussed algorithms as well as future advanced concepts in network based localization.

1.1 Outline

The thesis document is structured as follows.

Chapter 2 summarizes the basics of radio wave based localization. The most common methods are listed and explained on a high level. Subsequently several interesting application examples are presented.

An in-depth review of the time difference of arrival (TDOA) approach to localization, that is followed throughout the thesis, is given in Chapter 3. The following Chapter 4 considers the localization problem under the assumption of spatial sparsity and applies a solution inspired by the area of compressed sensing. Next, the problem of sensor self-localization is treated in Chapter 5. Finally an implementation of a distributed SDR system is presented, that is used to experimentally evaluate some of the algorithms developed in the aforementioned chapters. The thesis is concluded in Chapter 7.

Localization systems rely on reference points in space. It is important to point out that there exists a number of different terms for this points that are frequently used. Depending on the research community, author or context, all the terms anchor, anchor node, anchor point, access point, base station, receiver, transmitter, sensor, sensor node are often used to identify objects with the same localization-related task in different systems. In the different chapters of this thesis several of the terms are used interchangeably. Another confusion involves the terms localization and positioning. This thesis follows the common definition that positioning purely determines coordinates in form of numbers, while localization determines the location of an object relative to its environment, for example using a map. Therefore, mainly the term localization is used.

Parts of the work presented in this thesis have already been published in [7, 8, 9, 10, 11]. Further, [12] has been submitted for publication.

2 | Technical Background of RF-Based Localization

This chapter will give a compact review of radio frequency (RF)-based localization techniques, followed by a number of typical application examples which are related to the approach of the thesis. The typical underlying digital signal processing stack of most modern localization systems can be generalized as shown in Figure 2.1. First, the utilized RF signal has to be acquired from the antenna in the analog domain. Usually this is carried out by a homodyne or (super)heterodyne receiver architecture comparable to a communication system, followed by an analog-to-digital converter (ADC). Next, one or several physical features are extracted from the sampled signal using an estimation algorithm. Subsequently, a second algorithm is employed to derive the location based

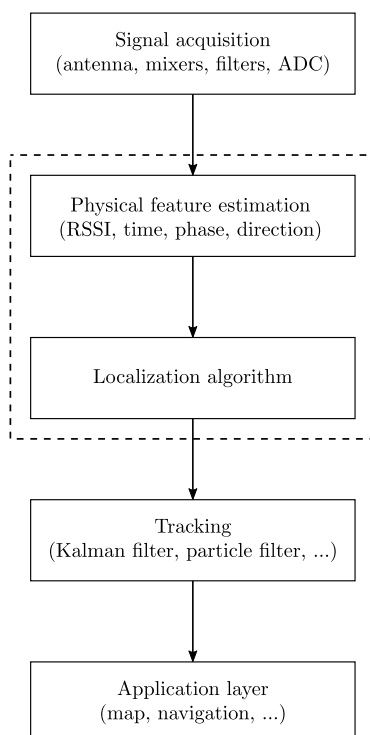


Figure 2.1: Typical receiver signal processing stack for RF-based localization, the stages in the dotted box are performed jointly in some cases.

on the estimated physical features. In some cases the last two steps are performed jointly and the location is directly estimated based on the sampled signals. Optionally, the system might feature a tracking stage that exploits the spatial correlation in the time series of estimated locations, as well as a knowledge about the movement behavior of the target. This is typically done with a Kalman or particle filter. Finally, the results are handed over to the application layer where they can be displayed to a human user or further processed for navigation purposes.

2.1 Physical Principles

To begin with, in the following subsections a closer look is taken at the second step of Figure 2.1 and how it relates to the third step. A variety of different physical features relate to spatial information about the signal emitter. This is the interface between the feature estimation and the localization algorithm. Different features can be used either alone or jointly, where joint approaches are also denoted as hybrid. Considering only the feature estimation step without the localization, some major practical disadvantages can be noted. Accurate estimation of received signal strength (RSS) requires calibration. Further, knowledge about the transmit power or the expected RSS at a particular location is needed. Approaches with direction of arrival (DOA) estimation require more than one antenna per receiver and also require calibration of the resulting antenna array. Time measurement-based approaches require very accurate synchronization. These distinct physical layer issues, together with cost, size and other constraints, often decide about which approach is used in a new system.

2.1.1 Uplink and Downlink Localization

For the characterization of localization systems it is important to distinguish between two major scenarios. We denote these two basic cases as the uplink and the downlink scenario. In the downlink scenario, the network infrastructure provides the necessary signals while the mobile node performs the localization algorithm, whereas in the uplink scenario the mobile node transmits the signal and the network performs the localization algorithm. GNSS is an example for a downlink system, in contrast, tag-based wildlife or asset tracking are representatives of uplink scenarios. In cellular networks the uplink as well as the downlink can be used for localization. Infrastructure-free localization, e.g., with active methods such as RADAR, LIDAR or passive optical systems for automotive applications, obviously can not clearly be categorized in the two classes above. However, as the localization is performed on the mobile node they rather resemble a downlink configuration and are often combined with further infrastructure-based downlink methods. The choice of an uplink or downlink approach is an important design criterion for a localization system due to several reasons. It determines where the location information is first available and how much additional communication overhead occurs, it may

limit the accessibility of the system in terms of number of simultaneous users and it may also have an impact on the accuracy. This is due to the differences in processing power and the quality of the hardware for different network nodes. For example, the amplifiers and clocks of base stations are usually more expensive and better than the parts used in user equipments. In some safety critical real-time applications, downlink localization is inevitable because the additional delay introduced by communicating the results over the network and the limited update rate, due to bandwidth limitations, can not be tolerated. Finally, power constraints due to battery powered devices are also a very important design criteria, that can heavily influence design decisions in localization systems. For example, if localization tags should achieve a very long lifetime of one year or more on a single set of batteries, it is essential that they spend most of the time in a deep sleep mode and use a localization scheme and transmission protocol with the lowest number of transmissions possible. Thus, each localization solution has to be carefully designed and adopted for its specific application. In the following the possible physical principles used by RF localization systems are explained.

2.1.2 Ranging

The simplest feature that can be used for localization is RSS also known as received signal strength indicator (RSSI). It can be estimated using a single channel receiver and accurate synchronization is not required. Together with a model for the signal propagation this can be used for ranging, i.e., the distance between the transmitter and the receiver can be determined, in this case based on the attenuation of the signal. Localization based on the range is known as tri- or multilateration. The localization step itself is usually solved by using a least squares approach that takes the measured ranges to several anchor points as an input. Performing ranging, based on the estimated signal strength, is known to have limited accuracy as studied in [13]. One known issue with RSS, that deteriorates performance, is that the exact transmit power is often unknown and also depends on the antenna characteristic and thus the direction.

Another way to perform ranging is to estimate the time of flight (TOF) between the transmitter and receiver. The term TOF is often confused with time of arrival (TOA), however they are only equivalent when synchronization between transmitter and receiver is ensured. TOF can be converted to range based on the propagation speed c of the wave, the speed of light in the case of radio waves. The most popular example for time-based ranging is GNSS, i.e., European Galileo, US American GPS [2], Russian globalnaya navigatsionnaya sputnikovaya sistema (GLONASS) and Chinese Beidou, which carries highly accurate clocks on board the satellites. A SDR-based implementation for GNSS reception has been implemented in [14, 15]. Without the atomic clocks used in GNSS systems, highly accurate TOF measurements would not be possible. In ground-based sensor networks, to avoid the necessity for the accurate but very expensive and large clocks, the two-way ranging method can be used. In this case a signal is transmitted

and promptly returned by the receiver such that the distance can be determined as half of the round-trip time, carefully taking into account the processing times.

2.1.3 Time Difference of Arrival

If synchronization between the transmitters and receivers in the system as well as two-way ranging is not possible, the method of TDOA can be used. This can be especially useful for uplink and remote sensing applications when a radio wave emitter has to be localized. One of the earliest applications was the British GEE system used for bomber guidance over German territory. For optimum results the TDOA localization method requires very good synchronization between the anchor points of the system, e.g., the receivers in an uplink localization scenario. The TDOA is the difference in arrival time between pairs of anchor points. In a free-space wave propagation environment each TDOA translates into a hyperboloid while the location of the target object is found at the intersection. In case of the GPS and predecessor system Transit the surface of the earth was used as an additional constraint to obtain a position fix. Further ground-based systems for naval and aerial applications that use or have been using TDOA are DECCA, OMEGA, GEE and LORA. One of the critical challenges of TDOA-based systems is the synchronization of the anchor nodes. Three major approaches are usually used in order to solve this problem. The *common clock* approach delivers a common clock signal to each of the anchor nodes. It can be achieved by cabling all units to a central clock unit. This achieves very high synchronization accuracy at the price of complex network infrastructure and difficult installation. Further, a *calibration emitter* can be used, that transmits another wireless signal, additionally to the localization signal, which is used to constantly track and correct the time offsets of all nodes in the system. In some systems one of the sensors takes the role of the calibration emitter and the network follows some type of common protocol for synchronization. This approach has the disadvantage that purely passive operation is not possible. Alternatively, a GNSS system can be leveraged in order to perform time synchronization of all the anchors. This requires a GNSS receiver at each of the nodes that disciplines the local clocks of the nodes. Such a unit is known as GPS disciplined oscillator (GPSDO). This technology is mainly used in wide area multilateration (WAM), for example for airspace surveillance [16] or lightning detection [17, 18, 19, 20, 21].

2.1.4 Direction of Arrival

Another principle is based on the estimation of the directions of the impinging waves. This is also known as triangulation because the location estimation depends on the angles of the wave vectors with the antenna baselines. The technique was used as early as World War II by the Germans under the code name *X-Gerät* in order to guide bombers towards their targets over England. DOA estimation requires multiple signal processing channels and antenna elements at the receiver. Synchronization between sensors is

not critical for this scheme. However, due to the working principle, the main challenge in DOA-based systems is antenna and receiver design. In order to apply algorithms like multiple signal classification (MUSIC) [22] and estimation of signal parameters via rotational invariance techniques (ESPRIT) [23] a DOA-enabled sensor requires an absolutely phase coherent synchronization between its different internal receive channels. Note that this requirement is different from a MIMO communication receiver and therefore makes it difficult to design a DOA sensor based on commercial off-the-shelf (COTS) hardware components. In communication systems phase offsets are estimated and corrected using pilot information during channel estimation and equalization. This is often not possible in a passive localization system. Hence, it leads to the need of calibration methods for the antenna as well as each signal processing chain in the receiver.

Besides calibration, another issue of DOA systems is the large number of antenna elements which sometimes permits a deployment as a result of constraint space. An advantage is the low effort in terms of network infrastructure. This is because DOA estimation is usually performed inside each sensor and only the bearing information is exchanged. Altogether, the reasons described above have so far mostly prevented RF-based DOA from being deployed in the consumer mass market. Networked DOA-based systems are mainly used for highly specialized applications. Further, in experimental research applications TDOA-based systems often seem to be preferred to DOA-based systems because the complexity and calibration issues of the DOA receivers outweigh the network design and synchronization issues present when using TDOA. Examples are tracking systems for biology [24, 25]. DOA systems exhibit advantages in mobile single sensor applications, e.g., search and rescue missions in disaster scenarios or law enforcement. An approach to enable DOA estimation with a single antenna is a virtual antenna array. To build the virtual array an inertial measurement unit (IMU) and sometimes a GPS is combined with a moving antenna [26]. Then, by using the information about the movement obtained by the IMU after Kalman filtering, the measurements at different locations and times can be combined. The accuracy of this approach is limited by the estimation of the antennas locations. Further, the transmitted signal should be present at all measurement times.

2.1.5 Hybrid Methods

If high complexity is tolerable or a system consists of a heterogeneous set of sensors with different abilities, then a hybrid algorithm can be used that exploits the diversity in the best possible way. Hybrid algorithms that combine ranging and DOA measurements are investigated in [27, 28]. Another interesting approach, that can be characterized as hybrid, is the idea of so called lighthouses [29, 30]. The idea of the lighthouses is to transmit from at least two anchor nodes with a narrow rotating beam. The same principle is used in VHF omni directional radio range (VOR) for the radio navigation of aircraft. VOR uses an RF beam whereas small scale systems designed for indoor use, typically utilize a rotating laser beam to achieve the desired directionality and avoid

multipath propagation. As the location of the anchor and the frequency of the rotation is exactly known to the receiver, it can perform triangulation based on time difference measurements between two consecutive detections. An additional synchronization signal can be issued for every rotation of the beam in order to determine the baseline angle and to avoid measurements of differences. Another related approach using RF signals is described in [31]. Here a rotating unidirectional antenna emits a constant amplitude sine wave. Another fixed antenna transmits a second sine together with a synchronization signal such that using interferometric evaluation of the received signal allows for a triangulation.

2.1.6 Carrier Phase-Based Methods

Similar to communication receivers, receivers for localization applications may operate in a coherent or non-coherent way. The coherent receiver is able to obtain information about the carrier phase. Many direction finding systems strictly rely on this and estimate the phase difference of the impinging wave at the different antenna elements. Ranging-based systems can also greatly improve accuracy if carrier phase measurements are available. A prominent example for this is Real Time Kinematic (RTK) [32, 33] where differential phase measurements of GNSS signals are used in order to achieve centimeter-level accuracy. Carrier phase-based methods have two main issues: they are strongly affected by signal multipath propagation and the phase measurement is highly ambiguous. Moreover, accurate carrier phase estimation needs a constant tracking of the signal in the receiver. In a ground-based system, especially the effects of multipath propagation can not completely be eliminated, therefore the experimental part of the thesis focuses on non-coherent receivers. A way of circumventing the multipath problem for short range applications, e.g., indoor localization is the use of near-field electromagnetic ranging (NFER) [34, 35, 36, 37]. The idea of NFER is to use the difference of the electric and magnetic fields that prevail in the near-field region of an antenna for ranging. As the effect in practice is limited to about one-third of the wavelength, very low frequencies (usually below 2 MHz) have to be used. This has the advantage that the effect of multipath propagation in the targeted indoor environment is weak. However, attenuation of the signal is relatively large because very large antennas usually required for long wavelengths can not be used indoors. Another solution against multipath is to create a very large virtual bandwidth using channel hopping. The resulting set of phase measurements at very different frequencies and hence very different wavelength can be used to perform ranging based on the Chinese remainder theorem [38, 39, 40].

2.1.7 Fingerprinting

To overcome several of the issues with geometric approaches to localization, a data-driven approach called fingerprinting has been proposed [41, 42]. Fingerprinting divides localization in two phases. During the offline phase measurements of signal features,

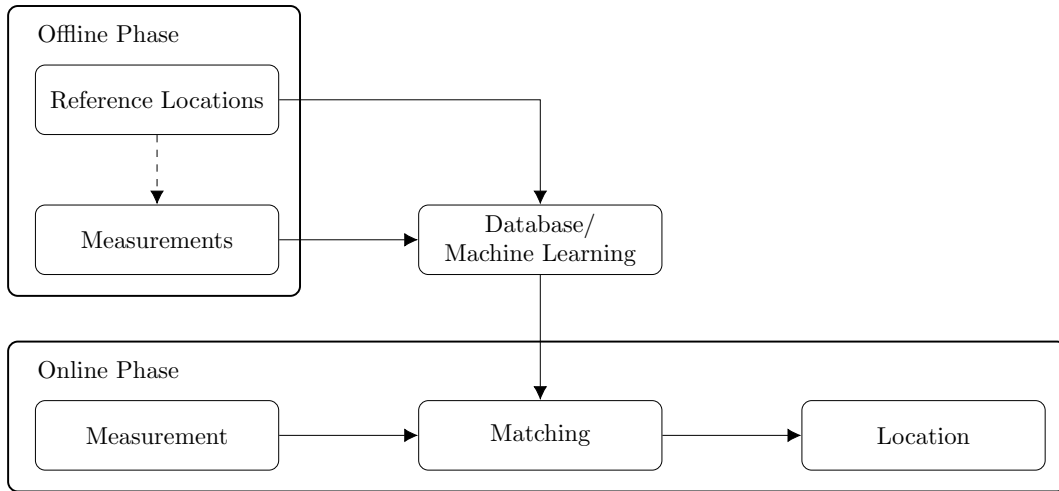


Figure 2.2: The fingerprinting approach to localization.

e.g., RSSI, on a grid of exactly known locations are taken and stored. The online phase is the actual localization step where measurements are taken at unknown locations and are then matched with the stored data to determine the location. By taking a large set of measurements covering the complete region of interest, many of the static effects of the signal propagation, e.g., antenna patterns, multipath, NLOS can be implicitly accounted for. For storage and matching of the data, several approaches are possible. A classical database can be used. After a rough lookup step based on the ID of the involved anchor nodes, measured feature vectors can be mapped to the stored data vectors using a distance measure. The output location is then an interpolation between the most likely grid points. Another approach is to use machine learning and store the information in a neural network [43]. In this example, during the offline phase, a deep neural network learns a representation of the RF environment and therefore yields higher localization accuracy. An issue of fingerprinting is its difficulty to be studied and justified analytically and therefore making it difficult to find optimum solutions. Some approaches such as [44] exist but are very limited.

Classical fingerprinting for localization is usually associated with RSSI measurements. Typical commercial applications also combine RSSI information from cellular networks and WiFi. However, generalizing the concept, any type of signal feature can be used. In [45] channel state information (CSI) information is used, i.e., the phases rotation and attenuation of the orthogonal frequency-division multiplexing (OFDM) subcarriers underlying the IEEE 802.11 WiFi standard. Another approach presented in the thesis, cf. Section 4.3, uses TDOA-based features [8]. In an effort to ease the effort of the offline phase, it further uses a model of radio wave propagation instead of the typical measurement campaign. If several antenna elements are available at the receiver it is also possible to use DOA features as studied in [46].

In order to completely remove the necessity of initializing the fingerprinting with measurements or simulations, simultaneous localization and mapping (SLAM)-based ap-

proaches have been developed to build up and update the database [47, 48, 49]. For reasonable results, just few available absolute location information is sufficient, e.g., the location of connected cellular base stations or sporadic GPS positions. However, a large amount of users and measurements is necessary to refine the data set. Hence, on a global scale this approach is only feasible for organizations with a large user base. So far this resulted, on the one hand, in proprietary solutions from corporations that are large enough to maintain their own global data base and, on the other hand, several providers that offer access to databases for fingerprinting with global coverage for application development.

2.1.8 Range Free Methods

In contrast to all the methods described above, another class of methods called *range free localization* does not rely on explicit measurements of the received signal's features. These methods have been developed for very simple sensor networks where the sensors need to have a low complexity as well as power consumption and lower accuracy of the localization is acceptable. This topic is strongly related to sensor network self-localization, cf. Section 2.1.11. Instead of physical layer measurements, connectivity information from higher layers is used. Network connectivity and routing is inherently interlinked with the geometry of the network and therefore enables an inference of the nodes' locations. The simplest approach in this regard is the centroid method [50]. With this method a sensor node determines its location as the centroid of the three closest anchor nodes it is connected to. There exist several extensions such as weighted centroid methods, where the weights are based on the quality of the links [51]. Another method, distance vector-hop (DV-Hop), goes a step further and uses the hop count of messages, that are broadcasted by the anchor nodes as an input. This increases the accuracy because a larger part of the network geometry is taken into account. Both methods have weaknesses when the geometry is irregular or the nodes are moving. A third method, approximate point in triangle (APIT) [52], improves on this by increasing the range of the anchor node transmissions and calculating the center of gravity of multiple centroids of triangles formed by all possible anchor triples. The name *range-free* is insofar misleading, as the information about the radio links does implicitly contain information about the range, albeit in some kind of highly quantized way. This quantization yields an inherent bound to the accuracy.

2.1.9 Importance of Physical Layer, Protocols and Topology in Network-Based Localization

In network-based localization, besides the design criterion of uplink and downlink localization, there exist the problem of physical layer waveform design and the problem

of multi user access to the system. These problems are very similar to the design problems encountered in communication networks. For example, 3G cellular networks use code-division multiple access (CDMA) to differentiate between the user equipments in the cell, while GPS and Galileo use the same approach to differentiate between the different satellites. In communications systems, the physical layer waveform design puts strict limits on the capacity of the system as has been described in Claude E. Shannon's seminal works [53, 54]. Similarly in localization systems, the waveform inflicts a limit on the accuracy, typically evaluated using the Cramér-Rao Bound [55]. Further limitations are caused by the network geometry and are analyzed with the dilution of precision concept [56].

A special case to be considered is the localization of signals from non-cooperative transmitters, i.e., the structure of the waveform is either partially or completely unknown. Under this constraint, a *matched filter*-based receiver is not feasible and alternative sub-optimal techniques have to be used. In this thesis we consider the case of known and unknown waveforms and perform TDOA-based localization. An unknown waveform implies the exchange of baseband samples between the nodes in order to perform the TDOA estimation. In practice for modern wide-band signals this requires a powerful backhaul network. If the signal structure was known at the receiving sensors, matched filter-based processing could reduce this communication overhead to a fraction. This shows that, although the localization algorithm which solves for the coordinates in a map based on the TDOAs is essentially the same in both cases, the consequences of certain constraints can be critical for the practical feasibility.

2.1.10 Cooperative Localization

Contrary to the cooperative signaling described above, the term cooperative localization often has a different meaning as described in [57, 58]. In cooperative localization two or more user equipments or mobile nodes in a communication network cooperate in order to improve their localization accuracy. The benefit of this is a large increase in the number of anchor points that each user can see, because the other users act as a type of additional virtual anchor point. Thus, it can be shown that the accuracy of localization of each node can be improved substantially. It can also help to resolve situations where insufficient anchor points are visible for each user, therefore entirely prohibiting a fix in the non-cooperative case. This also means that if the mobile nodes cooperate, a smaller amount of fixed anchor points is necessary.

2.1.11 Sensor Network Self-Localization

A problem that is related to cooperative localization is sensor network self-localization [59, 60]. The problem is to find the location of the anchor points in the network. This can be split into two subproblems:

1. Finding a configuration, i.e, the relative positions of the sensors with respect to each other.
2. Mapping this configuration to the absolute location on the map.

Obviously, some kind of absolute reference points is needed to perform the second step. However, compared to determining an absolute localization of all anchors, only a small subset of points is sufficient to provide the anchoring for the complete network. Furthermore, in some cases, e.g., sensor swarm navigation [61], absolute locations are not always required and therefore only the first step of the self-localization is needed.

2.2 Application Examples

The following section provides a examples of current infrastructure ground-based localization technology. Due to the myriad of deployed systems in the research community as well as the commercial market, completeness is not the scope of this listing. Rather, the reader should gain a basic understanding of possible solutions for different types of localization problems.

2.2.1 2G/3G/4G/5G Cellular Networks

Localization in cellular networks is desired due to several reasons. Among others these are localization services for the customers, emergency response, law enforcement and localization for the improvement of the service, such as improved handover among base stations [62, 63] One of the most known authoritative measures in this area is the Enhanced 9-1-1 (E911) system, which is mandatory, according to an Federal Communications Commission (FCC) order from 1996 and the 1999 Wireless Communications and Public Safety Act, for all cellphone networks operated in the US [3]. The system is also used for law enforcement purposes. It resulted in many base station and networks being equipped with the necessary technology, such as direction finding, TDOA measurements and uplink fingerprinting. Another method is to use the GNSS chipsets deployed in most modern user equipments (UEs) and to retrieve this information from the network side. Methods for network-based localization are described in the standards for 2G–Global System for Mobile Communications (GSM), 3G–Universal Mobile Telecommunications System (UMTS) and 4G–Long Term Evolution (LTE) networks [64, 65, 66, 67, 68, 69]. More specifically in LTE observed time difference of arrival (OTDOA), i.e., downlink TDOA observed by the UE has been introduced in release 9 and uplink time difference of arrival (UTDOA) in release 11 [70]. The accuracy of the 4G–LTE localization has been studied in [71, 72, 73]. Although the accuracy in line-of-sight conditions can be quite high due to the larger signal bandwidth compared to 2G and 3G systems, in NLOS it can deteriorate harshly. Errors of 50-100 m and more are reported under such worst

case conditions. In future 5G systems the signal bandwidth is expected to be further increased and therefore the localization accuracy will be improved. Together with cell site planning that is optimized for roadways, this is expected to be an important assisting technology for autonomous driving [74]. Although, most currently deployed networks possess some degree of localization capabilities, these services are typically not available to the user. Localization of the UE from the user perspective, as necessary for personal navigation software is mostly done using a combination of GNSS and a fingerprinting approach that takes the RSSI of all available RF signals into account.

2.2.2 Personal and Industrial Indoor Localization

Due to the missing availability of interfaces on the user side and the insufficient accuracy, cellular network-based localization is often not adequate for many indoor applications. This and the poor coverage with GNSS signals leads to a strong demand for additional methods which are often based on short range communication systems. The authors of [75] and [76] provide surveys about the commonly used approaches. Indoor localization can be used for guidance systems in shops, museums and conferences and for personal mobility in airports, train- and subway stations. It is also used in the industrial context for warehouse management and autonomous systems such as robots. Personal navigation is often based on IEEE 802.11 WiFi and Bluetooth due to their broad availability on the end user hardware. Localization is typically carried out with RSSI-based fingerprinting. Together with further sensors of the used hardware platform, i.e., IMU, camera, the accuracy and the experience for the user can be further improved [77]. More recently ultra-wideband (UWB) technology has been introduced and studied extensively. The very short time, high bandwidth pulses of UWB provide a simple means of multipath resilience. Typical UWB implementations cover several 100 MHz of bandwidth and enable positioning errors in the order of cm [78]. A disadvantage is the limited range due to very low regulatory limits on the transmitted power. As of today, the proliferation of UWB technology has been limited and it is mostly used for specific industrial applications. Further, there is a large range of proprietary real-time locating system (RTLS) technologies [37, 79, 80] requiring custom made anchors as well as tags.

2.2.3 Localization in Aviation

In commercial civil aviation a large range of RF-based technologies is used in order to obtain location information about the aircrafts [16]. The different technologies can be grouped in two categories, systems that help the aircraft to self-localize and systems that are used for surveillance of the airspace from the ground. For self-localization, besides the relatively new GNSS, various ground infrastructure-based systems are used. The distance measuring equipment (DME) enables the aircraft to perform ranging, it is composed of very simple transponder ground stations that respond to the interrogation of the aircraft. Another system called VOR, depicted in Figure 2.3 provides directional



Figure 2.3: The VOR transmitter at the former airfield Berlin Tempelhof. The runway is now open to the public.

information by emitting a rotating RF beam together with an omnidirectional synchronization signal. A joint DME and VOR station is able to provide information about the absolute location of the aircraft by a combination of range and direction. This is an older implementation of the rotating lighthouse principle as described in [29, 30] which is now also used for indoor localization. Finally, in case of bad weather conditions instrument landing system (ILS) is used to support aircraft landing. ILS uses antenna arrays to transmit directed RF beams towards the sky. The beams are transmitted pairwise on two different frequencies and are used by the aircraft for navigation by staying in the equilibrium line of the amplitudes of the two signals. The localizer beams enable the aircraft to align its flightpath with the runway, while the glideslope beams indicate a slope of 3 degrees towards the touchdown point at the beginning of the runway. To provide additional information, the aircraft may use further onboard sensors that do not rely on any network architecture, these are the inertial measurement unit, air pressure sensor, Pitot tube for airspeed measurement and the radio altimeter, which is a RADAR that measures the distance to the ground.

To determine the location of the aircraft from the ground two major systems are in use. The primary surveillance radar (PSR) is a classical RADAR that emits a strong signal and receives the reflection from the aircraft. A more modern system is secondary surveillance radar (SSR), it requires a transponder hardware aboard the aircraft that responds to the transmission of the ground station similarly to DME. However, additional information about the identification and current location of the vehicle is included in the response. The active transponder technology allows for a significantly lower transmit power of the ground station. In order to perform the localization the information inside the response message, that is obtained by the aircraft through GNSS, can be trusted or the signals can additionally be used by the ground stations in order to per-

form their own localization of the vehicle, e.g., using a WAM network. The airborne transponder can also be used for a second mode called automatic dependent surveillance - broadcast (ADS-B), where a message is regularly transmitted at a frequency of 1 Hz or higher. This enables a passive localization from the ground using WAM [81, 82] and also for aircraft among each other for the purpose of collision avoidance.

2.2.4 Maritime Localization

Besides classical optical lighthouses, modern maritime navigation also uses radio navigation. Infrastructure-based solutions are Decca, Omega and Loran-C, which are low frequency hyperbolic, i.e, TDOA, systems. These systems work based on a very widely spread out, synchronized network of anchor stations, that regularly emit RF pulses. Proliferation of these type of systems dates back to the Second World War era and the only system still in service among the three is Loran-C. Accuracy of classical Loran-C is rather low based on the fact that the signal bandwidth is low. This is one of the reasons why GNSS-based navigation experienced a steep rise in popularity. Other reasons are the ubiquitous world wide availability and lower cost per user. Nevertheless, there exist some undertakings, namely EUROFIX, eLoran and eDLoran, that aim to improve Loran-C and use it in combination with GNSS [83, 84]. The accuracy for the updated system has been shown to be in the order of 5-10 m for regions of good coverage [85, 86]. These ground-based backup and augmentation systems are also much less vulnerable to jamming compared to GNSS. Close to the shoreline, RADAR can be used very well to obtain a fix by comparing the RADAR image to stored map data. As the RADAR also provides a tool to avoid collisions during bad weather conditions, most larger vessels now are equipped with a combination of RADAR and GNSS navigation. To determine the depth of the water ships are also equipped with echo sounding; RF-based RADAR is not well suited for this application due to the poor penetration properties of the radio waves in water.

Another application of radio localization in the maritime context are radio buoys. These radio beacons are used for example in order to recover driftnets. The fishing vessel has to be equipped with a direction finder system and the net will be connected to the buoy which constantly emits a signal.

An interesting research field that requires localization in the ocean are swimming and floating sensor networks. Two examples are the international Argo project [87] and the swarm of underwater robots [25] developed at the university of California San Diego. Argo is a cooperation of 29 countries and has almost 4000 ocean floats with sensors all over the world. The floats are able to dive down to a depth of 2000m to generate measurement data. Data is collected using a satellite link when the floats return to the surface. Float locations are also determined when they are at the surface using GNSS. The underwater robot swarm [25] is a system that covers smaller regions of hundreds of square meters to a few square kilometers. It is used to very accurately measure the flows occurring in a volume of ocean water. Two components are necessary for this,

a number of floating buoys as anchor points and the underwater robots. The anchors are synchronized using GPSDOs and emit an acoustic underwater signal whose times of arrival are recorded by the robots on a large memory. Localization is performed offline using the complete dataset [88].

2.2.5 Spectrum Regulation and Surveillance

The task of spectrum regulation is a duty of the national spectrum agencies. In order to provide a sufficient level of standardization under such a constraint, the decisions of the national organizations are based on International Telecommunication Union (ITU) recommendations and standards. According to the Handbook on National Spectrum Management [89] the issues that the agencies shall be supervising are

- Monitoring to assist frequency assignment,
- Monitoring to assess spectrum occupancy,
- Monitoring for compliance with national rules and regulations,
- Detection and identification of unauthorized transmissions,
- Monitoring to identify the source of, and, resolve interference.

Especially for the latter tasks, localization of the emissions is mission critical. For CR applications it is also interesting to have maps of the spectrum occupancy which requires a sensor network with the ability to provide location information. A good overview and understanding of the topic of localization for spectrum surveillance can be gained from the spectrum monitoring handbook [90]. Of further importance concerning the topic is the ITU spectrum management series, where several recommendations have been published that are concerned with direction finding systems. General tasks of a monitoring service are summarized in [91]. Methods for direction finding and emitter localization using monitoring stations are described in [89, 90, 92]. More detailed recommendations for time division multiple access and code division multiple access signals are provided in [93]. In [94] testing procedures for the accuracy of direction finding stations are described, while [95] is concerned with the precision of TOA-based sensors.

2.2.6 Search and Rescue

In disaster scenarios localization technology can be a life-saving tool. The E911 clearly defines requirements for localization of user equipment in case of emergencies. In the European Union a similar system under the name Enhanced 1-1-2 (E112) is partially implemented. As described in Section 2.2.1, this has led to enhancing the base stations and networks with the required capabilities. In situations where no sophisticated network infrastructure is available, yet search and rescue is required, other approaches

might be used. An example is large destructions and collapsed buildings due to earthquakes. Buried people might still carry their phones and this presents an opportunity for mobile search and rescue teams to perform the localization. In [96] it has been shown how the mobile device can be triggered to transmit from an improvised mobile GSM base station. The emergency responders can then setup up a temporary network and perform multilateration as demonstrated in [97]. A simpler method is to use simple single antenna sensors [98] and manually perform signal strength-based localization by moving around with the sensor. Similar approaches are used to recover buried skiers and snowboarders from avalanches. There are two options available in the market for athletes to carry. A *RECCO* reflector is a passive device that is usually embedded in a jacket. Using a special RADAR device the reflector can be detected and localized below the surface. More sophisticated *avalanche transceivers* include a transmitter and a receiver using a standardized frequency of 457 kHz. In case of an accident of a member of a group, the device is switched to receive mode and can then be used to localize the buried person. Currently available receivers possess direction finding and ranging capabilities. Similarly, for marine use active beacons are used for search and rescue. An automatic identification system - search and rescue transponder (AIS-SART) is a simple transmitter that can be detected by a suitable receiver up to 10 nautical miles. In contrast an emergency position-indicating radio beacon (EPIRB) allows to transmit a local signal together with an emergency message over a satellite network, thereby dramatically increasing the range.

2.2.7 Wildlife Radio Tracking

Wildlife radio tracking is a process of tagging animals with some type of RF-based tags in order to observe their movements and behavioral patterns among the population. A good overview of such techniques can be found in the books of Kenward [99] and White [100]. Typical systems either use GPS-based tags or local base station-based systems that track custom made tags using an RSSI, DOA or TDOA-based approach. The design decision for a certain technology is clearly based on a trade-off between range, update rate, lifespan and cost. GPS-based tags, as shown in Figure 2.4, are either heavy due to the large energy consumption or have low update rate as well as lifespan. Another design criterion is the question of data extraction. Systems can either perform in real-time and constantly report back the animal's location to the scientists or record data for later interrogation. If the location is calculated in the tag, data backhauling further limits the battery lifetime. Infrastructure-based systems, e.g., with WAM can support small tags with high update rate and real-time capability because the tags can be very simple transmitters and the majority of signal processing is performed at the sensors and FC. Real-time capable systems enable further applications such as finding the animals in their sleeping spots for close observation. Using the output data of the

¹Pictures have been taken during a research stay in Israel, the author thankfully acknowledges the support by the Minerva short-term research grant of Max Planck Society.

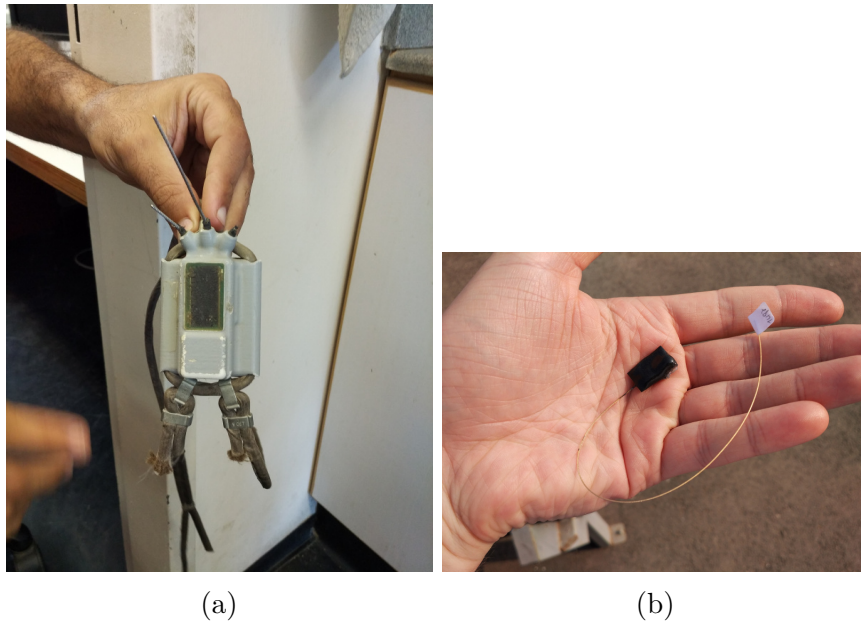


Figure 2.4: (a) A GPS-based wildlife tracking tag for eagles and other large birds, (b) a tag for the ATLAS [24] tracking systems with a weight of about 1-2 g.¹

wildlife tracking system scientist can perform a number of examinations about a species in the observed habitat. Among others they can answer questions about the home range, size of the habitat, locations of sleeping hideouts, survival rate, movement patterns, mating habits, interaction and sleeping patterns. As the quality of these results directly depends on the accuracy of the localization, it is important to constantly improve such systems with state-of-the-art hardware and algorithms. Examples of recent state-of-the-art infrastructure-based scientific wildlife tracking systems are [101, 102, 24]. As demonstrated by the ATLAS system [24] SDR technology enables fast prototyping as well as deployment of advanced tracking system.

The ATLAS system

The ATLAS system is a wildlife localization and tracking system, developed jointly by the biology department of Hebrew University and the computer science and electrical engineering department of Tel-Aviv University. This system is basically a WAM system using TDOA measurements for the localization. Various birds as well as bats with a minimum bodyweight of about 20 g are tagged with battery powered transmitting tags. The tagging process is depicted in Figure 2.5. Afterwards, the animals can be localized in quasi real-time by an array of 9 base stations distributed in an area of about 10 km by 20 km in Hula Valley in the north of Israel. Backhauling of the sensor measurement data is performed over the Internet using cellular network connections. A TDOA localization algorithm is then run in a FC server at the university. On the physical layer the system uses 433 MHz frequency-shift keying (FSK) signals transmitted



Figure 2.5: The process for tagging birds in Hula Valley, (a) small birds are not heavy enough to carry the tags, (b) a tag being glued to the back of a slightly larger bird (a Bulbul), (c) antenna of the tag, the tag is hidden beneath the feathers, cellular base station tower co-locating the ATLAS system (d).

by the tags at intervals of 1 or 2 seconds, depending on the battery lifetime requirements. The transmit bandwidth is about 2 MHz and the power about 1 mW. Multiple access is achieved by assigning each tag its unique 8 ms long, 8192 length code sequence. Using this approach, several hundred animals can be tracked in parallel. Similar to GNSS signals, the coding gain that can be achieved with the knowledge of these long codes allows the reception of the signals under very low signal-to-noise ratios (SNRs). The typical achievable accuracy of the localization is in the order of 5-10 m if the signal is received by most of the base stations. An analysis of the accuracy of the system extended to asynchronous clock operation is given in Section 3.8.

3 | Localization with TDOA

In the remainder of the thesis the focus lies on various techniques and algorithms that deal with TDOA-based localization. Therefore, after defining a system model, the present chapter begins with the basics of measuring and estimating TDOAs and explaining how the location estimation can be performed for single snapshots. It then goes on to deal with fundamental accuracy limits of such systems that are on the one hand determined by the network geometry and on the other hand by the measurement noise. The former is often analytically treated using the dilution of precision (DOP) concept while the latter is modeled using bounds such as the Cramér-Rao lower bound (CRLB). The DOP and CRLB are closely related and essentially perform the same analysis. An interesting special case is the case of differential measurements, where additional beacons are present in the system that serve as calibration emitters. This improves the synchronization at the cost of additional noise introduced by the additional measurements. Finally, tracking methods that take into account several observations over time can help to overcome the limits of single snapshots. A Kalman filter (KF) approach that takes into account the geometry of the network is introduced for that purpose at the end of the chapter.

Parts of the following results have been presented in [12].

3.1 TDOA System Model and Geometry

During the course of the thesis several slightly different signal models are considered. The main differences are the sensors are the transmit capability of the sensors, the number of transmitting targets, and different models for signal propagation. If none of the sensors performs any transmission in the observed frequency band we define the system as passive. This chapter begins with the simplest model and extensions are added when needed. Consider a system of M distributed receivers that are trying to localize P moving transmitters. We define an index set for the sensors as $\mathcal{S} = \{1, \dots, M\}$ and an index set for the transmitters as $\mathcal{T} = \{1, \dots, P\}$. The system is considered to be passive and has no communication from the transmitting target to the receivers for the purpose of the localization. For the sake of simplicity begin with $P = 1$, assuming a

single transmitter and model the transmitted signal as

$$y_i(t) = h_i s(t - t_i) + w_i(t), \quad i \in \mathcal{S}, \quad (3.1)$$

where $w_i(t)$ is a Gaussian noise process and t_i models the delay which is proportional to the propagation distance $d_{i,k}$ between the transmitter k and receiver i . Similarly $h_i \propto \frac{1}{d_{i,k}}$ models the attenuation of a free space propagation channel. A TDOA capable sensor system is able to observe time differences $\tau_{i,j,k} = t_i - t_j$ between receiver i and the reference j resulting from a signal of transmitter k . In a two-dimensional space this translates to equations of the form

$$\begin{aligned} \tau_{i,j,k} &= \frac{1}{c} \left(\|\mathbf{p}_k - \mathbf{r}_i\|_2 - \|\mathbf{p}_k - \mathbf{r}_j\|_2 \right), \quad i, j \in \mathcal{S}, \quad k \in \mathcal{T} \\ &= \frac{1}{c} \left(\sqrt{(p_{k1} - r_{i1})^2 + (p_{k2} - r_{i2})^2} - \sqrt{(p_{k1} - r_{j1})^2 + (p_{k2} - r_{j2})^2} \right), \end{aligned} \quad (3.2)$$

with the speed of light c and the coordinates of the transmitter $\mathbf{p}_k = [p_{k1}, p_{k2}]^\top, k \in \mathcal{T}$ and the coordinates of the receivers $\mathbf{r}_k = [r_{k1}, r_{k2}]^\top, k \in \mathcal{S}$. Based on the measurements, a solution for the location \mathbf{p}_k can be found as explained in Section 3.2. Geometrically the problem goes back to an intersection of hyperbolic functions. An example is shown in Figure 3.1.

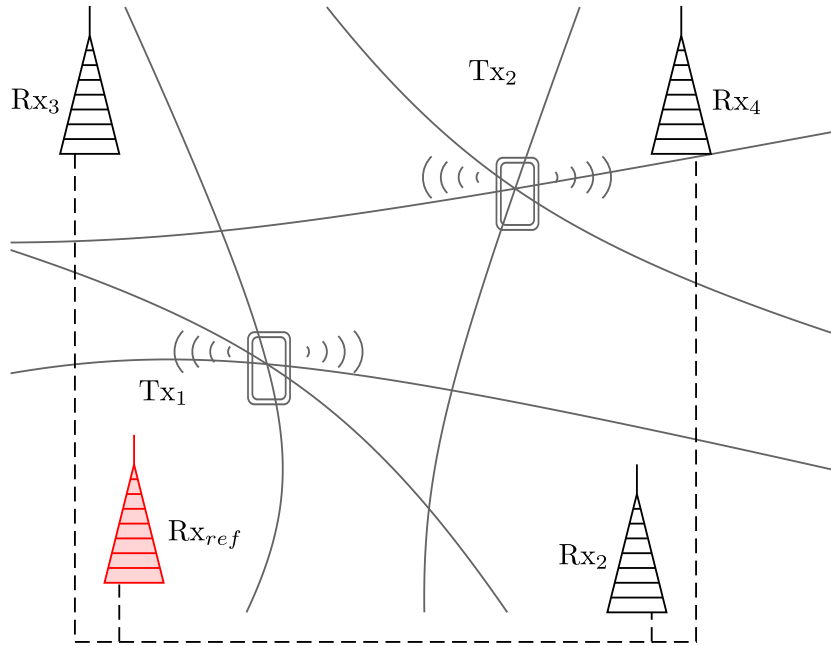


Figure 3.1: Exemplary TDOA localization system with four receivers and two transmitters, often one receiver is selected as a reference for the TDOA estimation.

3.2 TDOA Localization Algorithms

TDOA measurements are used for localization in the situation where no absolute TOF measurements are possible, i.e., transmitter and receiver are not synchronized but synchronization of the anchor points is possible. Assuming the TDOAs between the sensors are exactly known or have been estimated, several methods exist that can determine the position of the transmitter. Overviews about the most important known methods may be found in [103, 104]. In [105] a performance comparison of different methods is provided. The minimum number of sensors needed to perform TDOA localization in two dimensions is three. This yields a so called full set of TDOAs of size three. In general there are $M(M-1)/2$ TDOAs in the full set for M sensors. It turns out that for the noiseless case the full set is redundant and a reduced set or spherical set that uses only one sensor as the reference is sufficient. However, in the more realistic case of noisy measurements the single reference approach can yield slightly suboptimum results [106] and improvements can be achieved by an optimum full set to reduced set conversion [107].

Assume a single target transmitter $P = 1$, the following algorithm [108, 109] provides a solution for the target coordinates in the three sensor case ($M = 3$). It uses the two non-redundant TDOAs $\tau_{i,j,k}$ where the reference sensor $j = 1$ and $i \in \{2, 3\}$. With the auxiliary terms

$$g_{i,1} = r_{i1} - r_{11}, \quad (3.3)$$

$$g_{i,2} = r_{i2} - r_{12}, \quad (3.4)$$

$$\delta_{i,1,k} = c\tau_{i,1,k}, \quad (3.5)$$

$$\delta_{i,1,k} = d_{i,k} - d_{1,k}, \quad (3.6)$$

$$d_{1,k} = \|\mathbf{p}_k - \mathbf{r}_1\|_2, \quad (3.7)$$

$$K_i = r_{i1}^2 + r_{i2}^2, \quad (3.8)$$

the target coordinates \mathbf{p}_k can be determined as

$$\mathbf{p}_k = \begin{bmatrix} g_{3,2} & -g_{2,2} \\ -g_{3,1} & g_{2,1} \end{bmatrix} \frac{1}{(g_{3,2}g_{2,1} - g_{2,2}g_{3,1})} \times \begin{bmatrix} \delta_{2,1,k}d_{1,k} + \frac{1}{2}\delta_{2,1,k}^2 - K_2 + K_1 \\ \delta_{3,1,k}d_{1,k} + \frac{1}{2}\delta_{3,1,k}^2 - K_3 + K_1 \end{bmatrix}, \quad (3.9)$$

This can be rewritten as follows:

$$p_{k1} = d_{1,k} \underbrace{\left[\frac{g_{2,2}\delta_{3,1,k} - g_{3,2}\delta_{2,1,k}}{g_{3,2}g_{2,1} - g_{2,2}g_{3,1}} \right]}_A + \frac{g_{2,2} \left(\frac{1}{2} (\delta_{3,1,k}^2 - K_3 + K_1) \right) - g_{3,2} \left(\frac{1}{2} (\delta_{2,1,k}^2 - K_2 + K_1) \right)}{\underbrace{g_{3,2}g_{2,1} - g_{2,2}g_{3,1}}_B}, \quad (3.10)$$

$$p_{k2} = d_{1,k} \underbrace{\left[\frac{g_{3,1}\delta_{2,1,k} - g_{2,1}\delta_{3,1,k}}{g_{3,2}g_{2,1} - g_{2,2}g_{3,1}} \right]}_C + \underbrace{\frac{g_{3,1} \left(\frac{1}{2} (\delta_{2,1,k}^2 - K_2 + K_1) \right) - g_{2,1} \left(\frac{1}{2} (\delta_{3,1,k}^2 - K_3 + K_1) \right)}{g_{3,2}g_{2,1} - g_{2,2}g_{3,1}}}_D. \quad (3.11)$$

Introducing eqs. (3.10) and (3.11) into (3.7) leads to

$$d_{1,k}^2 = d_{1,k}^2 \cdot \underbrace{(A^2 + C^2)}_{\alpha+1} + d_{1,k} \cdot \underbrace{2(AB + CD - Ar_{11} - Cr_{12})}_{\beta} + \underbrace{r_{11}^2 + r_{12}^2 - 2r_{11}B - 2r_{12}D + B^2 + D^2}_{\gamma}. \quad (3.12)$$

Then, $d_{1,k}$ can be solved as

$$d_{1,k} = \frac{-\beta \pm \sqrt{\beta^2 - 4\alpha\gamma}}{2\alpha}. \quad (3.13)$$

This yields two roots, normally one of them positive and the other negative. By introducing the positive root into eqs. (3.10) and (3.11) the final solution is obtained. An ambiguity can occur when both roots are positive.

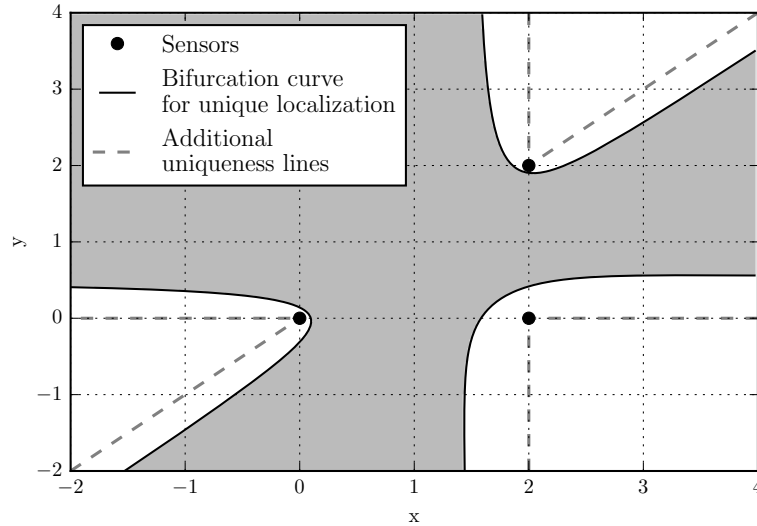


Figure 3.2: The three sensor TDOA localization problem has a region where the solution is unique (gray area and dashed lines), in the white region two different solutions are obtained. Reproduced and plotted based on results from [110].

Clearly, with three sensors the solution is in general not unique, due to the fact that the two linearly independent hyperbolas may have two intersections in some cases. The

region of uniqueness can be analytically derived as shown in [110, 111] and depicted in Figure 3.2.

A fourth sensor can resolve the uniqueness problem and provide redundancy for the unique region. Further sensors provide additional redundancy to the solution and therefore lead to a least squares approach

$$\hat{\mathbf{p}}_k = \arg \min_{\mathbf{p}_k} \|\hat{\boldsymbol{\tau}}_k - \boldsymbol{\tau}_k\|_2, \quad (3.14)$$

where $\hat{\boldsymbol{\tau}}_k = [\hat{\tau}_{2,1,k}, \dots, \hat{\tau}_{M,1,k}]^T$ are the estimated TDOAs as described in Section 3.3. For this problem, in the literature, two major classes of algorithms can be identified.

- **Iterative algorithms:** These types of algorithms solve the problem by applying gradient descent or Gauss Newton types of algorithms, linearizing the problem with Taylor series approximation. The algorithms of Foy [112] and Torrieri [113] fall under this class. Due to the non-linear nature of the TDOA problem, a large number of iterations might be necessary for some target locations.
- **Direct algorithms:** Another class of methods derives closed form direct solutions for the problem, thereby avoiding large numbers of iterations. The first popular approach in this direction has been a transformation of the hyperbolic problem to spheres by introducing an additional variable that describes a fixed virtual time reference. This idea has been used by Friedlander [114], Schau [108], Fang [115] and Smith [116, 117]. Those methods need at least one additional sensor per dimension, e.g., four sensors in two dimensions. Further, the results are suboptimum as the solution depends on the choice of the fixed virtual time reference. An improvement is provided by the two step approach that takes this dependency into account. It has first been proposed by Chan [109] and reaches the CRLB (described in Section 3.6). This particular method performs very well under optimum conditions but is biased for low SNR, erroneous sensor locations and problematic geometries. Later it has been slightly improved by Huang in [118] and also by the initial co-author in [119], in order to decrease the bias. A rather different formulation, that also leads to the reduced bias performance, has been proposed by Wei [120]. It formulates the passive source localization problem using multidimensional scaling (MDS) by introducing two additional dimension to the problem.

3.3 TDOA Estimation from Known and Unknown Waveforms

In order to perform the algorithms listed in Section 3.2 the TDOAs have to be estimated from the received signals first. Depending on the knowledge on and the waveform structure of the emitted signal, there exist two possible ways

- **Direct TDOA estimation:** For the direct estimation access to the baseband samples of both sensors is needed. Technically this implies a large amount of information communicated between the sensors and the FC where the calculation is performed. This is a problem that is partially addressed by the approach described in Chapter 4. For a direct estimation of the TDOAs usually a cross-correlation approach is used. The direct method is useful especially if the observed signal structure is unknown or if insufficient pilots are embedded in the signal.
- **Estimation based on TOAs:** In case of a known signal and pilot structure, each sensor can estimate a TOA of the signal independently from the others. In this way the amount of data that needs to be transmitted to the FC can be decreased considerably. TDOAs are in this case straightforwardly calculated as a difference of TOAs.

The TDOAs between the anchor points can then be estimated based on the received signals. A well known estimator is the cross-correlation and its extended, i.e. filtered, versions called generalized cross-correlation (GCC) [121, 122]. The basic unfiltered estimator is given as

$$R_{y_i y_j}(\tau) = E\{y_i^*(t)y_j(t + \tau)\}, \quad (3.15)$$

$$\hat{\tau} = \arg \max |R_{y_i y_j}(\tau)|. \quad (3.16)$$

An estimator for $R_{y_i y_j}(\tau)$ is given as

$$\tilde{R}_{y_i y_j}(\tau) = \frac{1}{T} \int_{\tau}^T y_i^*(t)y_j(t + \tau)dt, \quad (3.17)$$

with the observation time T . Using the equivalent baseband model at each sensor i one obtains $y_i(t)$, that contain ideally low pass filtered, Nyquist sampled version of the received signals, where $t = nT_s$ and $n \in \mathbb{Z}$. Here T_s is the sampling interval. The cross-correlation function can then be estimated as

$$\hat{R}_{y_i y_j}[\eta] = \frac{1}{N} \sum_{n=0}^{N-1} y_i^*[n]y_j[n + \eta]. \quad (3.18)$$

In practice the length N of the available signal vector

$$\mathbf{y}_i = (y_i(t_0 - \gamma), \dots, y_i(t_{N-1} - \gamma))^T \in \mathbb{C}^{N \times 1}, \quad (3.19)$$

with the delay γ is limited. The estimate of cross-correlation is therefore biased as the number of samples available for the calculation of each lag is not constant. Instead one might use an unbiased version of the estimator

$$\hat{R}_{y_i y_j}[\eta] = \frac{1}{N - \eta} \sum_{n=0}^{N-1-\eta} y_i^*[n]y_j[n + \eta], \quad (3.20)$$

where it has to be taken care that $\eta \ll N$, such that enough samples are available for the estimation. A fast version based on the fast Fourier transform (FFT) can be implemented as [123, p. 188]

$$\hat{R}_{y_i y_j}[\eta] = \frac{1}{N} \sum_{m=0}^{M-1} Z_i^*[m] Z_j[m] e^{j \frac{2\pi \eta m}{M}}, \quad (3.21)$$

with

$$Z_i[m] = \sum_{n=0}^{N-1} z_i[n] e^{j \frac{2\pi m n}{N}}, \quad (3.22)$$

$$Z_j[m] = \sum_{n=0}^{N-1} z_j[n] e^{j \frac{2\pi m n}{N}}, \quad (3.23)$$

where $y[n]$ needs to be zero-padded if the acyclic cross-correlation function is desired

$$\mathbf{z}_i = [\mathbf{y}_i^T \ \mathbf{0}^T]^T, \quad (3.24)$$

$$\mathbf{z}_j = [\mathbf{0}^T \ \mathbf{y}_j^T]^T. \quad (3.25)$$

3.4 Interpolation

Due to the discrete nature of the cross-correlation function estimate $\hat{R}_{y_i y_j}[\eta]$ the accuracy of $\hat{\tau}$ is limited by the sampling time step T_s . Several different methods for interpolation exist in the literature. An overview of different methods used in digital signal processing is given in [124, Chapter 5.6]. A rather simple but computationally expensive method is to upsample the signal to a higher sampling rate T_s that provides sufficient accuracy for time delay estimation. For very high accuracies this does not only require a large amount of computation but can also result in an enormous memory footprint. Therefore other analytic methods, that provide virtually infinite accuracy are preferable. This can be achieved by using a single polynomial interpolation based on the so called Lagrange form first discovered by Waring [125]. It requires solving a linear system of equations in order to determine the coefficients of a polynomial that goes through each sample point. Interpolation with a single polynomial however has well known limitations, i.e., the Runge phenomenon that describes the often occurring strong oscillation, especially at the endpoints. Therefore, the method of spline interpolation is preferable for signal processing applications. Splines are piecewise defined polynomials that can be constructed as the sum of B-spline basis functions with limited support. The pieces of the B-spline can be constructed using the Cox-de Bor formula [126]

$$B_{i,0}(\tau) := \begin{cases} 1 & \text{if } t_i \leq \tau < t_{i+1} \\ 0 & \text{otherwise,} \end{cases} \quad (3.26)$$

$$B_{i,k}(\tau) = \frac{\tau - t_i}{t_{i+k} - t_i} B_{i,k-1}(\tau) + \frac{t_{i+k+1} - \tau}{t_{i+k+1} - t_{i+1}} B_{i+1,k-1}(\tau), \quad (3.27)$$

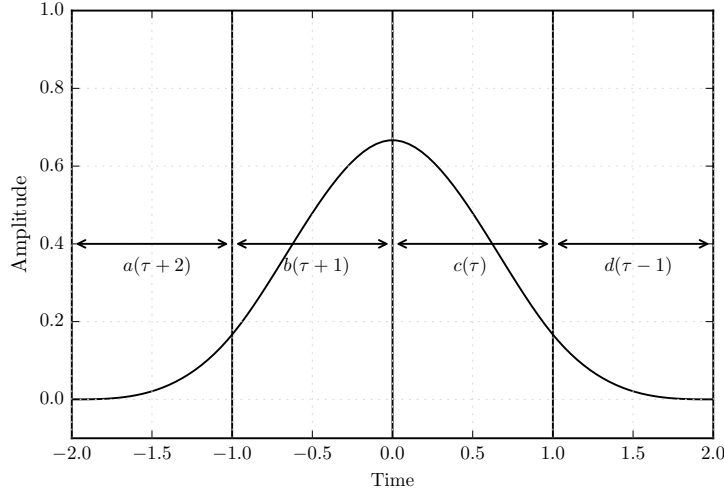


Figure 3.3: Single B-spline basis function

where t_i are called the knots of the spline, which limit the different pieces. Figure 3.3 shows an example for a cubic B-spline basis function. In order to determine the weights for each basis, different methods exist that try to fit a spline in an optimum way to a given set of sample points, according to different criteria, e.g., smoothness [127, 128]. A beneficial property of the polynomial-based interpolations is the possibility to find the maximum of the interpolated function with arbitrary accuracy by the use of calculus. To simplify the process of the peak detection, a possible simplification is to omit the derivation of interpolation weights and use the sample values instead. For this it is necessary to have the spline knots located at the sampling points. Using an explicit formulation, a cubic spline piece for $\tau \in [0, 1)$ can be written as

$$\zeta(\tau)_3 = \nu_1 B_{1,3}(\tau) + \nu_0 B_{0,3}(\tau) + \nu_{-1} B_{-1,3}(\tau) + \nu_{-2} B_{-2,3}(\tau), \quad \tau \in [0, 1), \quad (3.28)$$

where ν_0 is the weight for the knot at $\tau = 1$, with

$$B_{-2,3}(\tau) = a(\tau + 2) = \frac{1}{6}(1 - 3\tau + 3\tau^2 - \tau^3) \quad \text{for } 0 \leq \tau < 1, \quad (3.29a)$$

$$B_{-1,3}(\tau) = b(\tau + 1) = \frac{1}{6}(4 - 6\tau^2 + 3\tau^3) \quad \text{for } 0 \leq \tau < 1, \quad (3.29b)$$

$$B_{0,3}(\tau) = c(\tau) = \frac{1}{6}(1 + 3\tau + 3\tau^2 - 3\tau^3) \quad \text{for } 0 \leq \tau < 1, \quad (3.29c)$$

$$B_{1,3}(\tau) = d(\tau - 1) = \frac{1}{6}\tau^3 \quad \text{for } 0 \leq \tau < 1. \quad (3.29d)$$

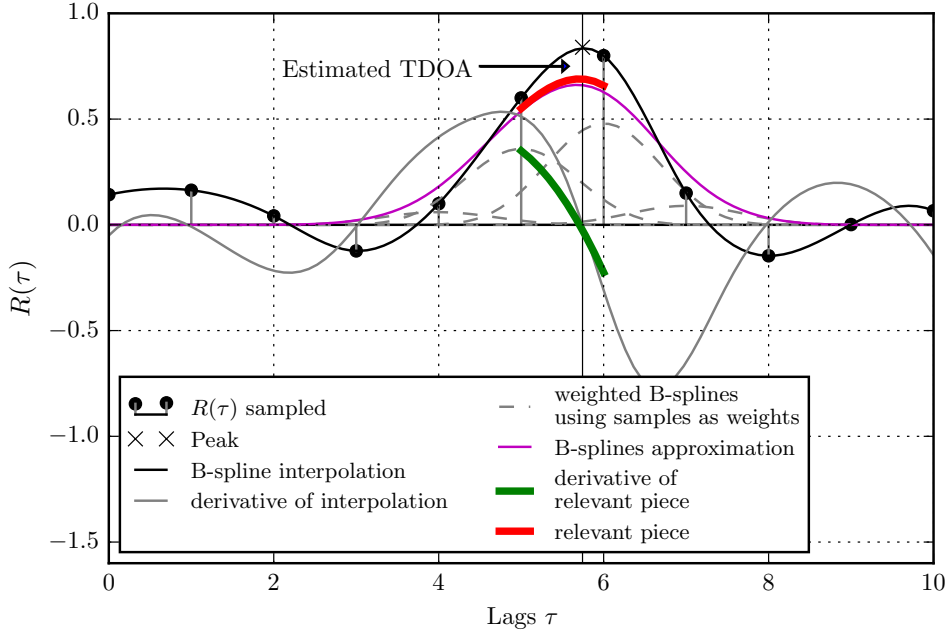


Figure 3.4: Interpolation of the cross-correlation function using B-spline interpolation, which is used in the experimental part of the thesis including, approximation and derivatives.

The associated derivatives are given as

$$\frac{d}{d\tau}B_{-2,3}(\tau) = \frac{1}{6}(-3 + 6\tau - 3\tau^2) \quad \text{for } 0 \leq \tau < 1, \quad (3.30a)$$

$$\frac{d}{d\tau}B_{-1,3}(\tau) = \frac{1}{6}(-12\tau + 9\tau^2) \quad \text{for } 0 \leq \tau < 1, \quad (3.30b)$$

$$\frac{d}{d\tau}B_{0,3}(\tau) = \frac{1}{6}(3 + 6\tau - 9\tau^2) \quad \text{for } 0 \leq \tau < 1, \quad (3.30c)$$

$$\frac{d}{d\tau}B_{1,3}(\tau) = \frac{1}{6}(3\tau^2) \quad \text{for } 0 \leq \tau < 1. \quad (3.30d)$$

Further, the relevant parts with the location of the maximum are assumed to be in the section directly left and right of the sample maximum of $R(\tau)$. Then the derivative $\frac{d}{d\tau}\zeta(\tau)_3$ of the spline from (3.28) with the weights ν_i given by the sample values of $R(\tau)$ is given as

$$\begin{aligned} \frac{d}{d\tau}\zeta(\tau)_3 = & \nu_1 \frac{d}{d\tau}B_{1,3}(\tau) + \nu_0 \frac{d}{d\tau}B_{0,3}(\tau) \\ & + \nu_{-1} \frac{d}{d\tau}B_{-1,3}(\tau) + \nu_{-2} \frac{d}{d\tau}B_{-2,3}(\tau), \quad \tau \in [0, 1], \quad (3.31) \end{aligned}$$

where ν_0 is assumed to be the sample maximum and the true peak is in the left interval towards ν_{-1} . An equivalent solution can be given for the peak in the right interval.

Then a solution to the peak detection problem is the solution of

$$\tau_{\max} = -0.5 \frac{6\nu_0 - 12\nu_{-1} + 6\nu_{-2}}{3\nu_1 - 9\nu_0 + 9\nu_{-1} - 3\nu_{-2}} \pm \sqrt{\left(0.5 \frac{6\nu_0 - 12\nu_{-1} + 6\nu_{-2}}{3\nu_1 - 9\nu_0 + 9\nu_{-1} - 3\nu_{-2}}\right)^2 - \frac{3\nu_0 - 3\nu_{-2}}{3\nu_1 - 9\nu_0 + 9\nu_{-1} - 3\nu_{-2}}} \quad (3.32)$$

located in the interval of interest. This explicit simple analytical solution yields a good compromise between accuracy and computational complexity. An example can be found in Figure 3.4, where the approximated solution is almost identical to the complete spline interpolation.

3.5 Time of Arrival Estimation using OFDM Signals

Exemplary for the case of known signals, some examples from the class of OFDM signals are discussed in the following. When known signals with pilot structures are received it is possible to estimate a TOA at each receiver in an uplink configuration. In the downlink configuration a single receiver needs to estimate all TOAs from the different anchors. TDOA-based localization can then be performed using the differences of the measurements. For example, in LTE systems this final step is always performed by the core network, which obtains the measurements either from the UE in the downlink, i.e., the so called OTDOA case or from the Evolved NodeB (eNB) in the uplink, i.e., the so called UTDOA case.

3.5.1 Estimation Based on Cyclic Prefix and Preamble

OFDM signals as used in point to point communication like in IEEE 802.11 wireless local area network (WLAN) are built from symbols that contain several subcarriers. Subcarriers are transmitted parallel on different frequencies in an orthogonal way. In order to protect each consecutive signal from the effects of multipath propagation and avoid inter symbol interference (ISI), a so called cyclic prefix (CP) is added in front of each symbol. The CP is a copy of the final part of the symbol itself as shown in Figure 3.5. The resulting signal can be written for a single OFDM symbol as

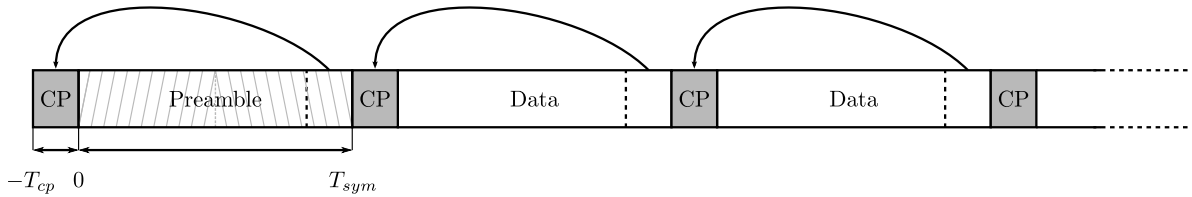


Figure 3.5: Basic OFDM signal structure.

$$x(t) = \frac{1}{\sqrt{N}} \sum_{k=0}^{N_{sym}-1} X_k e^{j2\pi f_k t} q(t - nT), \quad -T_{cp} \leq t \leq T_{sym}, \quad (3.33)$$

where N_{sym} is the number of subcarriers X_k is the message symbol transmitted over the k th subcarrier, T_{sym} the symbol duration and T_{cp} the cyclic prefix duration. The position of each subcarrier is

$$f_k = k\Delta f, \quad (3.34)$$

with the subcarrier spacing

$$\Delta f = \frac{1}{T_s N_{sym}}, \quad (3.35)$$

while $q(t)$ is a pulse shaping function, for example:

$$q(t) = \text{rect}(t). \quad (3.36)$$

The discrete realization of the OFDM signal without oversampling for this simple pulse shaping function and sampling times

$$t = nT_s, \quad (3.37)$$

becomes

$$x[n] = \frac{1}{\sqrt{N_{sym}}} \sum_{k=0}^{N_{sym}-1} X_k e^{j2\pi \frac{kn}{N_{sym}}}, \quad -N_{cp} \leq n \leq N_{sym}. \quad (3.38)$$

By generating the OFDM symbols in frequency domain each subcarrier can be individually modulated with signaling or user data. A number of OFDM symbols forms a frame. Usually each frame carries synchronization data on some of the subcarriers, e.g., on all subcarriers of the first symbol. A well known method has been proposed by Schmidl and Cox [129]. In this approach the first symbol of the preamble is loaded with two identical parts in time domain. Using such a pilot or preamble symbol, the beginning of the frame can be detected. The preamble symbol is often used together with the CPs [130] to continuously perform time synchronization using a running correlator, that correlates two different parts of the received signal

$$P[n] = \sum_{d=0}^{N/2} x^*[n+d]x[n+N/2+d]. \quad (3.39)$$

The normalized output of such a correlator, according to the two different metrics, is shown in Figure 3.6. For localization this provides a first approach for the estimation of the TOA. However, a communication receiver has very low requirements on the accuracy of the synchronization compared to a receiver aiming for localization. In communication an error of several samples is acceptable due to the cyclic properties of the OFDM symbol. Assuming a bandwidth between 1 and 20 MHz a synchronization mismatch of a single sample transforms to an error of up to 300 m. Therefore additional interpolation is necessary in order to achieve reasonable results. TOA estimation based on the CP and preamble is inherently limited by the fixed length of these structures [131]. Therefore it is useful to reserve additional data subcarriers and transmit additional pilot information in order to improve the localization accuracy. This is the approach followed in the LTE standard.

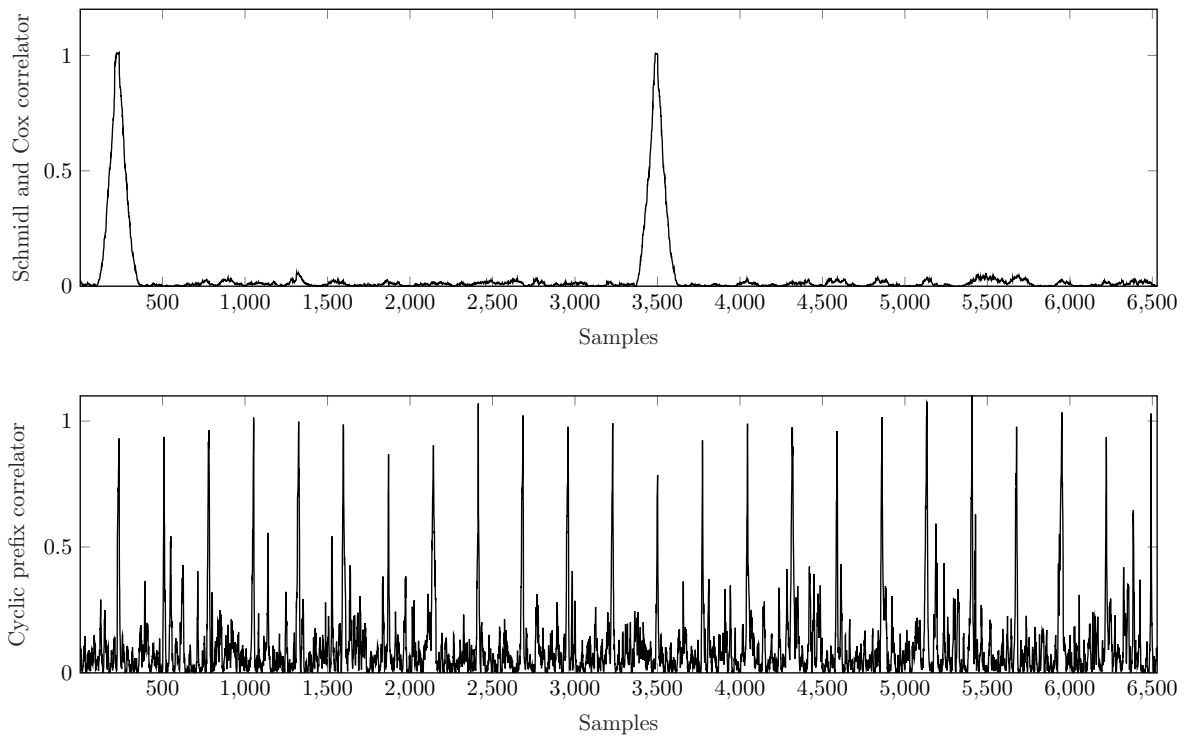


Figure 3.6: Correlator outputs for OFDM time synchronization. Based on the preamble design of Schmidl and Cox [129] (top), and the cyclic prefix [130] (bottom). The corresponding OFDM signal frame consists of 12 symbols.

3.5.2 OTDOA in LTE Downlink

The LTE downlink from the eNB to the UE uses orthogonal frequency-division multiple access (OFDMA) on the physical layer. This is essentially OFDM where the subcarriers are shared among all users in time and frequency. For localization, the network can make a request to the UE to take TDOA measurements between different detectable eNBs. During the measurement time a specially designed signal sequence called positioning reference signals (PRS) is embedded in the downlink signals. The measured TDOAs are reported back the network where the UE location is calculated. An example for the PRS in the OFDM time frequency grid can be seen in Figure 3.7. The exact sequence and all possible configurations are given in [69, §6.10.4]. PRS signals are transmitted on distinctive subcarriers for each neighboring eNB in order to avoid interference. Additionally, to further lower the interference, specifically in the case of localization, the transmissions in neighboring cells can be muted completely.

3.5.3 UTDOA in LTE uplink

In the LTE uplink the single-carrier frequency-division multiple access (SC-FDMA) is used for radio access from the UEs to the eNBs. For localization a set of eNBs that

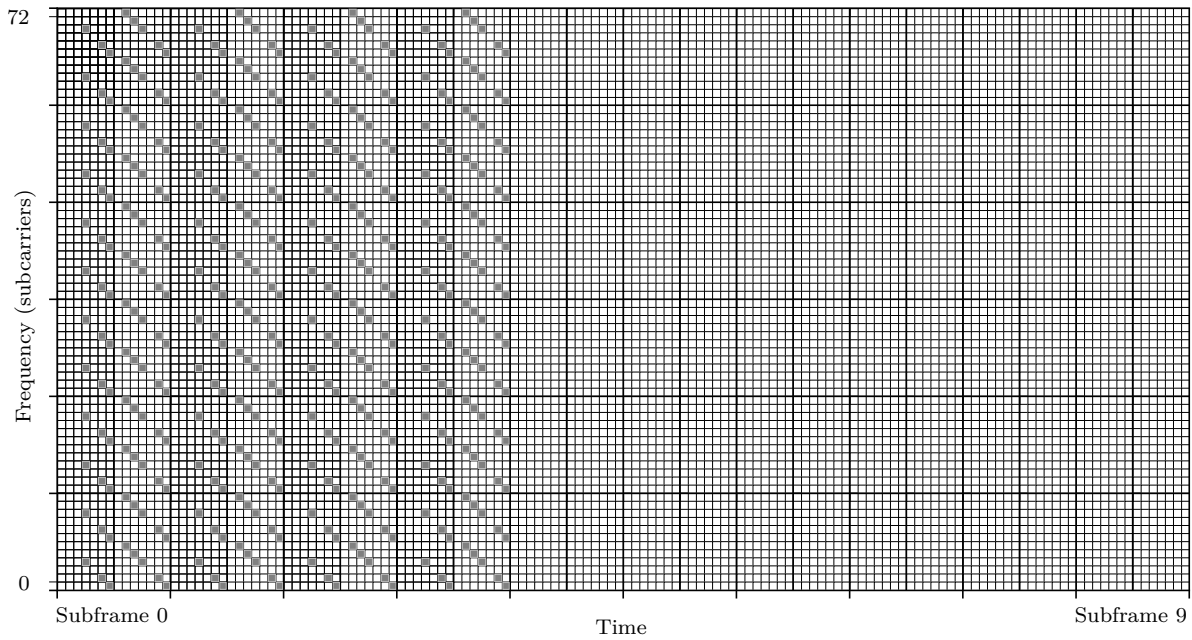


Figure 3.7: Example of the positioning reference signals (PRS) used for localization in an 1.4 MHz LTE downlink. The exact subcarrier pattern depends is different for each eNB.

are able to detect the uplink signal is ordered by the core network to obtain TDOA measurements. Simultaneously the UE is requested to embed the sounding reference signal (SRS) sequence into its transmit signal. Finally, similar to the downlink case the measurements are delivered to the responsible service of the core network and a localization is obtained. The SRS can be transmitted on the last OFDM symbol of each subframe as shown in Figure 3.8. In order to support multiple users, the SRS uses a Zadoff-Chu or a quadrature phase-shift keying (QPSK) sequence that is optimized for low cross-correlation. The exact sequence and all possible configurations are given in [69, §5.5.3]. The number of simultaneous users can be further increased by frequency alternating scheme and a frequency hopping scheme. As in the downlink case, muting of adjacent cells for interference management is possible.

3.6 Dilution of Precision and Cramér-Rao Bound

The dilution of precision (DOP) concept models how the sensor network geometry translates into localization errors with respect to the location of the target. This concept is most prominently known from GPS [56] and most of the available GPS receivers are able to calculate it. For TDOA-based localization it can be similarly applied. As shown

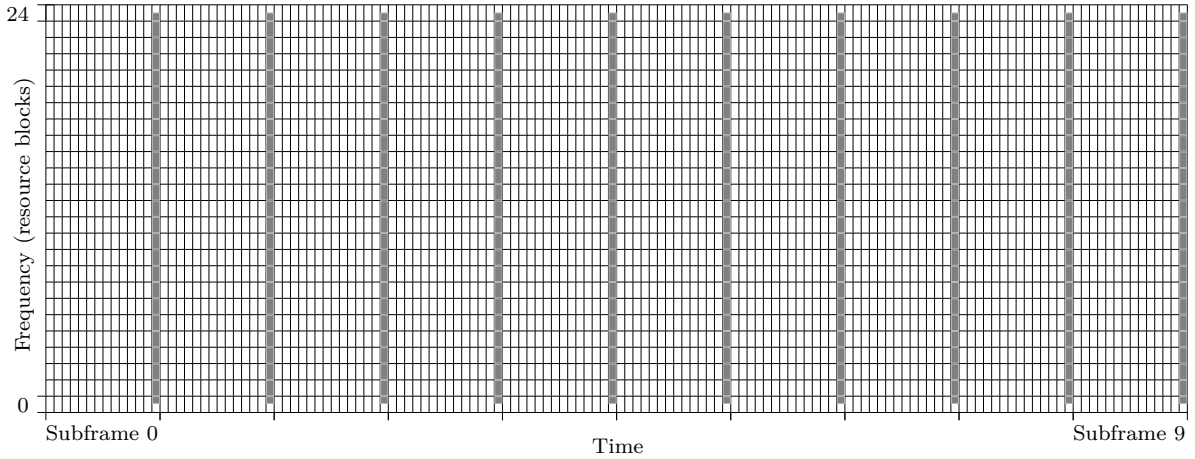


Figure 3.8: Example of the SRS used for localization in a 5 MHz LTE uplink. The SRS (gray) can be transmitted on the last symbol of each subframe.

in [132] define the Jacobian \mathbf{H}^j of the TDOAs with reference receiver j

$$\mathbf{H}^j = \begin{bmatrix} \vdots \\ (\frac{\partial}{\partial \mathbf{p}_k} \tau_{i,j,k})^\top \\ \vdots \end{bmatrix}, \quad i \in \mathcal{S} \setminus \{j\}, \quad (3.40)$$

where the partial derivative

$$\frac{\partial}{\partial \mathbf{p}_k} \tau_{i,j,k} = \frac{1}{c_0} \left(\frac{\mathbf{p}_k - \mathbf{p}_i}{\|\mathbf{p}_k - \mathbf{p}_i\|_2} - \frac{\mathbf{p}_k - \mathbf{p}_j}{\|\mathbf{p}_k - \mathbf{p}_j\|_2} \right), \quad (3.41)$$

describes the change in each TDOA measurement for a change in each dimension of the location \mathbf{p}_k . The DOP is then defined as

$$\text{DOP}^j = \sqrt{\text{tr}((\mathbf{H}^{j\top} \mathbf{H}^j)^{-1})}. \quad (3.42)$$

This value exclusively describes the effect of the precision loss due to the geometry. However, for a more comprehensive understanding of the system limitations the loss of the propagation channel and the resulting SNR as well as the limitations due to the limited signal bandwidth have to be taken into account. This leads to performance bounds such as the CRLB [55], which for TDOA systems is examined in [109, 133]. For low SNR the CRLB becomes loose. This is due to the behavior of the cross-correlation estimator. At high SNR the estimates will always be close to the main lobe. Whereas, for low SNR the main lobe will become so low that the estimate will become completely random, dominated by noise and secondary lobes, eventually the error will just be limited by the size of the search space. To describe this behavior the Ziv-Zakai and the Weiss-Weinstein [134, 135, 136] bounds can be used, which are much tighter and consistent with the real system behavior at low SNRs. Though, at high SNR the bounds

are identical. Most of the time the CRLB analysis provides sufficient insight, as often, due to the large performance degradation, it makes little sense to operate the system under conditions where the Ziv-Zakai bound becomes relevant.

The CRLB for time delay estimation has been studied in [137, 138, 139, 140]. As the bound depends on the power spectral density of the transmitted signal it always has to be evaluated individually for each individual localization system. In general the CRLB for the estimation of a signal parameter θ is given as

$$\text{var}(\hat{\theta}) \geq \frac{1}{-E \left\{ \frac{\partial^2 \ln p(\mathbf{x}; \theta)}{\partial \theta^2} \right\}}. \quad (3.43)$$

One basic approach to derive the bound for time delay estimation is given in [55]. This assumes the known transmitted waveform $s(t)$ received disturbed by additive Gaussian noise $w_i(t)$ at a single receiver with delay t_i

$$y_i(t) = x(t - t_i) + w_i(t). \quad (3.44)$$

For a signal parameter θ of the sampled signal $x[n]$ disturbed by additive Gaussian noise with variance σ_w^2 it can then be shown from (3.43) that the CRLB on the estimate of θ is given as

$$\text{var}(\hat{\theta}) \geq \frac{\sigma_w^2}{\sum_{n=0}^{N-1} \left(\frac{\partial x(n; \theta)}{\partial \theta} \right)^2}. \quad (3.45)$$

Then the bound of the variance of the TOA estimate \hat{t}_i results in [55, p. 53-56]

$$\text{var}(\hat{t}_i) \geq \frac{1}{\frac{E}{N_0/2} \bar{F}^2}, \quad (3.46)$$

with the signal energy E and noise power spectral density $N_0/2$. Further, \bar{F}^2 , called the mean square bandwidth of the signal, is

$$\bar{F}^2 = \frac{\int_{-\infty}^{\infty} (2\pi f)^2 |X(f)|^2 df}{\int_{-\infty}^{\infty} |X(f)|^2 df}, \quad (3.47)$$

where $X(f)$ is the Fourier transform of the transmitted signal $x(t)$. Looking at the term $(2\pi f)^2$ in 3.47 it becomes obvious that high frequency components of the signal play a more important role in localization than lower frequency components. This relationship becomes very relevant in some newer modulation schemes such as the binary offset carrier (BOC) modulation used in Galileo, which is also known as split-spectrum modulation as it possesses a spectrum divided into to parts with very low spectral

density around the carrier frequency. Assuming for a moment a flat signal spectrum with a constant power spectral density and the bandwidth $2W$, the CRLB becomes [138]

$$\text{var}(\hat{t}_i) \geq \frac{3}{8\pi^2} \cdot \frac{1}{\text{SNR}} \cdot \frac{1}{TW^3}. \quad (3.48)$$

The variance improves with the observation time T , which is proportional to the amount of samples taken, the SNR, which is defined as $\frac{E/T}{N_0W}$ and the bandwidth $2W$ of the signal.

If the signal waveform is unknown to the receiver and a cross-correlation based method of TDOA estimation shall be used, the CRLB is slightly different. Assuming TDOA estimation between two signals

$$y_1(t) = s(t - t_1) + w_1(t), \quad (3.49)$$

$$y_2(t) = s(t - t_2) + w_2(t), \quad (3.50)$$

one approach or deriving it is to express one of the two involved signals as a shifted and noisy version of the other one

$$y'_2(t) = y_1(t - t'_2) + w'_2(t), \quad (3.51)$$

where the variance of the noise $w'_2(t)$ becomes $\sigma_1^2 + \sigma_2^2$. The time shift t'_2 is equivalent to the TDOA. Then estimate t'_2 , treating $y_1(t)$ as deterministic and fully known and use (3.45) to derive the bound in the same way as before. After the same manipulations this leads to

$$\text{var}(\hat{t}'_2) \geq \frac{3}{4\pi^2} \cdot \frac{1}{\text{SNR}} \cdot \frac{1}{TW^3}, \quad (3.52)$$

Due to the two involved noise processes, the variance for the TDOA estimate is higher than that of the TOA estimate. However, calculating TDOAs from the estimated TOAs ultimately yields the same variance at the input of the localization algorithm.

Knowing the bound on the time delay estimation one may now wonder about the resulting bound on the localization. Analog to the DOP, the CRLB for TDOA localization is given as [109]

$$\mathbf{C}_p = (\mathbf{H}^{j\top} \mathbf{C}_\tau^{-1} \mathbf{H}^j)^{-1} \quad (3.53)$$

where $\mathbf{I}(\boldsymbol{\tau}) = \mathbf{H}^{j\top} \mathbf{C}_\tau^{-1} \mathbf{H}^j$ is called the Fisher information matrix. Equivalently one can say that the variance of the position estimate $\hat{\mathbf{p}}$ satisfies

$$\text{var}([\hat{\mathbf{p}}]_i) \geq [\mathbf{I}^{-1}(\boldsymbol{\tau})]_{ii}. \quad (3.54)$$

This accounts for the noisy TDOA measurements which are modeled with the covariance matrix \mathbf{C}_τ . However, perfect clock synchronization between the sensors is assumed. The case of imperfect synchronization and drifting clocks is tackled in Section 3.8. The covariance itself depends on the signal bandwidth and the receive SNR of each sensor.

$$\mathbf{C}_\tau = \begin{pmatrix} \sigma_1 + \sigma_2 & \dots & \sigma_1 \\ \vdots & \ddots & \vdots \\ \sigma_1 & \dots & \sigma_1 + \sigma_N \end{pmatrix}. \quad (3.55)$$

In practice this means that an SNR estimate for each sensor is necessary in order to achieve optimum system performance. In systems that perform TOA estimation based on known sequences this is relatively straightforward. However, in cross-correlation based TDOA systems accurate SNR estimation is difficult. Therefore, if no SNRs are available, a common assumption is $\sigma_i = \sigma_\tau$, i.e, equal sensor signal to noise ratio (SNR), and hence

$$\mathbf{C}_\tau = \sigma_\tau^2 \begin{pmatrix} 1 & \dots & 0.5 \\ \vdots & \ddots & \vdots \\ 0.5 & \dots & 1 \end{pmatrix}. \quad (3.56)$$

A suitable value for σ_τ has then to be determined empirically.

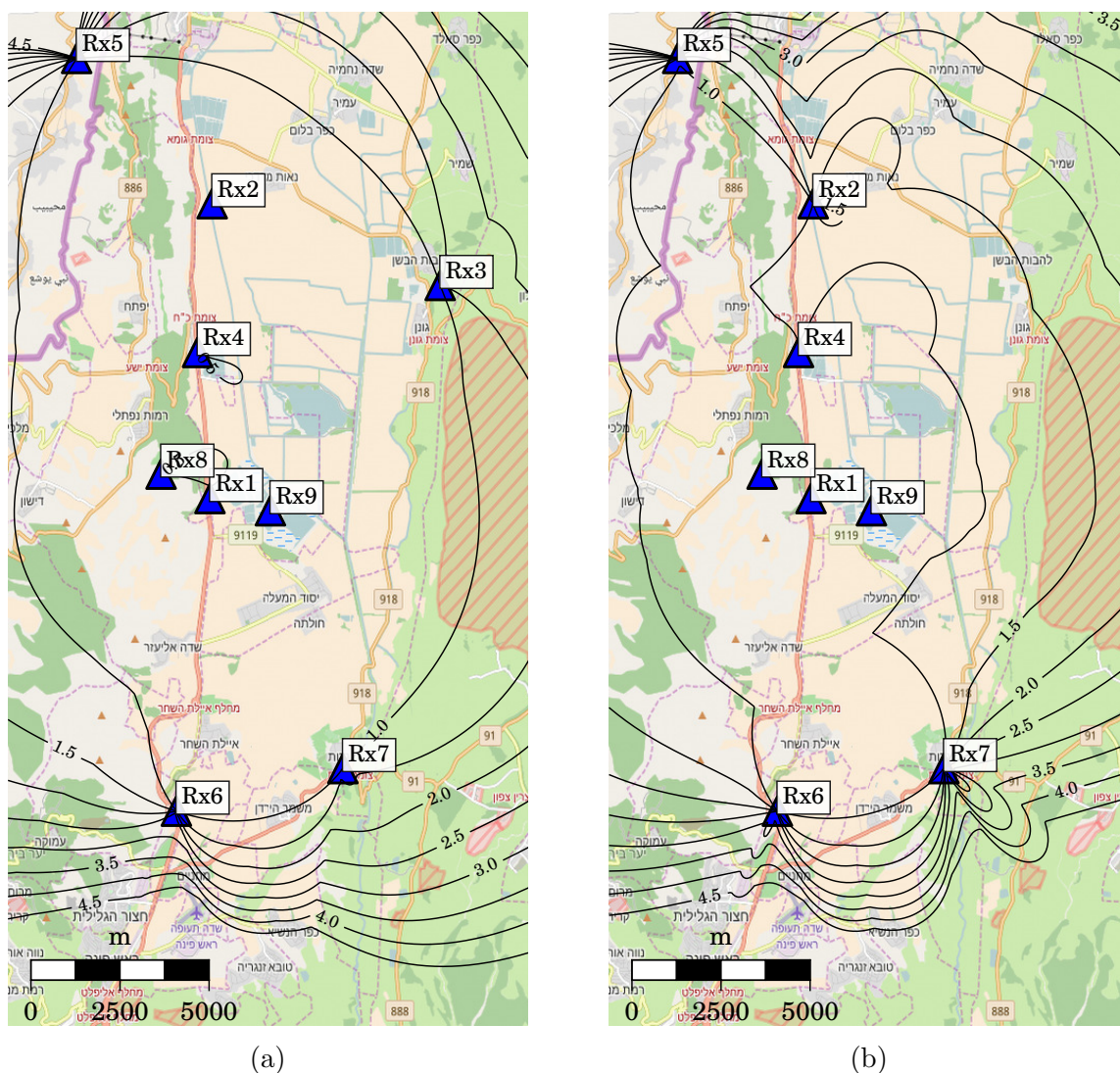


Figure 3.9: DOP of the ATLAS system with all sensors (a) and without sensor 3 (b).

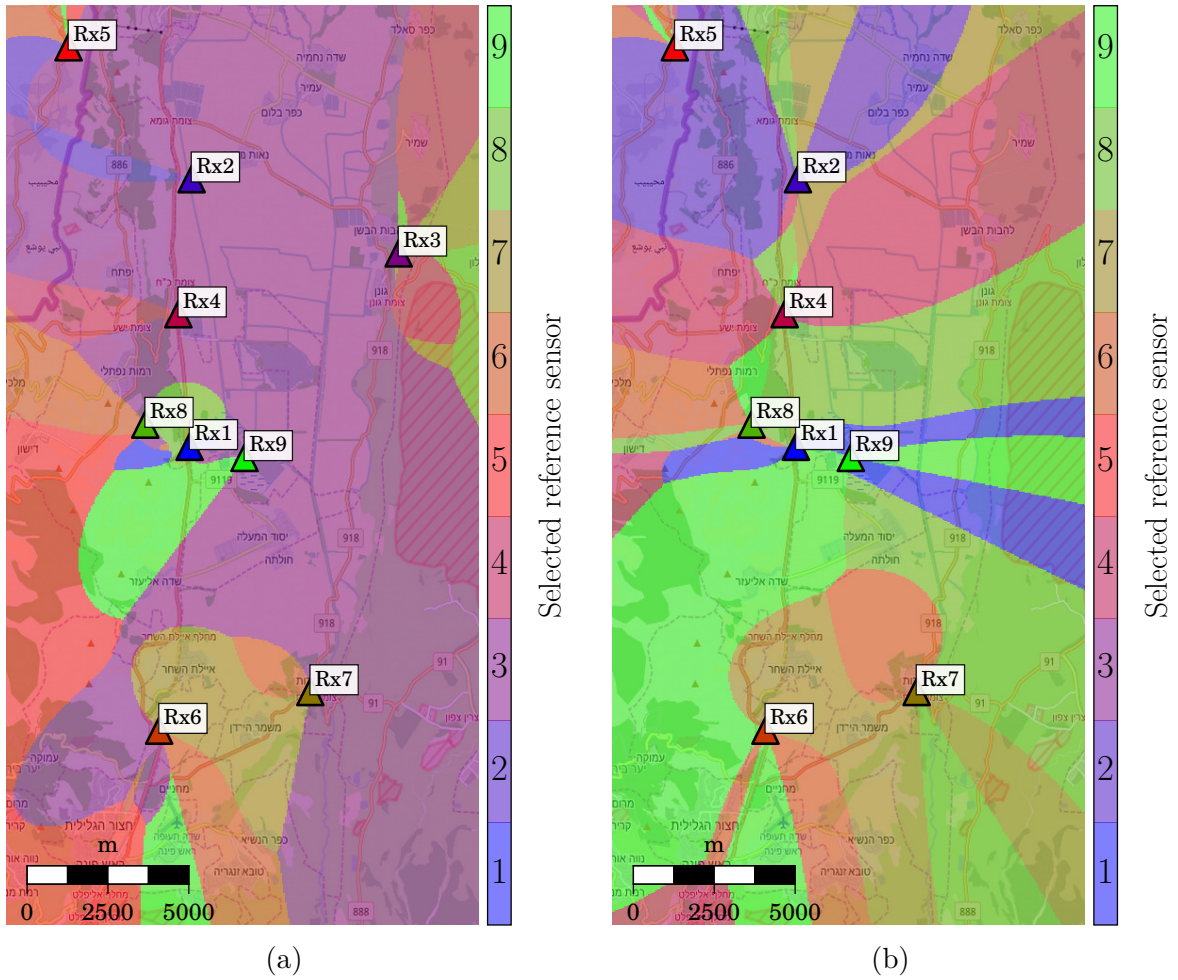


Figure 3.10: Optimum reference receiver selection based on minimization of the DOP in ATLAS with all sensors (a) and without sensor 3 (b).

Reference receiver selection

A way of improving the localization performance is to select the reference receiver for the localization algorithm based on the current location of the target. For high SNR this can be formulated as an optimization problem where the goal is to select the reference j from the set of M receivers such that

$$j = \arg \min_{r \in \{1, \dots, M\}} \text{DOP}^r. \quad (3.57)$$

An example for the reference receiver selection in a 3 sensor network is depicted in Figure 6.11(b).

Sensor Network and Coverage Planning

The DOP analysis can be used for coverage planning during installation and upgrading of the network. As an example the analysis of the deployed configuration of the ATLAS system [24] is presented in this section. Optimum sensor placement has been discussed in [141, 142, 143]. When fully functional, the ATLAS system consists of about 10 sensors distributed in an area of approximately 10 km by 20 km. In such a large-scale scenario sensor placement is subject to some hard constraints imposed by the availability of suitable sites. Similar as in cellular systems, to improve the reception, sensors need to be placed on towers of high buildings. For the case of ATLAS most sensors are colocated with cellular antennas. Figure 3.9 (a) shows the DOP for the full sensor configuration. Obviously this assumes that all sensors have received the signal with a sufficient SNR. In Figure 3.9 (b) receiver 3 is not available and the DOP is clearly deteriorated in some areas. Further, Figure 3.10 shows the selected reference receiver for both cases based on Equation 3.57. It implies that some knowledge about the last location of the target is available, which can be obtained through tracking.

3.7 Kalman Filter Based Tracking

For further improvement of the localization Kalman filter (KF) based tracking [144] is applied to the output of the localization algorithm. The KF updates the state $\boldsymbol{\pi}_\kappa$ for time instance κ based on a motion model contained in matrix $\boldsymbol{\Phi}$ and the measurement matrix \boldsymbol{M}

$$\boldsymbol{\pi}_\kappa = \begin{pmatrix} p_{k1}^{(\kappa)} \\ p_{k2}^{(\kappa)} \\ v_{k1}^{(\kappa)} \\ v_{k2}^{(\kappa)} \\ U_{k1}^{(\kappa)} \\ U_{k2}^{(\kappa)} \end{pmatrix} \quad \boldsymbol{\Phi} = \begin{pmatrix} 1 & 0 & \Delta t & 0 & 0 & 0 \\ 0 & 1 & 0 & \Delta t & 0 & 0 \\ 0 & 0 & 1 & 0 & 1 & 0 \\ 0 & 0 & 0 & 1 & 0 & 1 \\ 0 & 0 & 0 & 0 & \rho & 0 \\ 0 & 0 & 0 & 0 & 0 & \rho \end{pmatrix}$$

$$\boldsymbol{M} = \begin{pmatrix} 1 & 0 & 0 & 0 & 0 & 0 \\ 0 & 1 & 0 & 0 & 0 & 0 \end{pmatrix} \quad \boldsymbol{Q} = \begin{bmatrix} \mathbf{0}_{4 \times 4} & \mathbf{0}_{4 \times 2} \\ \mathbf{0}_{2 \times 4} & \sigma_a^2 \Delta t^2 \mathbf{I}_2 \end{bmatrix}.$$

acceleration is modeled as a random variable. Hence \boldsymbol{Q} is a covariance matrix where σ_a^2 is the covariance of the acceleration, ρ is a correlation coefficient of the acceleration and Δt the (usually fixed) time between observations. The KF algorithm consists of a recursive two-step procedure. First, the prediction step generates a-priori estimates

$$\boldsymbol{\pi}_{\kappa|\kappa-1} = \boldsymbol{\Phi} \boldsymbol{\pi}_{\kappa-1|\kappa-1} \quad (3.58)$$

$$\boldsymbol{P}_{\kappa|\kappa-1} = \boldsymbol{\Phi} \boldsymbol{P}_{\kappa-1|\kappa-1} \boldsymbol{\Phi}^\top + \boldsymbol{Q}. \quad (3.59)$$

Then the update step calculates the a-posteriori estimates by merging the a-priori estimates with the new observation of the target location $\mathbf{p}_k^{(\kappa)}$

$$\boldsymbol{\pi}_{\kappa|\kappa} = \boldsymbol{\pi}_{\kappa|\kappa-1} + \mathbf{K}_{\kappa}[\mathbf{p}_{\kappa} - \mathbf{M}\boldsymbol{\pi}_{\kappa|\kappa-1}] \quad (3.60)$$

$$\mathbf{P}_{\kappa|\kappa} = [\mathbf{I} - \mathbf{K}_{\kappa}\mathbf{M}]\mathbf{P}_{\kappa|\kappa-1} \quad (3.61)$$

$$\mathbf{K}_{\kappa} = \mathbf{P}_{\kappa|\kappa-1}\mathbf{M}^{\top}[\mathbf{M}\mathbf{P}_{\kappa|\kappa-1}\mathbf{M}^{\top} + \mathbf{R}_{\kappa}]^{-1}. \quad (3.62)$$

The covariance matrix \mathbf{R}_{κ} of the location estimate depends on the geometry of the sensor network. As explained before, the concept of geometric dilution of precision (DOP) is needed to capture this effect. Hence \mathbf{R}_{κ} can be determined in each update step using (3.53).

As shown in Section 3.2, TDOA algorithms with only three receivers exhibit an ambiguity problem in certain regions close to and behind the receivers. One way of resolve this ambiguity is to select the solution \mathbf{p}_k^l that lies closer to the KF prediction:

$$l = \arg \min_{n \in \{1,2\}} \left\| \mathbf{p}_k^n - \mathbf{M}\boldsymbol{\pi}_{\kappa|\kappa-1} \right\|_2. \quad (3.63)$$

This improves the performance in the vicinity of the receivers. However, as can be seen in Figure 6.11(a), locations exactly behind a receiver additionally suffer from a very high DOP, therefore the prediction works only well for high SNR and very good system synchronization.

3.8 Cramér-Rao Bound and Synchronization in Systems with Calibration Emitter

For the analysis until this point the synchronization between the receiving sensors of the localization network has been assumed perfect. In practice this is barely the case. If a common clock system is used where all the sensors are connected with cables or fibre optics, close to perfect synchronization can be achieved. To avoid the need of such a complex infrastructure many systems use wireless synchronization methods. This can be synchronization based on GPS signals or using a special scheme of messages exchanged between the sensors. Sometimes, if the sensors can not transmit or are too far from each other to communicate, additional calibration emitters at a known location, preferably in the middle of the network or with high transmit power are used as a synchronization aid. In any case synchronization can only be achieved down to a particular accuracy. The properties of some practical synchronization approaches based on GPS are discussed in Section 6.3. Current section studies the special case of a passive localization network with known stationary sensor locations, known stationary beacon locations which are not co-located with the sensors and a moving target that emits signals at different times compared to the beacon.

Time measurement based localization systems either rely on very accurate synchronization between the anchor points, or, in asynchronous systems, require accurate estimation of the clock offsets to achieve optimum performance. Network infrastructure assisted passive localization has been in the center of various research activities for several decades. In comparison, results on the operation of such systems with asynchronous, drifting clocks and wireless synchronization are rather young. The most common approach to localization is divided in two stages, where first a physical signal parameter is estimated, in our case the TOA, and second the target location is obtained using a second algorithm that takes the measurements, TOAs or the resulting time differences of arrival (TDOAs) as an input, see e.g., [112, 117, 109, 118]. Due to hardware imperfections and physical constraints, impairments of the first stage are not uncommon in practice. The requirement of nanosecond accuracy for decimeter level localization is challenging even for the most accurate clocks. For optimum localization performance, it is therefore necessary to apply correction methods to cope with the effects of asynchronous clocks. Accordingly, in [145] the idea of differential time difference of arrival (DTDOA) has been introduced in order to eliminate clock offsets. Further, in [146] the use of a calibration emitter, also known as beacon, has been proposed. However, the authors focus on inaccurate knowledge of sensor locations rather than asynchronous clocks. Later, [147] proposed a protocol for passive localization with asynchronous clocks where one of the anchors actively transmits a reference signal. The problem has also been investigated in a downlink fashion [148], where the transmitting anchors' clocks are assumed to be perfect, but the receiving target possesses a drifting clock. An extension of this scenario to cooperative localization is given in [149]. Most of the publications in this area apply the CRLB to derive theoretical performance limits. As described in [149], for problems with many interlinked parameters that all need to be estimated, the modified Cramér-Rao lower bound (MCRLB) is often more practical and provides more insight into the problem. It has been introduced in [150] and further thoroughly examined in [151] and [152]. In the present section, the methodology of the modified bound is followed, as it constitutes a feasible way of deriving theoretical performance limits.

In contrast to the previous works, a different system model is considered, where the investigated system consists of distributed passive sensors, i.e., they can only receive, and additional beacons, that can only transmit. The beacons are not colocated with the sensors, sensor and beacon locations are known and the sensor clocks are running asynchronously and experience drift over time. Recently, in [153] a similar system has been considered. However, this paper does not present any theoretical bounds and assumes a very precisely timed beacon signal, where the exact time difference between two beacon transmissions is known, which we do not have in our case. Another implementation of such a system for wildlife tracking has been described in [24]. Previously, the sensors have been synchronized with GPS and therefore the clock drift has been neglected in practice, while for the present section we consider the same system running with asynchronous, drifting clocks. For numerical evaluation we then obtain recorded TOAs from the fusion center of the system under this deteriorated conditions. Due to

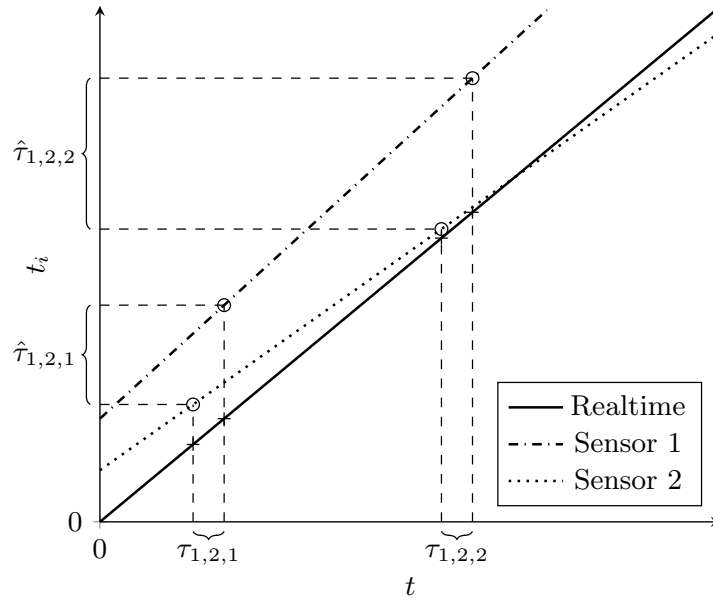


Figure 3.11: Visualization of the linear model for the receiver clocks and the resulting error in TDOA measurements if the effect is not compensated.

stringent constraints in battery size of the target and beacons, the rate of transmissions in the system is strictly limited. Further, target and beacon transmissions are not synchronized and therefore the time difference between the received messages can lead to large differences in the local clocks, during one set of measurements. Hence, we derive the necessary clock correction algorithms and evaluate their performance using simulations and a comparison with the MCRLB. For validation, we then apply the correction algorithms to the recorded TOAs.

3.8.1 System and Clock Model

Similar as before a system of M distributed receiving sensors that are localizing a moving transmitter is considered. The system is assumed to be passive and has no communication between the sensors and the transmitting target. Additionally, two transmitting beacons at known locations are available for synchronization. We assume that each sensor i is independently able to estimate the TOA $t_{i,k}$ of the received signal from either the target $k = 0$ or the two beacons $k \in \{1, 2\}$, based on a pilot sequence. The location can then be determined using the TDOAs $\tau_{i,j,k} = t_{i,k} - t_{j,k}$ between receiver i and the reference receiver j . Note that this is slightly different compared to the case of cross-correlation-based TDOA estimation. In the following we apply [109] to find the solution and exclusively focus on the problem of correctly determining the TOAs and resulting TDOAs respectively. For that, the time offset caused by the drifting clocks at receiver i is modeled as [154]

$$t_i = \epsilon_i t + \phi_i, \quad (3.64)$$

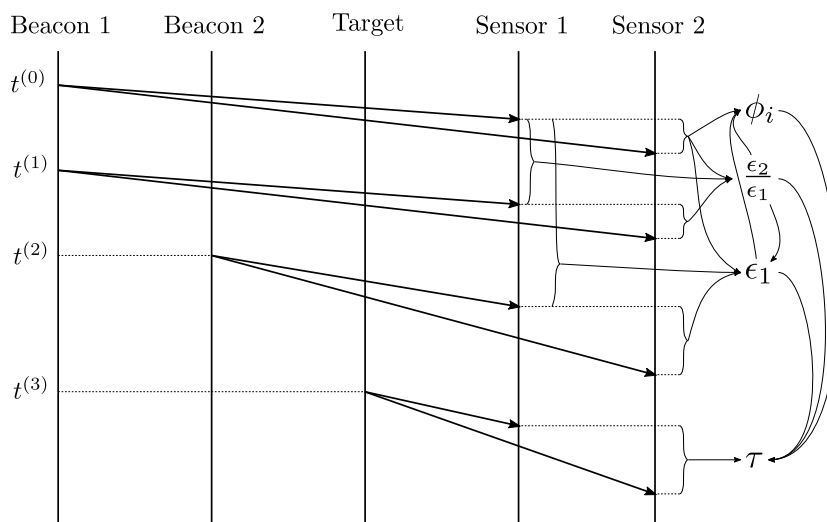


Figure 3.12: Transmission sequence of a beacon augmented passive TDOA localization system using TOA measurements. Different combinations of measurements can be used to estimate the clock parameters and subsequently localize the target.

where t is the real time, ϕ_i a constant initial offset at time instance $t^{(0)} = 0$ and ϵ_i the drift rate, which is assumed to be constant over the course of a measurement period and Gaussian distributed with respect to different clocks. The mean of ϵ_i is 1 and its standard deviation σ_{ϵ_i} depends on the specific clock type, it can reach as low as 10^{-12} for GPS disciplined oscillators (GPSDOs) and up to 10^{-5} for a temperature compensated crystal oscillator (TCXO). This especially means that in a system with several sensors, their clocks will often drift in different directions with respect to real time. Hence, assuming that target and beacon transmissions occur at a relatively low rate, e.g., 1 Hz, considerable relative errors between sensor clocks might be introduced. An example for drifting clocks and the growing error of TDOAs is depicted in Figure 3.11. The drifting clocks can also lead to an association problem of the received transmissions at the different sensors. We assume that a mechanism exist to resolve this problem, such as unique message identifiers embedded in the signal. Another physical layer approach is to perform a plausibility check by comparing known and estimated beacon locations.

In order to perform clock synchronization between two sensors, two beacons at different locations are needed. However, a single beacon is sufficient to achieve a reasonable approximate solution as described later. Figure 3.12 shows the transmission sequence of the involved signal bursts at time instances $t^{(q)}$. Note that it is important that all the beacon and target signals are detected by all involved sensors. If that is not the case, as depicted in Figure 3.13, clock correction can not be performed and localization is not possible. However, in practice with a large number of sensors, the probability of receiving all signals at all sensors can be low. In that case older beacon transmissions could be used as long as they are detected both by the reference sensor and at least one other sensor. It is preferable not to use very old detections as in general the clock rates

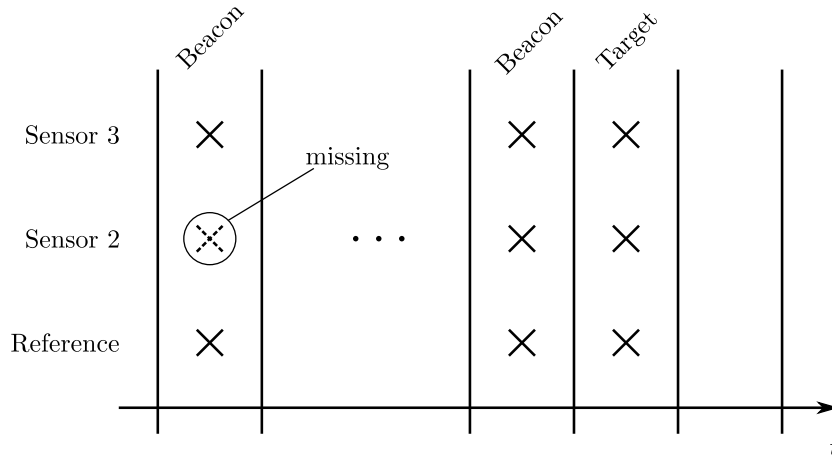


Figure 3.13: For beacon based clock correction it is important that the same transmitted signal bursts are received at the reference sensor and at least one other sensor. If the signals are partially missing, the target can not be localized. As a replacement older beacon transmissions can be used but this leads to performance degradation.

ϵ_i are time dependent and the model from (3.64) could be violated.

A transmitted signal from beacon or target k at time index q receives the sensor i at the TOA

$$t_{i,k}^{(q)} = \epsilon_i \left(t^{(q)} + \frac{d_{i,k}}{c} \right) + \phi_i + n_i^{(q)}, \quad (3.65)$$

where $n_i^{(q)}$ is a realization of zero-mean Gaussian noise with variance $\sigma_{n_i}^2$ and $d_{i,k}$ is the distance

$$d_{i,k} = \|\mathbf{p}_k - \mathbf{r}_i\|_2, \quad (3.66)$$

between the beacon or target k and the sensor i with the two dimensional coordinate vector \mathbf{p}_k . The TDOA is then given as the difference

$$\begin{aligned} \tau_{i,j,k} &= t_{i,k}^{(q)} - t_{j,k}^{(q)} \\ &= (\epsilon_i - \epsilon_j)t^{(q)} + \epsilon_i \frac{d_{i,k}}{c} - \epsilon_j \frac{d_{j,k}}{c} \\ &\quad + \phi_i - \phi_j + n_i^{(q)} - n_j^{(q)}. \end{aligned} \quad (3.67)$$

Localization algorithms eventually require the distance differences

$$\delta_{i,j,k} = d_{i,k} - d_{j,k}, \quad (3.68)$$

in order to geometrically determine the target coordinates. Hence, correction of the parameters ϵ_i and ϕ_i is necessary. A possible way to remove parameters that are constant between two TDOA measurements is the differential time difference of arrival (DTDOA)

$$\Delta\tau_{i,j,k,l}^{(q,r)} = \tau_{i,j,k}^{(q)} - \tau_{i,j,l}^{(r)}. \quad (3.69)$$

Different types of DTDOA measurements are possible. A DTDOA between receptions of the same transmitter, e.g., the same beacon, at different time instance yields

$$\Delta\tau_{i,j,k,k}^{(q,r)} = (\epsilon_i - \epsilon_j)(t^{(q)} - t^{(r)}) + n_i^{(q)} - n_j^{(q)} - n_i^{(r)} + n_j^{(r)}. \quad (3.70)$$

Clearly, the constant term $\phi_i - \phi_j$ is cancelled out. Another type of DTDOA is between different transmitters k and l , i.e., two different beacons or one beacon and the target, at different time instances

$$\begin{aligned} \Delta\tau_{i,j,k,l}^{(q,r)} = & (\epsilon_i - \epsilon_j)(t^{(q)} - t^{(r)}) \\ & + \epsilon_i \left(\frac{d_{i,k}}{c} - \frac{d_{i,l}}{c} \right) - \epsilon_j \left(\frac{d_{j,k}}{c} - \frac{d_{j,l}}{c} \right) \\ & + n_i^{(q)} - n_j^{(q)} - n_i^{(r)} + n_j^{(r)}, \end{aligned} \quad (3.71)$$

again this eliminates the offset $\phi_i - \phi_j$. However, the simple formation of DTDOAs is not able to remove ϵ_i and hence, for larger time spans between beacon and target transmissions, ignoring these erroneous clock rates leads to a drastic degradation of the system accuracy.

3.8.2 Clock Error Correction

Next, four different estimators are defined that are useful in different situations, which depend on the amount of noise, the quality of the clocks and the time span between transmissions.

TDOA estimation without correction

Assuming that the clocks are of very high accuracy and synchronization is close to perfect, i.e, $\epsilon_i = 1$ and $\phi_i = 0$, simple TDOA estimation without further clock synchronization may be used based on (3.67).

TDOA estimation with offset correction

If very accurate clocks ($\epsilon_i = 1$) are available, that are not absolutely synchronized, i.e., $\phi_i \neq 0$, a DTDOA with a single beacon may be used based on (3.71). Equivalently, the difference $\phi_i - \phi_j$ can also be estimated explicitly using a single TDOA (3.67) from a beacon if the clock rates ϵ_i are known

$$\Delta\hat{\phi}_{1,j} = \tau_{1,j,k} - \frac{1}{c}\delta_{1,j,k}, \quad (3.72)$$

where without loss of generality, one may set the time of transmission $t^{(0)} = 0$. The distance differences needed by the localization algorithm are then

$$\hat{\delta}_{1,j,l} = c \cdot (\tau_{1,j,l} - \tau_{1,j,k} + \delta_{1,j,k}). \quad (3.73)$$

TDOA estimation with approximate offset and rate correction

When lower quality, unsynchronized clocks are used, i.e. $\epsilon_i \neq 1, \phi_i \neq 0$ it becomes necessary to correct for both parameters. This can be approximately achieved using a single beacon, however, two transmissions from that beacon are now required. The estimation of ϕ_i depends on ϵ_i , hence we begin with the estimation ϵ_i then subsequently estimate ϕ_i and correct the initially measured TOAs.

Let $i = 1$ be the reference sensor. The time $t^{(0)} - t^{(1)}$ between two beacon transmissions of a single beacon k can be estimated using a single sensor's clock. Compared to the true time difference between transmission this time difference is scaled

$$t^{(0)} - t^{(1)} = \frac{1}{\epsilon_1} (t_{1,k}^{(0)} - t_{1,k}^{(1)} - n_1^{(0)} + n_1^{(1)}). \quad (3.74)$$

Considering this scaling, the DTDOA for the same beacon can be written as

$$\Delta\tau_{1,j,k,k}^{(0,1)} = \left(1 - \frac{\epsilon_j}{\epsilon_1}\right) (t_{1,k}^{(0)} - t_{1,k}^{(1)}) + \frac{\epsilon_j}{\epsilon_1} (n_1^{(0)} - n_1^{(1)}) - n_j^{(0)} + n_j^{(1)}. \quad (3.75)$$

From this, obviously not all clock rates can be estimated but it is possible to estimate them relative to the reference sensor, as $\beta_j = \frac{\epsilon_j}{\epsilon_1}$. The estimator of β_j can be written as

$$\hat{\beta}_j = \frac{-\Delta\tau_{1,j,k,k}^{(0,1)} + (t_{1,k}^{(0)} - t_{1,k}^{(1)})}{(t_{1,k}^{(0)} - t_{1,k}^{(1)})}, \quad j \in 2, \dots, M. \quad (3.76)$$

Further, $\hat{\epsilon}_1 = 1$ is a reasonable choice based on the mean value of the distribution. Therefore, the estimate of clock rates will become $\hat{\epsilon}_j = \hat{\beta}_j$. Using those estimated values for the rates, next the absolute clock offsets of all sensors is estimated

$$\hat{\phi}_j = t_{j,k}^{(0)} - \hat{\epsilon}_j \frac{d_{j,k}}{c}, \quad j \in 1, \dots, M. \quad (3.77)$$

With all of this the TOAs and the respective distance differences of the target can be corrected as

$$\hat{\delta}_{1,j,l} = c \cdot \left(\frac{t_{1,l}^{(3)} - \hat{\phi}_1}{\hat{\epsilon}_1} - \frac{t_{j,l}^{(3)} - \hat{\phi}_j}{\hat{\epsilon}_j} \right), \quad (3.78)$$

and then used by the localization algorithm to determine the location \mathbf{p}_0 . Neglecting estimation error, the clock correction essentially enforces equal clock rates in all sensors, which are identical to the true value of ϵ_1 . A look at (3.67) reveals that this approach is reasonable as the term $(\epsilon_i - \epsilon_j)t^{(q)}$ becomes zero and the scaling in the term $\epsilon_i \frac{d_{i,k}}{c} - \epsilon_j \frac{d_{j,k}}{c}$ is less critical due to the errors in the rates being relatively small.

TDOA estimation with offset and rate correction

Finally, if the system dimensions become very large, e.g., satellite based systems, or the speed of the wave is low, e.g., ultrasound based systems, the error in the approximation of ϵ_1 can no longer be neglected any more. Fortunately, using a second beacon at a different location, an estimate for ϵ_1 can be obtained. Considering the time difference of two transmission from the two different beacons k and k'

$$t^{(0)} - t^{(2)} = \frac{1}{\epsilon_1}(t_{1,k}^{(0)} - t_{1,k'}^{(2)}) - \left(\frac{d_{1,k}}{c} - \frac{d_{1,k'}}{c} \right) - \frac{1}{\epsilon_1}(n_1^{(0)} - n_1^{(2)}), \quad (3.79)$$

this further results in

$$\begin{aligned} \Delta\tau_{1,j,k,k'}^{(0,2)} &= (1 - \beta_j)(t_{1,k}^{(0)} - t_{1,k'}^{(2)}) \\ &\quad + \epsilon_1\beta_j\left(\frac{d_{1,k}}{c} - \frac{d_{1,k'}}{c}\right) - \epsilon_1\beta_j\left(\frac{d_{j,k}}{c} - \frac{d_{j,k'}}{c}\right) \\ &\quad + \beta_j(n_1^{(0)} - n_1^{(2)}) - n_j^{(0)} + n_j^{(2)}, \end{aligned} \quad (3.80)$$

and leads to an estimator for ϵ_1

$$\hat{\epsilon}_1 = c \cdot \frac{\Delta\tau_{1,j,k,k'}^{(0,2)} - (1 - \hat{\beta}_j)(t_{1,k}^{(0)} - t_{1,k'}^{(2)})}{\hat{\beta}_j(\delta_{1,j,k} - \delta_{1,j,k'})}. \quad (3.81)$$

where $\hat{\beta}_j$ is estimated using (3.76). Analogously to the last case, using (3.77) and (3.78), the necessary input values for the localization algorithm can be obtained.

3.8.3 Cramér-Rao Bound Analysis

Counting the noise terms for the four different methods above, as listed in Table 3.1, it becomes obvious that the TDOA estimation with offset and rate correction is sub-optimum for moderately large system sizes and clock rate errors. This is because the impact of the additional measurement noise is, for certain parameter settings, much larger than the gain of the knowledge of the ϵ_1 estimate. To analytically describe this

Correction Method	Noise terms for two sensors
No correction	2
Offset correction	4
Approximate offset and rate correction	6
Full offset and rate correction	8

Table 3.1: Number of additive noise terms for different TDOA clock correction methods

behavior, next the MCRLBs [155, 152] are derived for the different cases and compared with Monte Carlo simulation results.

For any unbiased estimator, a lower bound on the variance of the error is provided by the CRLB [55]. It is based on the inverse of the Fisher information matrix (FIM) which is in our case given as

$$[\mathbf{I}(\mathbf{u})]_{m,n} = -\mathbb{E} \left\{ \frac{\partial^2 \ln p(\boldsymbol{\tau}_k; \mathbf{u})}{\partial u_m \partial u_n} \right\}, \quad (3.82)$$

where $\boldsymbol{\tau}_k = [\tau_{1,2,k}, \dots, \tau_{1,M,k}]^T$ is the vector of TDOAs (3.67) of the target when sensor $i = 1$ is the reference sensor, and the vector \mathbf{u} of parameters to be estimated.

For the problem at hand \mathbf{u} consists of the target coordinates as well as the clock parameters. The relationship between these parameters makes an analytical derivation of the CRLB very challenging. An approach that provides a less tight bound but simplifies the computation is the MCRLB for vector parameter estimation [151]. To derive the MCRLB expression, the estimation parameters are split into \mathbf{u} , the vector of estimation parameters, and \mathbf{v} , the vector of unwanted parameters, which are defined differently for each case considered below. We assume \mathbf{u} to be deterministic but unknown, and \mathbf{v} to be random with known probability distribution function. Then, the conditional FIM $\mathbf{I}(\mathbf{v}; \mathbf{u})$ is calculated using the expectation operator as

$$[\mathbf{I}(\mathbf{u}; \mathbf{v})]_{m,n} = -\mathbb{E}_{\boldsymbol{\tau}_k|\mathbf{v}} \left\{ \frac{\partial^2 \ln p(\boldsymbol{\tau}_k|\mathbf{v}; \mathbf{u})}{\partial u_m \partial u_n} \right\}, \quad (3.83)$$

with the probability density function $p(\boldsymbol{\tau}_k|\mathbf{u}; \mathbf{v})$

$$p(\boldsymbol{\tau}_k|\mathbf{v}; \mathbf{u}) = \frac{1}{(2\pi)^{\frac{M-1}{2}} \det(\mathbf{C}^{-1})^{\frac{1}{2}}} \cdot \exp \left(-\frac{1}{2} (\boldsymbol{\tau}_k - \boldsymbol{\mu})^T \mathbf{C}^{-1} (\boldsymbol{\tau}_k - \boldsymbol{\mu}) \right), \quad (3.84)$$

The conditional FIM can be calculated as [55]

$$[\mathbf{I}(\mathbf{u}; \mathbf{v})]_{m,n} = \left[\frac{\partial \boldsymbol{\mu}}{\partial u_m} \right]^T \mathbf{C}^{-1} \left[\frac{\partial \boldsymbol{\mu}}{\partial u_n} \right] + \frac{1}{2} \text{tr} \left(\mathbf{C}^{-1} \frac{\partial \mathbf{C}}{\partial u_m} \mathbf{C}^{-1} \frac{\partial \mathbf{C}}{\partial u_n} \right). \quad (3.85)$$

According to [151], taking the expectation over \mathbf{v} , one can then obtain the modified Fisher information matrix (MFIM) $\mathbf{I}_{\text{mod}}(\mathbf{u})$ with

$$[\mathbf{I}_{\text{mod}}(\mathbf{u})]_{m,n} = \mathbb{E}_{\mathbf{v}} \{ [\mathbf{I}(\mathbf{u}; \mathbf{v})]_{m,n} \}. \quad (3.86)$$

This leads to the modified lower bound on the estimation variance

$$\text{var}(\hat{u}_n) \geq [\mathbf{I}_{\text{mod}}(\mathbf{u})^{-1}]_{n,n}. \quad (3.87)$$

Next, this can be used to determine the bounds for the localization with the different clock correction approaches.

TDOA estimation without correction

In this case there is only a single transmission from the target $k = 0$ available. We consider $\mathbf{u} = [x_0, y_0]^\top$ as estimation parameters and $\mathbf{v} = [\epsilon_1, \dots, \epsilon_M, \phi_1, \dots, \phi_M]^\top$ as the unwanted parameters. To calculate the lower bound on the estimation error, we directly use the MCRLB from (3.87) with the mean $\boldsymbol{\mu} = [\mu_2, \dots, \mu_M]^\top$ and the covariance matrix \mathbf{C} of $\boldsymbol{\tau}_k$

$$\mu_i = (\epsilon_1 - \epsilon_i)t^{(q)} + \epsilon_1 \frac{d_{1,k}}{c} - \epsilon_i \frac{d_{i,k}}{c} + \phi_1 - \phi_i, \quad (3.88)$$

$$\mathbf{C} = \text{diag}(\sigma_{n_2}^2, \dots, \sigma_{n_M}^2) + \sigma_{n_1}^2 \mathbf{1}_{M-1} \mathbf{1}_{M-1}^\top. \quad (3.89)$$

For the cases that beacon transmissions are available, this simple MCRLB is unacceptably loose and we resort to a two-step approach, where we first obtain bounds for the clock parameters and then, in the second step, derive the bound for the target location.

TDOA estimation with offset correction

In this case a single beacon $k = 1$ is available and the clock offsets ϕ_i can be estimated. Hence, the estimation parameter vector for the first step becomes $\mathbf{u} = [\phi_1, \dots, \phi_M]^\top$ and the vector of unwanted parameters $\mathbf{v} = [\epsilon_1, \dots, \epsilon_M]^\top$. Then, the MCRLB on the estimation of the clock offsets ϕ_i is calculated using the mean and covariance matrix from (3.88) and (3.89). In the second step, we have $\mathbf{u} = [x_0, y_0]^\top$, and $\mathbf{v} = [\epsilon_1, \dots, \epsilon_M]^\top$. We model the clock offsets as $\hat{\phi}_i = \phi_i + \omega_i$, where $\hat{\phi}_i$ is an estimate with the error ω_i modeled as a Gaussian random variable, $\omega_i \sim \mathcal{N}(0, \sigma_{\phi_i}^2)$, where $\sigma_{\phi_i}^2$ is given by the bound from the first step. The second step mean and the covariance matrix then become

$$\mu_i = (\epsilon_1 - \epsilon_i)t^{(q)} + \epsilon_1 \frac{d_{1,0}}{c} - \epsilon_i \frac{d_{i,0}}{c} + \hat{\phi}_i - \hat{\phi}_j, \quad (3.90)$$

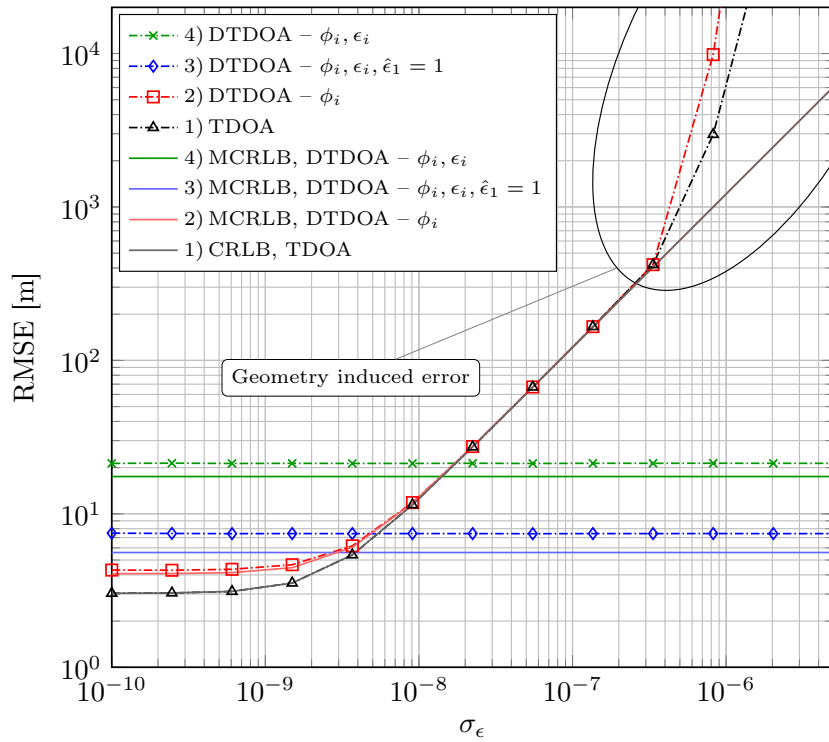
$$\mathbf{C} = \text{diag}(s_{1,\phi}^2, \dots, s_{M,\phi}^2) + s_{1,\phi}^2 \mathbf{1}_{M-1} \mathbf{1}_{M-1}^\top, \quad (3.91)$$

where $s_{i,\phi}^2 = \sigma_{n_i}^2 + \sigma_{\phi_i}^2$. This leads to the MCRLB of the target location.

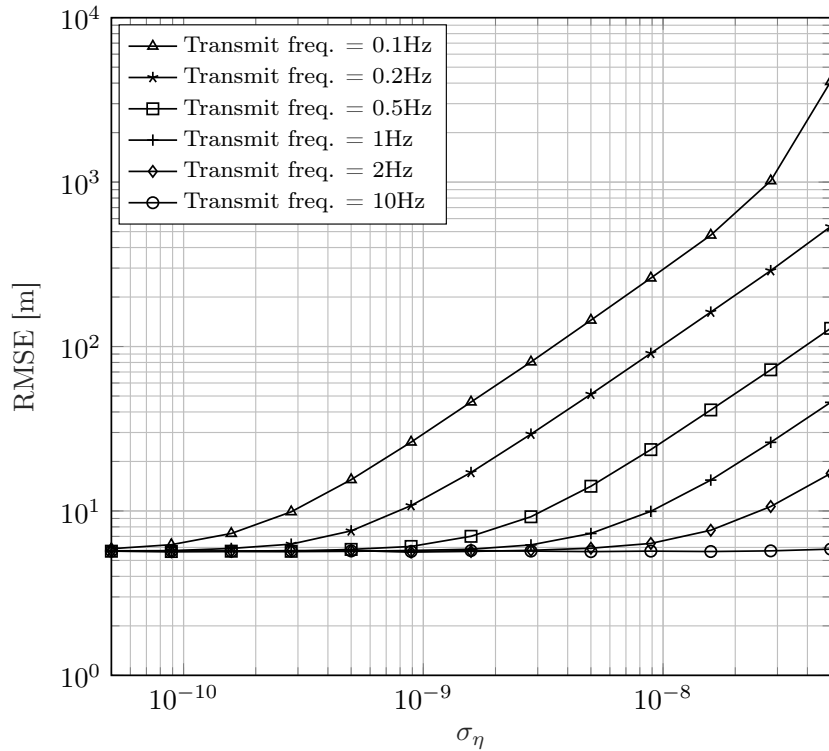
TDOA estimation with approximate offset and rate correction

When two transmissions of the beacon $k = 1$ are available, it is possible to estimate the clock offsets ϕ_i as well as the clock rates ϵ_i , except for one, e.g., ϵ_1 . Thus, similar to the last case, in the first step, we define the vectors as $\mathbf{u} = [\epsilon_2, \dots, \epsilon_M, \phi_1, \dots, \phi_M]^\top$ and $\mathbf{v} = [\epsilon_1]$.

In the second step, we model both the clock offset and rate as Gaussian random variables $\hat{\phi}_i = \phi_i + \omega_i$, $i = 1, \dots, M$ and $\hat{\epsilon}_i = \epsilon_i + \xi_i$, $i = 2, \dots, M$, where ω_i and ξ_i are the errors in the clock offset and rate estimation, modeled as Gaussian random variables



(a)



(b)

Figure 3.14: (a) The MCRLB compared with simulations for different availability of beacon messages with $\phi_i = 0$. 1) Baseline, no beacons used. 2) Single beacon message, estimation of ϕ_i . 3) Two messages from the same beacon, estimation of ϕ_i and ϵ_i while $\hat{\epsilon}_1 = 1$. 4) Three messages from two beacons, full estimation of ϕ_i and ϵ_i . (b) Impact of time dependent clock rate modeled as a random walk, using method 3).

$\omega_i \sim \mathcal{N}(0, \sigma_{\phi_i}^2)$ and $\xi_i \sim \mathcal{N}(0, \sigma_{\epsilon_i}^2)$. Variances $\sigma_{\phi_i}^2$ and $\sigma_{\epsilon_i}^2$ are derived using the first step MCRLB. To calculate the MCRLB on the estimation of the target position we incorporate the clock offset and clock rate models into (3.67). The second step mean and covariance matrix for this case are

$$\mu_i = (\epsilon_1 - \hat{\epsilon}_i)t^{(q)} + \epsilon_1 \frac{d_{1,0}}{c} - \hat{\epsilon}_i \frac{d_{i,0}}{c} + \hat{\phi}_i - \hat{\phi}_j, \quad (3.92)$$

$$\mathbf{C} = \text{diag}(s_{1,\epsilon}^2, \dots, s_{M,\epsilon}^2) + s_{1,\phi}^2 \mathbf{1}_{M-1} \mathbf{1}_{M-1}^T, \quad (3.93)$$

where $s_{i,\epsilon}^2 = \sigma_{\epsilon_i}^2 (t^{(q)} + \frac{d_{i,0}}{c})^2 + \sigma_{n_i}^2 + \sigma_{\phi_i}^2$ and $s_{1,\phi}$ is the same as in the last case. Similarly, the second step parameter vectors are $\mathbf{u} = [x_0, y_0]^T$ and $\mathbf{v} = [\epsilon_1]$.

TDOA estimation with offset and rate correction

Finally, with the aid of two beacons $k \in \{1, 2\}$, it is possible to estimate the clock rates of all the sensors. Hence, in this case there are no unwanted parameters, neither in the first nor in the second step. The first step estimation parameter vector is $\mathbf{v} = [\epsilon_1, \dots, \epsilon_M, \phi_1, \dots, \phi_M]^T$. We calculate the variance of the clock parameters estimation error using the standard CRLB. Analogous to the last case in the second step, we model all the clock rates and offsets with Gaussian random variables. Thus, the bound for the target location is derived with the estimation parameter vector $\mathbf{u} = [x_0, y_0]^T$, mean

$$\mu_i = (\hat{\epsilon}_1 - \hat{\epsilon}_i)t^{(q)} + \hat{\epsilon}_1 \frac{d_{1,0}}{c} - \hat{\epsilon}_i \frac{d_{i,0}}{c} + \hat{\phi}_i - \hat{\phi}_j, \quad (3.94)$$

and covariance matrix

$$\mathbf{C} = \text{diag}(s_{1,\epsilon}^2, \dots, s_{M,\epsilon}^2) + s_{1,\epsilon}^2 \mathbf{1}_{M-1} \mathbf{1}_{M-1}^T. \quad (3.95)$$

3.8.4 Results

Simulative as well as experimental results have been obtained for verification. In the simulation, 5 sensors have been placed using the same geometry as given in the experimental system, depicted in Figure 3.15 (a). First, receiver clocks have been modeled according to (3.64) and the time between transmissions is 2 s. The standard deviation of the error in each TOA measurement is $\sigma_{n_i} = 10^{-8}$. It is then possible to compare the analytical expressions for the bounds with Monte Carlo simulation result. This is shown in Figure 3.14 (a). From the plot it is found that if very good clocks are available it is recommendable to not apply any correction. That is due to the additional noise terms introduced into the solution due to additional measurements of the beacon signals. Note that this assumes that the offsets ϕ_i are close to zero. When the error in the TOA becomes large due to uncompensated differing clock rates, it leads to large outliers of the estimated location, caused by the nonlinear nature of the hyperbolic geometry.

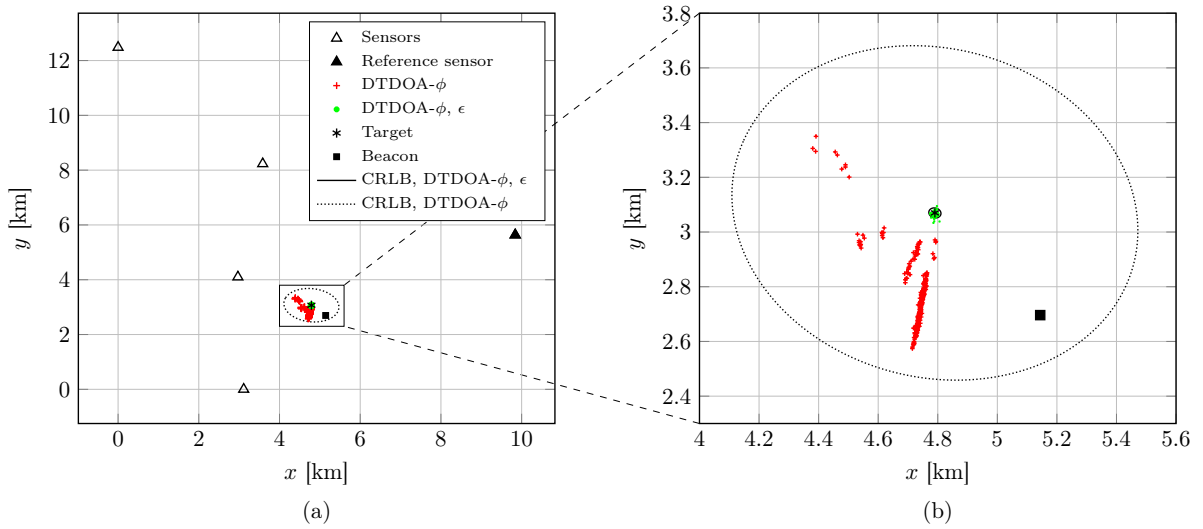


Figure 3.15: (a) Geometry of the considered localization sensor network [24], (b) drift in the location of a stationary target with correction of ϕ_i compared to the case with correction of ϕ_i and ϵ_i while $\hat{\epsilon}_1 = 1$.

This can be observed in the upper right corner of Figure 3.14 (a). Further, due to bad conditioning of the problem, as seen in (3.81), for the given system dimensions, full correction of all ϵ_i provides much worse performance than the approximation $\hat{\epsilon}_1 = 1$, which itself should be used only for clocks with $\sigma_\epsilon \geq 4 \times 10^{-9}$. However, this threshold obviously depends on the time between the beacon transmissions and also the measurement noise. Therefore, in a second simulation, the time dependence of the clock rates ϵ_i is modeled using a Brownian random walk approach where σ_η^2 is the variance of the additional Gaussian noise, that is cumulatively added. We then vary the time between the transmissions and observe the degradation of the localization in terms of root-mean-square error (RMSE). The resulting plot is presented in Figure 3.14 (b). This can be used to select the rate of the beacon transmission based on the specification of the used sensor clocks.

Experimental measurements have been obtained from the ATLAS system [24] with a subset of 5 sensors as shown in Figure 3.15 (a). Target tags, which are usually attached to birds for tracking, transmit a binary frequency shift keying signal every 1 s with a bandwidth of 2 MHz. Beacons transmit an identical signal every 2 s. Transmitted data is a 8192 long random code sequence, that yields a large correlation gain at the receiver and enables simultaneous channel access for a large number of tags. The sensors are based on software defined radio with Ettus USRP N200 frontends that contain a TCXO frequency reference specified with 2.5 ppm. However, according to the estimation for the recorded data set, all 5 sensor clock rates are within less than 1 ppm. Figure 3.15 (b) shows the drift in the location of a stationary target when just the offset correction from Section 3.8.2 or the offset and rate correction from Section 3.8.2 is used. The average of the stationary target is 5.39 dB. This results in a RMSE for the two cases of 334.71 m

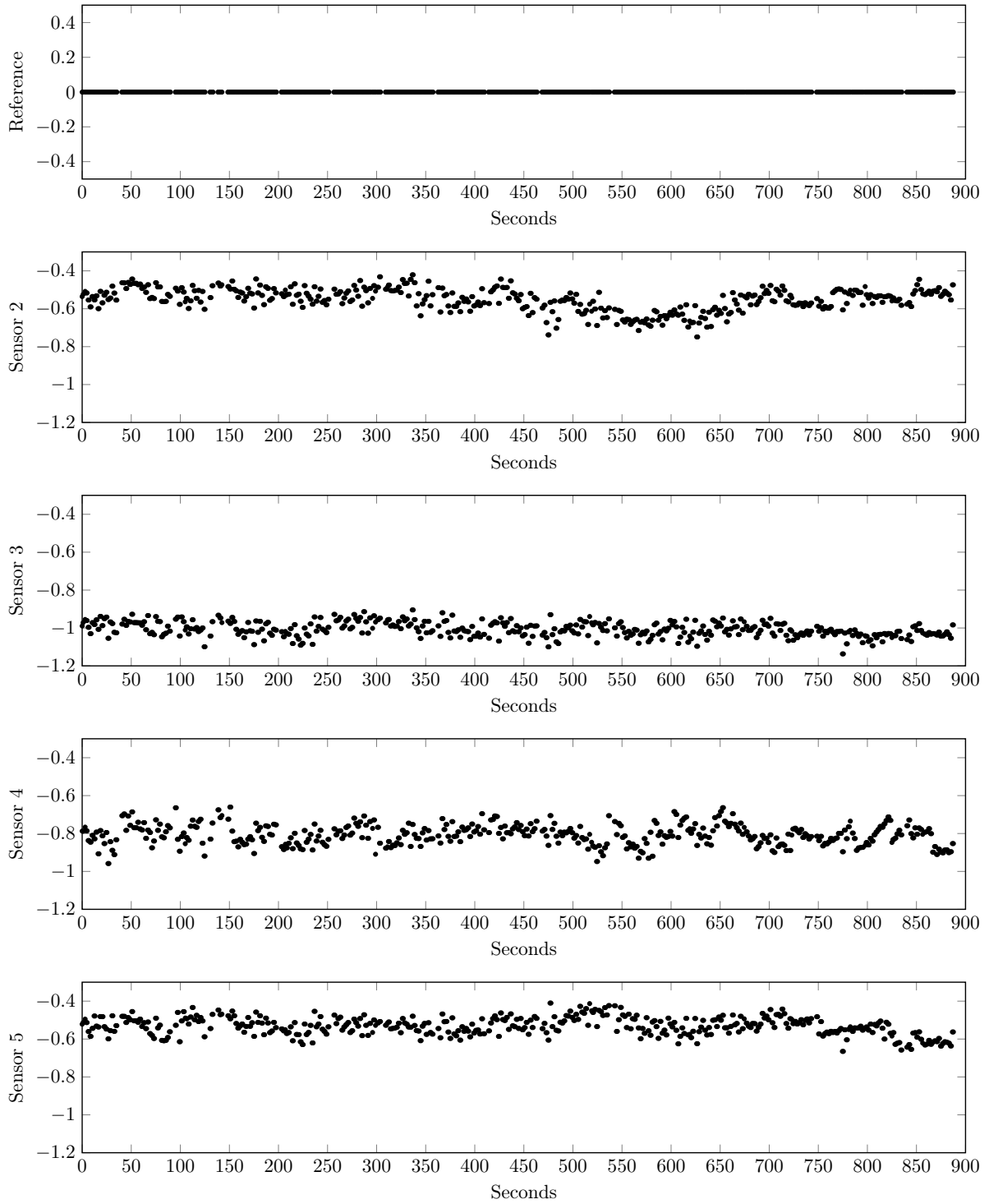


Figure 3.16: Estimated clock rate error in ppm, $(\epsilon_i - 1) \cdot 10^6$.

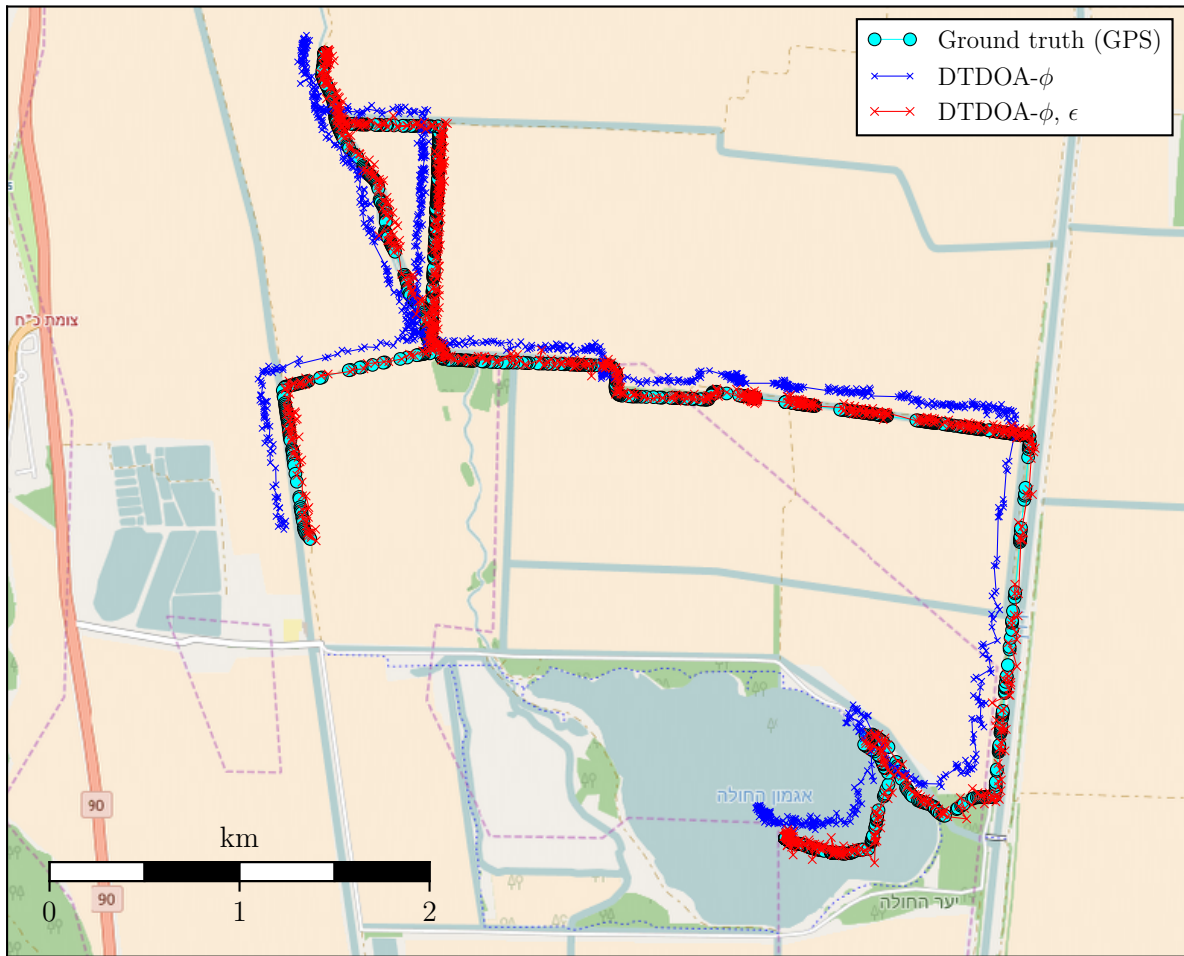


Figure 3.17: Drive test results from a tag mounted on top of a vehicle together with a GPS antenna that generates the ground truth track.

and 8.40 m respectively. In parallel, Figure 3.16 shows the estimated values of the clock parameters ϕ_i and ϵ_i . It is clearly visible that for the reference sensor it is assumed that ϵ is one and all other values are estimated accordingly.

In a second series of measurements, drive tests have been performed with the tag transmit antenna mounted on top of a vehicle, together with a GPS reference antenna that collects the ground truth. The GPS receiver is a SkyTraq Venus 828. Note that the accuracy of a standard GPS receiver is limited to approximately 1-3 m and is improved by the internal KF of the GPS receiver. Ground truth and TDOA localizations can be accurately compared based on the collected Coordinated Universal Time (UTC) timestamps. For comparison, again the RMSE criteria is used. One result of the drive test, using measurements from 4 sensors, is shown in Figure 3.17. The average SNR of the tag signal is -1.37 dB, resulting in a RMSE of 140.78 m when the offsets of the clocks are corrected and 24.17 m when offset as well as rates are corrected. Compared to the stationary case, the higher SNR after clock rate correction is due to the worse SNR.

On the other hand, the lower RMSE before clock rate correction is due to the shorter transmission interval of the beacon, which in this case has been configured to 1 s. In summary, it can be said that clock rate estimation is essential to improve the system accuracy. Further improvements could be achieved by tracking the change of the clock rate over time, e.g., using linear prediction or a KF. Using a KF in the localization step would also yield significant improvements.

4 | Grid-Based Sparse TDOA Localization

This chapter discusses an alternative approach to location estimation based on a TDOA type of system. Explicit TDOA estimates are not taken, instead the location is directly estimated from the signal samples. The necessity of solving a system of nonlinear hyperbolic equations is avoided. Moreover, the high sampling rate and long sample duration necessary for a precise localization in low SNR scenarios implies a large amount of data exchange between the sensor nodes. Therefore, the absence of high data rate enabled backbone links, connecting the nodes, restricts the system performance or may even render it dysfunctional in some cases. In order to approach this problem the novel method applies a compressed time difference of arrival based localization. Here, due to the spatial sparsity of the problem, the usage of the compressed sensing (CS) paradigm enables a trade off between the transmitted number of samples and the robustness against noise. Another severe problem for most RF based localization methods is multipath propagation. Therefore, in a second step the grid based approach is further amended with TDOA fingerprinting using ray tracing. Similar to the classical RSSI based fingerprinting, the TDOA fingerprinting is able to improve the localization results.

Parts of the following results have been presented in [7, 8].

4.1 TDOA Localization Using Spatial Sparsity

More recently another step of innovation in the context of localization was enabled by the introduction of CS. The concept of CS [156], [157] is a new paradigm for the sampling of signals that are sparse in a certain domain. It has been shown that under certain conditions concerning the involved matrices, e.g., the so-called restricted isometry property [158], it is possible to subsamples the sparse signal with respect to the Nyquist-rate while still being able to fully reconstruct it with a very high probability. CS has led to new approaches in signal processing as well as in localization where it is assumed that the location of the object to be observed and the location of the observers are sparsely distributed in the spatial domain as described in [159, 160, 161]. By finding an appropriate formulation that physically relies on the RSS of the signal, the localization problem is then solved using algorithms that are based on ℓ_1 -norm

minimization. In contrast, the authors of [162, 163] make use of the TDOAs of the signals assuming sparsity, while in [164] the Doppler shift is used additionally to obtain a direct location estimate. However, these papers do not investigate the impact of the number of recorded samples on the estimation performance.

This is important due to the fact that systems with TDOA-based localization using radio waves are usually distributed, with widely separated receiver nodes. A widely spread out system is necessary in order to fulfill the geometric requirements of the localization problem and to guarantee a good coverage. However, large distances impose some limitations on the transmission data rate achieved between the nodes. In practice, optical fiber links are still not available in a range of possible scenarios, e.g., in rural areas. Therefore, it is often necessary to use locally available landline, cellular network or other types of small data rate wireless links, to interconnect the sensor network. On the other hand, TDOA estimation methods require wide bandwidths in order to increase accuracy. These conflicting requirements may severely restrict the performance of the system or may even render it useless in case of quick target movements that demand high update rates.

To tackle this problem, a CS inspired method for localization based on TDOA is proposed, that particularly aims at a reduction of the number of samples that need to be transmitted between the distributed nodes. More specifically, the reduction can be achieved by the choice of the CS measurement matrix at the cost of estimation performance. As the approach determines the transmitter location directly based on the received signals, it avoids solving nonlinear hyperbolic equations that occur in the problem, as described in [112, 165, 109]. In [166] a group of receive antenna elements performs direction finding by applying CS. This work describes how the signal at a single antenna element is sampled at Nyquist-rate, yielding a reference signal, while the remaining elements are subsampled following a CS based approach. A distributed (multi-static) active radar system described in [167] performs non-coherent combining of the received signals in order to obtain joint sparsity. Following these ideas and applying it to TDOA-based location estimation, a novel approach including ideas from CS is derived next.

4.2 Location Estimation

In this chapter let R be the number of receivers and Q the number of transmitters that emit a signal $s_q(t)$, then the received signal at each receiver is given as

$$y_r(t) = \sum_{q=1}^Q h_{q,r} s_q(t - \tau_{q,r}) + w_r(t),$$

where $w_r(t)$ is assumed to be a realization of a white Gaussian noise process and $\tau_{q,r}$ stands for the delay which is related to the free-space propagation distance between

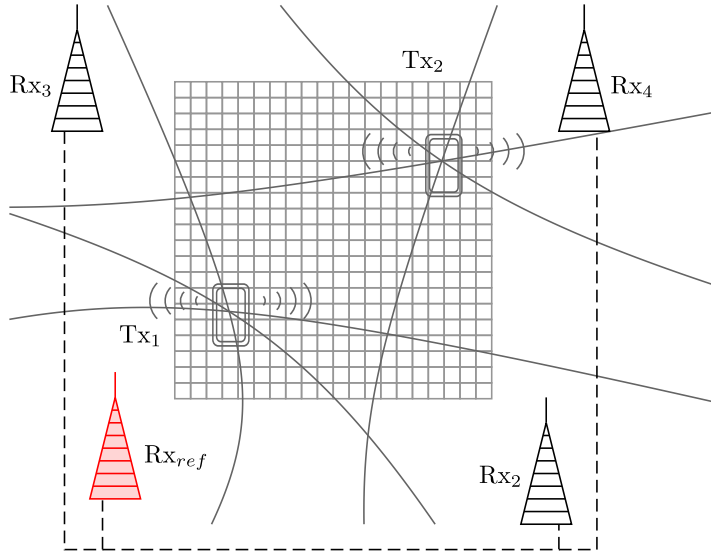


Figure 4.1: TDOA-based localization system with reference receiver marked in red, target locations are estimated on the underlying grid.

transmitter q and receiver r and $h_{q,r}$ models the corresponding attenuation. Additionally, we assume the transmitted signals to be mutually uncorrelated when the observation time goes to infinity. For the sake of simplicity, the derivation of an equivalent baseband model is omitted and the vector $\mathbf{y}_r(\gamma)$ is assumed to contain an ideally low pass filtered, Nyquist sampled and delayed version of the received signal:

$$\mathbf{y}_r(\gamma) = (y_r(t_0 - \gamma), \dots, y_r(t_{N-1} - \gamma))^T. \quad (4.1)$$

Inspired by [166], select one receiver, e.g., $r = 1$ as a reference and denote its output as $\mathbf{y}_{ref}(\gamma)$. Furthermore, set

$$\bar{\mathbf{y}}_{ref}(\gamma) = \frac{\mathbf{y}_{ref}(\gamma)}{\|\mathbf{y}_{ref}(\gamma)\|_2} \quad (4.2)$$

to denote the normalized version of $\mathbf{y}_{ref}(\gamma)$. Since from the remaining receivers $r = 2, \dots, R$ only a fraction of the samples is given to the localization algorithm (see Section 4.2.2), they are termed *CS receivers*.

Define an estimator $\tilde{\mathbf{y}}_r$ for the received signal \mathbf{y}_r at a CS receiver:

$$\tilde{\mathbf{y}}_r = \mathbf{\Psi}_r \mathbf{b}_r. \quad (4.3)$$

Here, the $N \times K$ matrix $\mathbf{\Psi}_r$ contains time shifted versions of the normalized reference signal vector with time shifts $\gamma_{r,1}, \dots, \gamma_{r,K}$, i.e.,

$$\mathbf{\Psi}_r = [\bar{\mathbf{y}}_{ref}(\gamma_{r,0}), \dots, \bar{\mathbf{y}}_{ref}(\gamma_{r,K-1})], \quad (4.4)$$

and \mathbf{b}_r is a vector with sparse support corresponding to the TDOAs of the transmitters' signals between receiver r and the reference receiver. If only one transmitter is active

and no noise is present in the system, the estimator $\tilde{\mathbf{y}}_r$ matches \mathbf{y}_r if the nonzero entry of \mathbf{b}_r contains the quotient of channel coefficients $h_{1,r}/h_{1,ref}$. In general, this does not hold due to noise and the different combinations of time shifts between the transmitter and receiver locations. Nevertheless, given the received signal \mathbf{y}_r , one can try to reconstruct \mathbf{b}_r . More specifically the nonzero entries in \mathbf{b}_r which are related to the TDOAs corresponding to the transmitter locations.

It should be emphasized that a single TDOA does not correspond to a unique transmitter location. In order to resolve this ambiguity and be able to directly determine the location, further restructuring of the problem is necessary in order to reveal a type of joint sparsity between the different receiver pairs.

4.2.1 Joint Sparsity

To localize the transmitters, a discrete grid \mathcal{G} is introduced for the two-dimensional plane containing potential location bins:

$$\mathcal{G} = \{\mu \cdot (u, v) \mid u \in \{1, \dots, L_1\}, v \in \{1, \dots, L_2\}\}, \quad (4.5)$$

where μ is a resolution parameter. This leads to a total number of $K = L_1 \cdot L_2$ bins. Assuming that $\mathbf{x}_1, \dots, \mathbf{x}_K$ is an enumeration of all bins in \mathcal{G} and the locations of the reference receiver and the CS receivers are denoted as \mathbf{z}_r and \mathbf{z}_{ref} , the time shifts in (4.4) are defined using (5.13) as

$$\gamma_{r,k} = \Delta(\mathbf{x}_k, \mathbf{z}_r, \mathbf{z}_{ref}), \quad k = 1, \dots, K. \quad (4.6)$$

This guarantees, that for all CS receivers the mapping from columns of Ψ_r to location bins is the same. It is then observed that the presence of transmitters in certain location bins yields a joint sparsity pattern for all vectors \mathbf{b}_r . Such type of structured sparsity has also been studied in [168].

4.2.2 Compressed Sensing

The joint sparsity makes it feasible to apply ideas from CS and therefore estimate all vectors \mathbf{b}_r recording only a subsampled signal $\hat{\mathbf{y}}_r$. Consider reduced versions of the received signal \mathbf{y}_r and the estimator $\tilde{\mathbf{y}}_r$ by introducing

$$\hat{\mathbf{y}}_r = \Phi_r \mathbf{y}_r, \quad (4.7)$$

$$\check{\mathbf{y}}_r = \Phi_r \tilde{\mathbf{y}}_r = \underbrace{\Phi_r \Psi_r}_{\mathbf{A}_r} \mathbf{b}_r = \mathbf{A}_r \mathbf{b}_r, \quad (4.8)$$

with the $m \times N$ matrix Φ_r which is obtained from the $N \times N$ identity matrix by randomly selecting m rows. This means that each CS receiver only transmits $m < N$ samples

to the reference receiver instead of N samples taken at Nyquist-rate. Nevertheless, CS theory suggests that the sparsity ensures that \mathbf{b}_r can be recovered. In fact, for the case of one active transmitter the recovery of \mathbf{b}_r from $\hat{\mathbf{y}}_r$ reduces to a classical CS problem. The latter can be solved by ℓ_0 -minimization searching for a solution with a low number of non zero elements which, however, is known to be NP-hard. It has been shown that under additional assumptions on the matrix \mathbf{A}_r the ℓ_0 -minimization can be relaxed by ℓ_1 -minimization [169]. In our case, it is expected that ℓ_1 -minimization similarly promotes sparse solutions and consider the relaxation

$$\text{minimize } \|\mathbf{b}_r\|_1 \quad \text{subject to} \quad \|\check{\mathbf{y}}_r - \hat{\mathbf{y}}_r\|_2^2 \leq \varepsilon_r, \quad (4.9)$$

where ε_r has to be adjusted to the current noise level. This relaxation can be solved using well-known linear and convex optimization methods. For fast numerical implementations, a greedy heuristic called orthogonal matching pursuit (OMP) [170] can be used as described in the Section 4.2.3.

In case that the time shifts in (4.4) are multiples of the sampling rate, the resulting matrices \mathbf{A}_r are closely related to so-called *partial random circulant matrices*. There exists a comprehensive theory for these matrices showing that they are feasible for the CS approach [171] and, indeed, the necessary number of measurements for sparse recovery basically grows linearly with the level of sparsity.

In our case, the matrices \mathbf{A}_r are determined by (4.6) and are less favorable for CS. This is due to the fact that different location bins might result in very close TDOAs and, hence, the columns of \mathbf{A}_r cannot be distinguished, anymore. Nevertheless, by exploiting the joint sparsity in a modified OMP algorithm, this drawback can be overcome.

4.2.3 Localization Algorithm

The standard OMP algorithm iteratively builds up an estimate for the unknown support set \mathcal{P} . If \mathcal{P} has been estimated at the $(i - 1)$ -th iteration, one uses the residual $\hat{\mathbf{r}}_{r,i}$ of the least squares approximation of $\hat{\mathbf{y}}_r$ by $\mathbf{A}_r \mathbf{b}_r$, where $\text{supp}(\mathbf{b}_r) \subset \mathcal{P}$, to choose an update for \mathcal{P} . This is achieved by selecting the index of an entry of the correlation vector $\mathbf{A}_r^H \hat{\mathbf{r}}_{r,i-1}$ with maximal norm.

For the jointly sparse case, the basic idea is to perform a non-coherent combining of the entries of the correlation at each receiver to obtain a measure of how likely a transmitter is present at a given location bin. This leads to a modified version of the OMP algorithm. Such modifications, in the presence of structured sparsity ("block" or "joint" sparsity), have already been studied by different authors [168], [172]. The resulting algorithm is depicted in Algorithm 1.

After termination, the set \mathcal{P} contains estimated location bins. A stopping criterion could either be to stop if the iteration count has reached the number of transmitters

Algorithm 1 Localization Algorithm

```

// Initialize:
1:  $\hat{\mathbf{r}}_{r,0} \leftarrow \hat{\mathbf{y}}_r$  ▷ (4.7)
2:  $\mathcal{P} \leftarrow \emptyset$ 
// for  $i$ -th iteration (beginning with  $i = 1$ ):
3: while stopping criterion is not met do
// Calculate correlations  $\beta_r$  and combine in  $\bar{\beta}$ :
4:  $\beta_r \leftarrow \mathbf{A}_r^H \hat{\mathbf{r}}_{r,i-1}$ 
5:  $\bar{\beta}[k] \leftarrow \sum_{r=2}^R |\beta_r[k]|^2$ 
// Estimate a new location bin and add it to the set:
6:  $p_i \leftarrow \arg \max_{k \in \{1, \dots, K\}} \bar{\beta}[k]$ 
7:  $\mathcal{P} \leftarrow \mathcal{P} \cup \{p_i\}$ 
// Calculate new residuals:
8:  $\hat{\mathbf{b}}_r \leftarrow \arg \min_{\text{supp}(\mathbf{b}_r) \subset \mathcal{P}} \|\hat{\mathbf{y}}_r - \mathbf{A}_r \mathbf{b}_r\|_2^2$  ▷ (4.9)
9:  $\hat{\mathbf{r}}_{r,i} \leftarrow \hat{\mathbf{y}}_r - \mathbf{A}_r \hat{\mathbf{b}}_r$ 
10: end while

```

(if previously known) or if the norm of the current residual is smaller than a given threshold.

Figure 4.2 shows a matrix version of the combined cross correlation vector $\bar{\beta}$ for the case of $R = 4$ receivers and $Q = 2$ transmitters. Here, the matrix entry (u, v) is equal to the entry $\bar{\beta}[k]$, with k chosen such that $\mathbf{x}_k = \mu \cdot (u, v)$.

4.2.4 Results

To confirm the theoretical considerations and to evaluate the performance of the proposed algorithm, numerical simulations of a two dimensional free-space radio wave propagation environment have been conducted as described in the following. A random BPSK modulated baseband signal with a sample rate of 100 MHz is generated for each transmitter location. In order to determine the received sum of signals, the transmit signals are time-shifted and attenuated according to their free-space path loss between each pair of transmitter and receiver. The sum of signals at each receiver is then added with white Gaussian noise, while for simplicity it is assumed that the SNR of each receiver's output signal is identical.

The scenario is a 100 m \times 100 m square and the receivers are located around the border at $\mathbf{z}_{ref} = (0, 0)$, $\mathbf{z}_2 = (0, 100)$, $\mathbf{z}_3 = (100, 0)$, $\mathbf{z}_4 = (100, 100)$, $\mathbf{z}_5 = (0, 50)$, $\mathbf{z}_6 = (50, 0)$, $\mathbf{z}_7 = (50, 100)$, $\mathbf{z}_8 = (100, 50)$. The transmitters are randomly placed in the region of interest, for each Monte Carlo iteration.

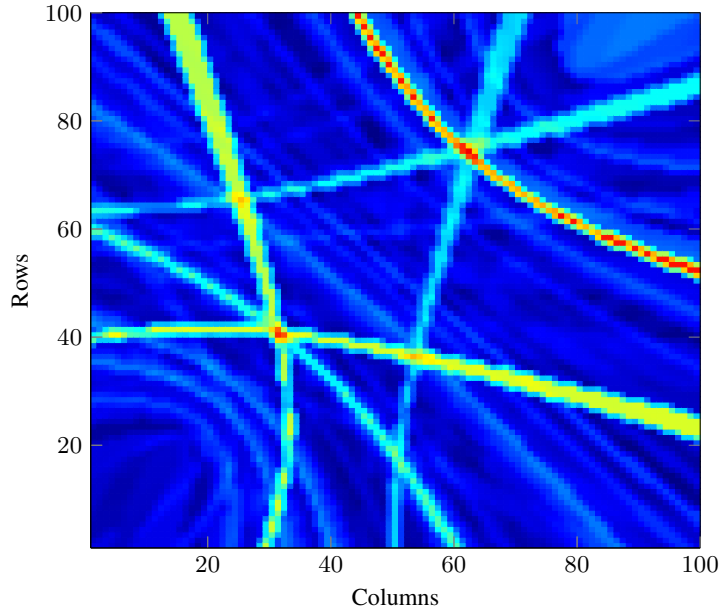


Figure 4.2: Example of matrix form of the combined cross correlations $\bar{\beta}$, blue colors denote low and red colors denote high values.

Additionally, the estimator grid dimension is set to cover the scenario with a resolution of one bin per square meter. In order to estimate the transmitter location, the reference receiver takes 1000 samples at Nyquist-rate and obtains compressed samples from the CS receivers. In the first experiment 1 transmitter and 4 receivers are active. The transmitter location is determined using a discrete uniform distribution placing it on the estimator grid in order to simplify the evaluation of the success rate. The estimation algorithm is performed for different numbers of compressed samples and determine the success rate as shown in Figure 4.3 (a). A location is estimated successfully if all TDOAs corresponding to the true and estimated bins are equal within a tolerance of one sample duration. It is noticed that for these parameters the estimator produces acceptable results up to a compression ratio of about 10.

A second experiment is performed with 4 receivers and 2 transmitters. As mentioned in Section 4.2.2, for a single transmitter one may apply classical CS solutions to our problem. For the case of multiple transmitters at different locations, slightly worse results are expected due to model mismatch. The corresponding success rate is depicted in Figure 4.3 (b), where a performance degradation can be observed. This is due to interference between the two transmitted signals that are added with a different relative delay at each receiver. Therefore, when using the signal of the reference receiver in the CS reconstruction, it remains inherently inaccurate. More specifically, the errors in the calculation of the residual can accumulated. However, unless the transmitted signal waveforms are known at the reference receiver this situation is difficult to resolve.

The third experiment considers the number of participating receivers. Placement of the single transmitter is now performed using a uniform distribution to allow arbitrary

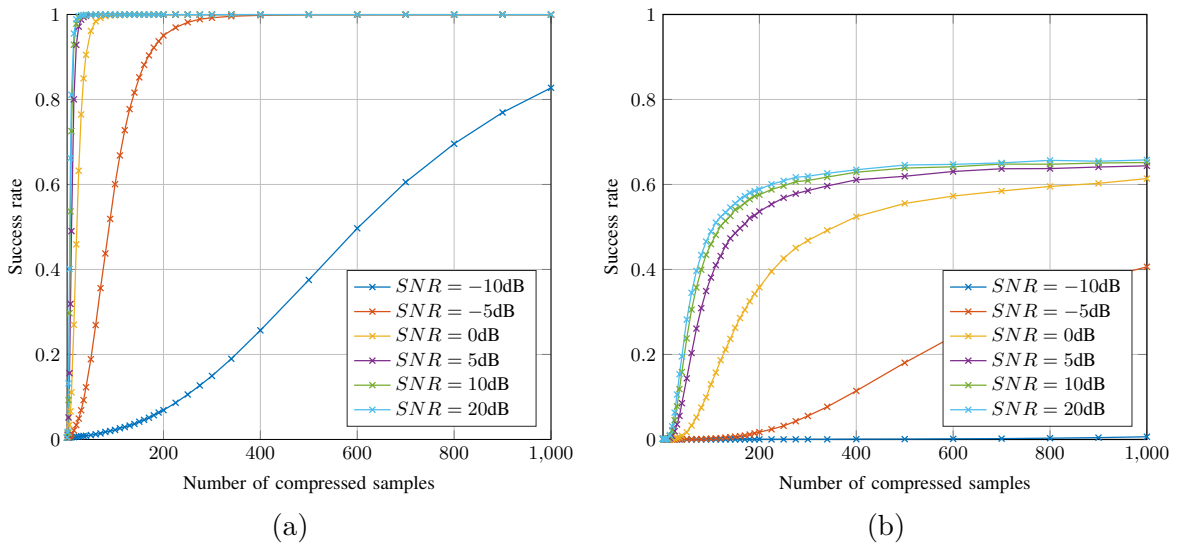


Figure 4.3: Success rate of localization for different number of compressed samples with 1 transmitter and 4 receivers (a) and with 2 transmitters and 4 receivers (b).

locations. Varying the number of receivers, including the reference receiver, between 3 and 8 the root-mean-square error (RMSE) between the true and estimated transmitter location is determined as shown in Figure 4.4. It is clearly visible how the error decreases for a higher number of CS receivers.

4.2.5 Localization of Many Sources

As expected and shown in the results above, additional receivers are able to decrease the localization error. Also, it is not possible to simultaneously distinguish and localize a large number of sources transmitting unknown signals in a non-orthogonal way. Therefore, next by scaling up the simulation it is examined if a larger number of sensors can help solving this problem and enable tracking of many sources at the expense of additional network infrastructure. For this purpose a network of 16 sensors is simulated that tries to localize 8 sources. The number of Nyquist samples is increased to 3000 in order to improve the effective SNR. Figure 4.5 shows a snapshot of the scenario including all the hyperbolas which are based on the reference sensor at coordinates $(0, 0)$. It is noted that the algorithm sometimes struggles with targets that are close together as well as it sometimes mistakenly detects two targets instead of a single one. Those are classical issues in the domain of multi target tracking. To overcome these, tracking over multiple time instances is necessary. However, Monte Carlo simulations indicate that if the number of sensors is high enough, the single snapshot approach already produces a reasonable baseline performance in terms of probability of detection. The result is shown in Figure 4.6. It shows the probability of detection all targets per snapshot, i.e., a probability of 1 signifies that all targets are always detected with 100% probability, while a probability of $\frac{1}{6}$ signifies that on average only one target is detected with 100%

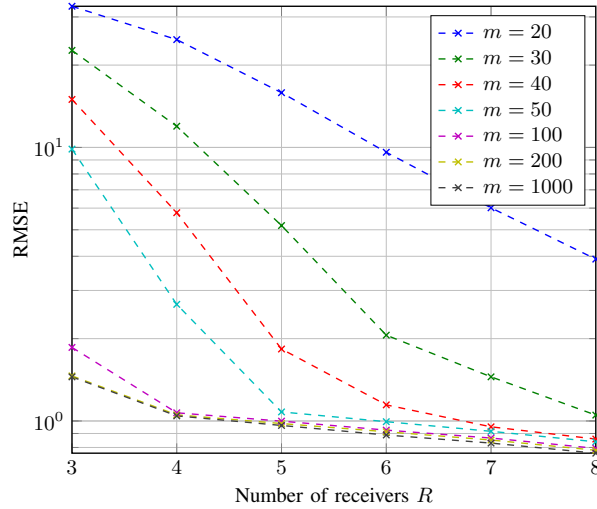


Figure 4.4: Root mean squared error of true and estimated location for a single transmitter and 0 dB SNR.

probability per snapshot. A solution is assumed correct if the target is localized with an error of one location bin in all directions. The result demonstrates that the model mismatch caused by the successive cancellation of sources inside the CS type algorithm can be mitigated to some extent using larger numbers of sensors.

4.3 Ray Tracing for Urban Scenarios

Localization in urban areas with no direct line-of-sight between the target and anchor nodes turns out to be challenging for many well-known localization methods. In combination with multipath propagation of employed radio waves, the performance of the location estimates can be heavily deteriorated. In this section, an extension to the sparsity based method that is able to cope with such conditions is introduced. Employing a discrete approach for the estimation of the emitter location, it is shown how prior knowledge of the environment, obtained from a ray tracer or ray launcher, can improve the system accuracy. A similar approach is followed in [173] and [174] in the context of GNSS, where 3D models of urban areas are used to improve the positioning accuracy. The localization algorithm in this section is based on the TDOAs between the observing sensors. However, in non-line-of-sight these time differences change as opposed to common signal models that assume free-space propagation. This mismatch is resolved taking into account information of the propagation paths provided by the ray launcher. Simulation results demonstrate that the proposed method effectively mitigates the impact of non-line-of-sight and multipath propagation on the location accuracy.

For the localization of wireless sensor nodes, mobile phones, or other types of radio wave emitters, numerous different approaches and related algorithms have been proposed. All approaches are based on explicit or implicit measurements of physical parameters

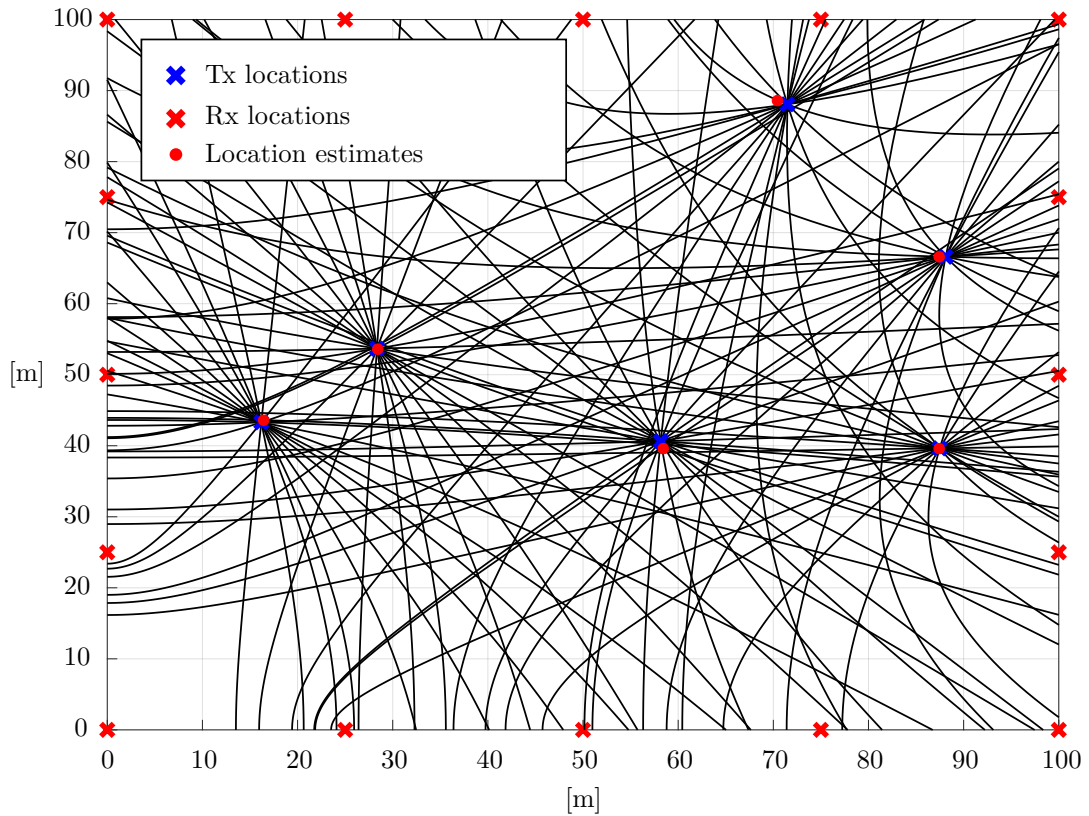


Figure 4.5: Localization of 6 targets using 16 sensors and the sparsity based algorithm. Targets are transmitting random BPSK signals without any pilots. The figure also shows all the TDOA hyperbolas with respect to the reference sensor at $(0, 0)$.

of the propagating waves. To assist the localization and relate it to a known coordinate system, the signals are usually transmitted or received by anchor nodes whose locations are known. Possible physical parameters at the receiver are the signal strength, time, frequency, phase or direction of the arriving wave, which are further processed by the localization algorithm, e.g., taking differences, averaging or other types of combining. However, all these parameters are affected if no direct line-of-sight (LOS) path exists which forces the radio waves to arrive at the receiving antenna by means of reflections and diffractions. Thus, the accuracy of all methods that assume free-space propagation in their system model, will be deteriorated.

Various approaches have been proposed in order to overcome or avoid such problems. A scheme that tries to track and discriminate between line-of-sight and non-line-of-sight (NLOS) propagation at the different receivers is proposed in [175] assuming range measurements. In case of NLOS, the range measurements of the particular receiver are corrected based on their statistics to obtain values resembling LOS. A similar error suppression approach is suggested by [176] which further investigates the statistics of the error in the NLOS case. Other approaches like [177] conduct more profound studies

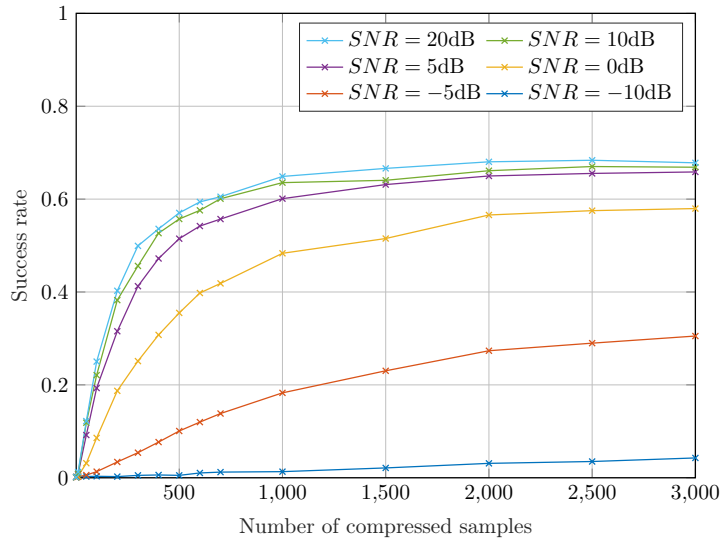


Figure 4.6: Detection probability of 6 targets using 16 sensors.

of geometrical properties of the wave propagation and thereby aim to suppress NLOS components in multipath propagation environments. The authors of [178] go a step further by assuming no line-of-sight component but wave propagation inside a completely closed room. An exact formulation of the differential equations of the wave field and a discrete grid enable the localization of an emitter behind a corner or in a another connected room. However, this last approach is only suitable for very specific scenarios with explicitly defined boundary conditions.

In order to tackle more generic scenarios with a good location accuracy, higher than that of statistics based methods but without detailed knowledge of the environment, fingerprinting has been introduced in [41] for example. Most literature about fingerprinting utilizes a metric based on the received signal strength indicator (RSSI) of the signals and assumes that a prior measurement campaign has taken place in order to obtain the fingerprints, which are calculated by the measured RSSIs at certain known positions. Those fingerprints are stored in a database and compared against the fingerprints obtained at runtime in order to perform the localization. In an attempt to reduce the effort and costs necessary for the collection of the fingerprints, the work in [179] suggests to obtain them from simulations by the means of a ray tracing or ray launching algorithm. In [180] this idea has been further extended to not only make use of the RSSI information but also the full information of the directions of arrival of different propagation paths at the receiver, which are available from the ray tracer. This is a powerful approach, however, it requires a calibrated antenna array at the receiver in order to obtain the same directional information from the received signal. As an alternative, ranging based methods have the advantage that they only need a single receive antenna and a single associated signal processing chain. Therefore, an approach based on the fingerprinting of the TDOA of a signal is proposed. The method utilizes a discrete grid of possible locations, which eliminates the need to explicitly solve the

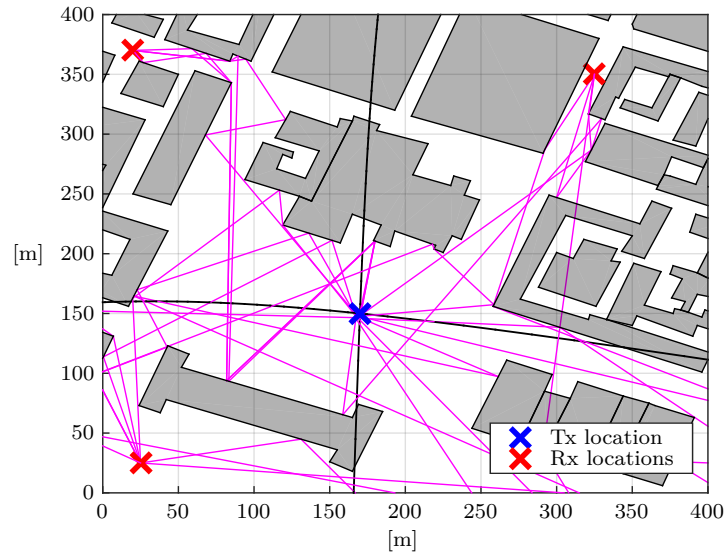


Figure 4.7: Footprint of buildings in the inner city of Munich with propagation paths between the transmitter and the receiving anchor nodes in magenta, TDOA hyperbolas in black.

nonlinear equations determined by the TDOAs and makes it suitable for fingerprinting. Thus, extending the algorithm in Section 4.2.3 the formerly developed ray launching algorithm [181] for multipath propagation leads to a TDOA-based fingerprinting approach introduced in current section.

4.3.1 Ray Launching Based Fingerprinting

For free-space propagation signal propagation follows a simple model. Denoting the emitted signal with $s(t)$ consider the signals $y_r(t)$ received at different nodes. The received signal at the r -th receiver with channel coefficients h_r is then given as

$$y_r(t) = h_r s(t - \tau_r) + w_r(t), \quad (4.10)$$

where $s(t)$ can be any type of signal and $w_r(t)$ is assumed to be white Gaussian noise, τ_r stands for the delay which is related to the free-space propagation distance between the transmitter and receiver r . In case of multipath propagation, the channel impulse response becomes a function of time and is convolved with the transmitted signal

$$y_r(t) = h_r(t) * s(t - \tau_r) + w_r(t). \quad (4.11)$$

For this case τ_r is the delay of the first arriving path.

In the beginning of the chapter the case of multiple transmitters for free-space propagation has been considered. For multipath propagation, multiple transmitters in the same band are extremely challenging as the assignment problem between the delays and

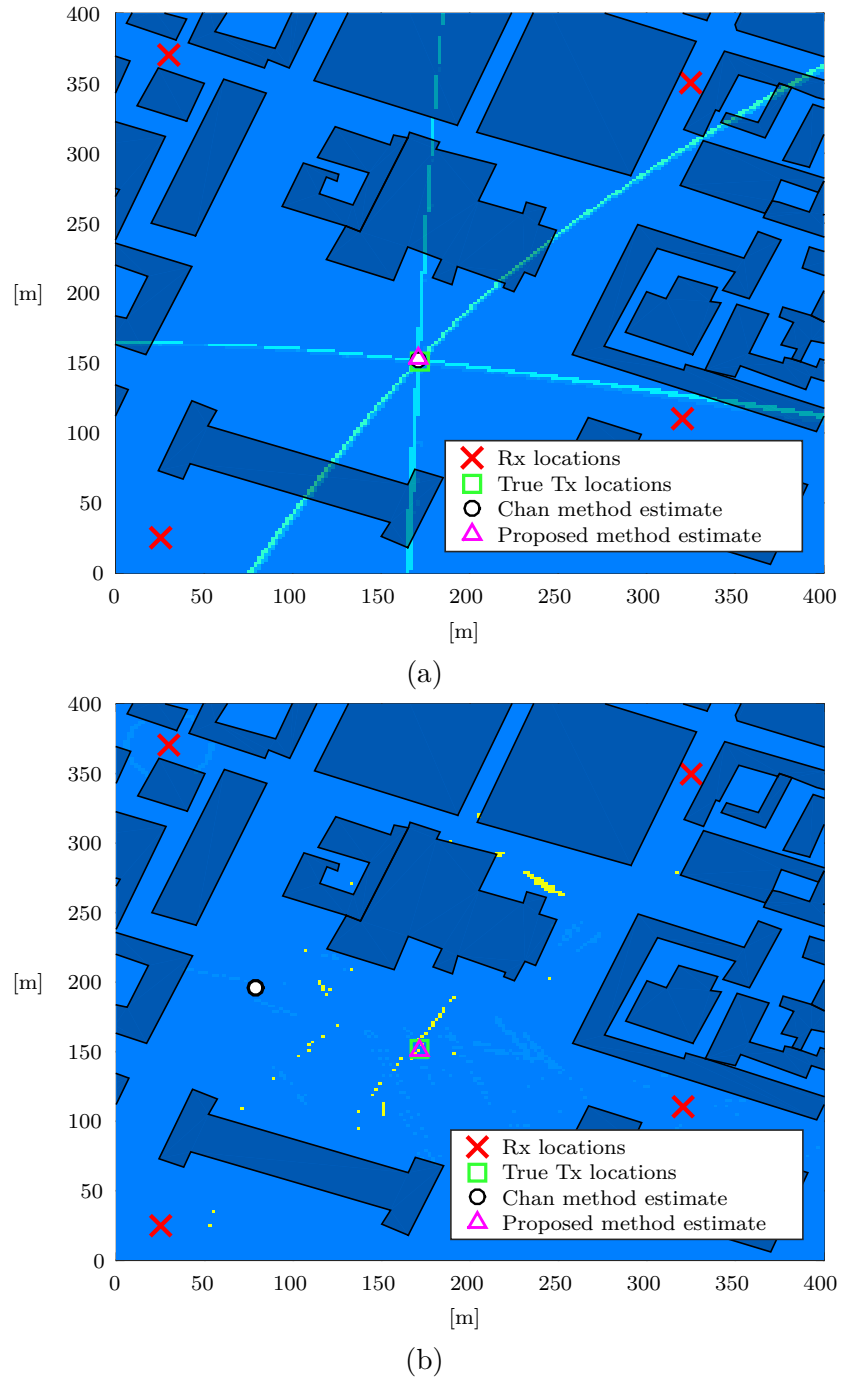


Figure 4.8: Comparison of the distortion encountered by Algorithm 1 from Section 4.2.3 in step 5 for (a) free-space and (b) multipath propagation. Our proposed method is able to estimate the location correctly in both scenarios while Chan’s method fails under NLOS.

the sources is further deteriorated. Therefore, the model in this section is restricted to a single transmitter to be able to obtain good location estimates under such adverse conditions.

Again a grid of K location cells $\Psi_r = [\bar{\mathbf{y}}_{\text{ref}}(\gamma_{r,1}), \dots, \bar{\mathbf{y}}_{\text{ref}}(\gamma_{r,K})] \in \mathbb{C}^{N \times K}$ on the region of interest is defined in order to determine the location. The time shifts are defined based on the TDOAs at the center of each location cell.

NLOS and multipath propagation of the radio waves introduce an inherent error into the localization as they alter the length of the propagation paths and add additional paths with different delays to the channel. In order to obtain the propagation information and resolve the problem by fingerprinting, either extensive measurement campaigns are necessary, or it can be simulated using ray tracing software and a model of the environment. For the results of the present section, the PIROPA ray launcher [181] was utilized. The algorithm is based on an input of 2.5D building data, i.e., buildings and other objects in the environment are modeled based on their footprints, as seen in Figure 4.7, and their heights. PIROPA provides a precise output of each segment of a propagation path, therefore providing information about the angles of departure and arrival, as well as the path lengths, which immediately lead to the power delay profile.

To include the ray launching data into the localization algorithm it is necessary to model the TDOA related time shifts in (4.4) for each entry of the matrices Ψ_r . Possible emitter location cells are straightforwardly represented by a grid of receivers in the ray launching algorithm. The algorithm is evaluated and a set of rays is obtained for each possible location. Based on the length of the rays the propagation delays, i.e., the times of arrival, can be evaluated. To resolve the multipath ambiguity in the delay, the dominant propagation path needs to be selected. Here the shortest, i.e., the first arriving ray has been selected to determine the time. However, it is also possible to select a weighted combination of rays. Then, to calculate the TDOAs, a pair of ray launching results of two receivers has to be combined by subtracting the times of arrival at both receivers for each location cell. In that way the relevant time shifts $\gamma_{r,1}, \dots, \gamma_{r,K}$ for the location cells can be obtained. The TDOA-based fingerprint data can be stored and used during runtime of the localization algorithm. As with other fingerprinting approaches this step has to be performed in an offline phase before the final deployment of the system. It has to be re-evaluated only whenever the position of one or more observing receivers or the scenario is changed, e.g., when a new base station is added as part of a mobile network.

4.3.2 Results

Simulation results have been obtained for scenarios in the inner cities of Aachen and Munich. The Munich data set comes from the land register data while the Aachen data is extracted from the OpenStreetMap (OSM) project [182]. Government data sets usually contain much better information about the building heights which can also be

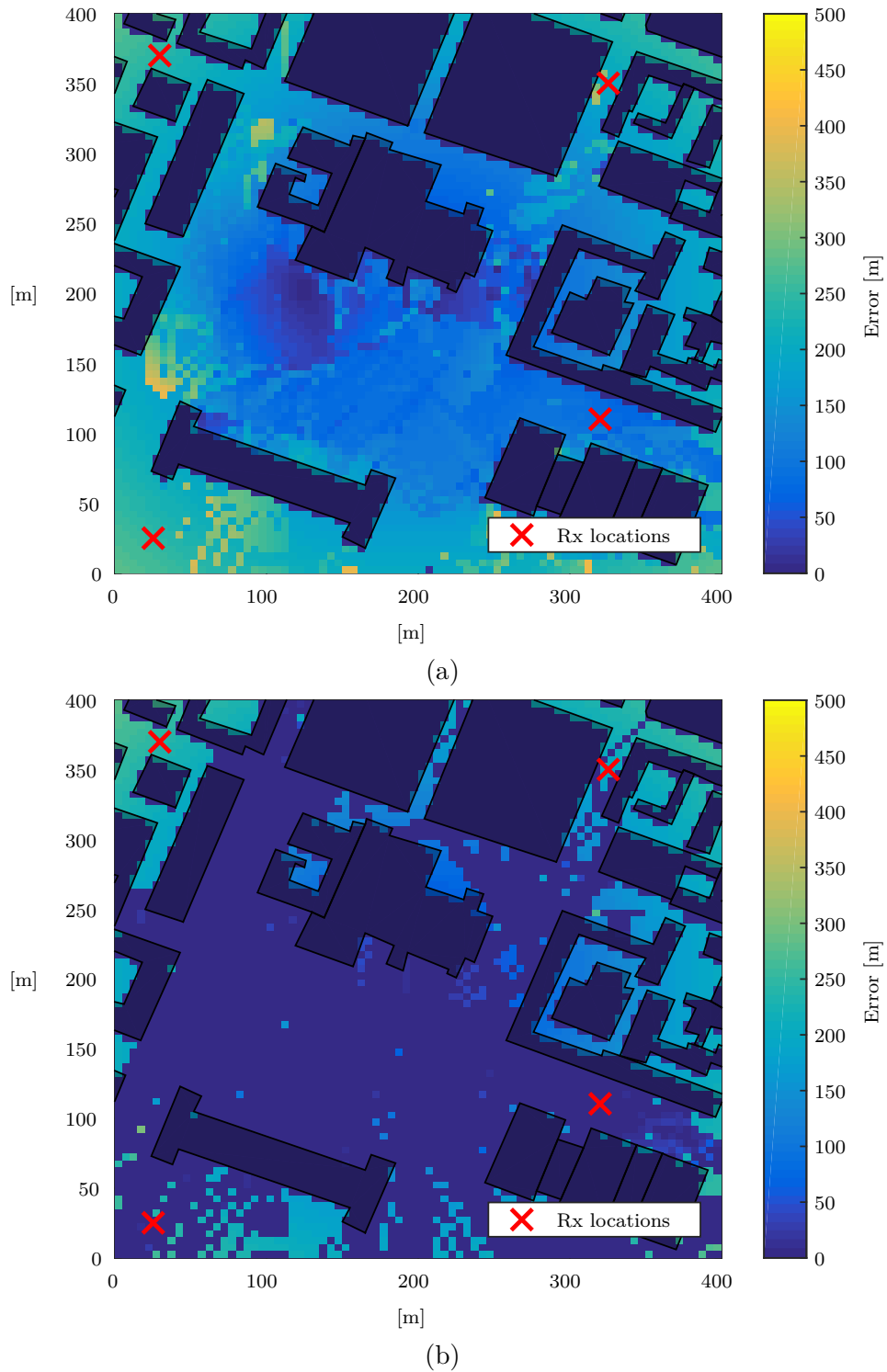


Figure 4.9: Error of localization in Meters evaluated on a 400 m \times 400 m region of interest, 5 m resolution, in the inner city of Munich, Germany for (a) Chan's method and (b) proposed method.

extracted from LIDAR scans. For the German state of North Rhine-Westphalia, where the authors' university is located, comprehensive LIDAR scan data is available and is updated by the local administration every 5 years. The OSM data on the other hand has proven to be a reasonable and royalty-free alternative with ever increasing accuracy. Therefore, the PIROPA ray launching tool supports various input filters for different data sets.

For the localization scenario three receivers are placed in a $400\text{m} \times 400\text{m}$ target area. A transmitter is placed on a location in the outdoor area as PIROPA does not support outdoor to indoor propagation modeling. The transmitted signal is a BPSK signal with a bandwidth of 100 MHz. Since no real world measurement data has been available, the channel impulse responses provided by the ray launching has been used to convolve it with the signal as given in (4.10). The size of the location cells for the proposed algorithm is $1\text{m} \times 1\text{m}$. In order to speed up and simplify the simulation the channel impulse responses is precalculated for each cell and the transmitter locations are only allowed to lie at those coordinates. In Figure 4.8, step 5 from the proposed Algorithm 1 of Section 4.2.3 is shown, in order to visualize how the NLOS propagation environment distorts the TDOAs. For each possible location the error of the localization is determined and compared to the well known algorithm for TDOA localization given in [109]. The results of this, as shown in Figure 4.9, indicate the error of both algorithms. It can be observed that the proposed approach results in a clearly improved accuracy.

5 | Sensor Network Self-Localization using TDOA

This chapter deals with the estimation of the locations of the sensors as opposed to the target. Determining the exact coordinates of the sensors in the respective coordinate system is an important step in the setup of a localization sensor network. The exact knowledge of the sensor locations is crucial for the accuracy of the target localization. When setting up a sensor network, it is not always possible or desired to perform measurements of the sensor locations by means of external measurement equipment. This is often the case in ad-hoc sensor networks. Interestingly enough there exist methods to let the network determine the location of all its sensor locations by itself. These methods either use some type of measurements between the sensor nodes or exploit the correlation in a time-series of target measurement, e.g., using Kalman filtering.

Parts of the following results have been presented in [11].

5.1 Active and Passive Methods

An important distinguishing property between different self-localization methods for sensor networks is the type of measurements that is used. Active methods require the sensors to receive, as well as transmit, while passive methods must rely on signals transmitted by the target, because the sensors can only receive. Passive self-localization approaches for time difference of arrival (TDOA) systems have been developed only very recently [183, 184]. In general, the optimization problems associated with active as well as passive self-localization are not convex. Research results on passive methods indicate that the underlying minimization problem severely suffers from many local minima, so greater effort is necessary to find the global optimum and thereby the sensor locations. Therefore, active self-localization based on time difference of arrival (TDOA) measurements between the sensors is considered in the current chapter. Due to the non-convex nature of the problem it is obviously difficult to provide mathematical rigorous proofs of convergence for both cases. However, numerical simulations show a more manageable behavior of the passive problem with respect to local minima as the passive problem tends to have no local minima close to the global optimum solution.

5.2 Self-Localization with Classical Multidimensional Scaling

Active self-localization relies on distance measurements between sensors [185, 186, 187]. The relative sensor locations can be determined from this distance measurements using the theory of classical multidimensional scaling (MDS) [188]. MDS is a mathematical method that places objects in a 2-, 3- or higher dimensional space according to known dissimilarities between the objects. In classical MDS the dissimilarities are Euclidean distances. For example, if M sensors with coordinates $\mathbf{x}_j = [x_{j1}, x_{j2}]^T, j \in \{1 \dots M\}$ are considered, this yields a $M \times M$ distance Matrix \mathbf{D} . The entries $[\mathbf{D}]_{jk}$ are given as $d_{jk} = \sqrt{(x_{j1} - x_{k1})^2 + (x_{j2} - x_{k2})^2}$. A common method to obtain all the pairwise distances and thereby \mathbf{D} , is two-way ranging, where sensors take turns to send a message that is immediately answered by a second one and the distance is determined as half of the sum of the propagation times.

Shepard and later Kruskal developed an iterative algorithm for the problem now known under the names of the authors [189, 190]. The algorithm iteratively decreases a cost function called *Stress*, much like a gradient descent type algorithm. A more thorough analysis including several extensions can be found in the more recent literature [191, 192, 193]. For the case of classical MDS where the dissimilarities are exact Euclidean distances, the literature also provides a closed form solution that takes \mathbf{D} as an input and based on eigenvalue decomposition outputs a coordinate for each object.

5.3 Procrustes Transform and Absolute Localization

It has to be emphasized that the solution obtained from MDS provides only a relative solution to the self-localization problem. That means, in general the solution is shifted, rotated and reflected with respect to the absolute solution that lies in a global coordinate system such as World Geodetic System 1984 (WGS84). In order to match the relative solution of the self-localization to an absolute solution some type of anchor points are required. Considering the two-dimensional problem, at least three anchor points are required to resolve the unknown shift, rotation and reflection. A well known solution to match the relative solution and the absolute anchor points onto each other is Procrustes analysis [194]. Procrustes analysis yields a linear transform that provides the best mapping of a set of points onto a reference set in a least squares sense, i.e., minimizing the Procrustes distance

$$\min_{\mathbf{T}, a, b} \sum_j (x_{j1} - \hat{x}_{j1})^2 + (x_{j2} - \hat{x}_{j2})^2, \quad (5.1)$$

between $\mathbf{x}_j = [x_{j1}, x_{j2}]^\top$ and $\hat{\mathbf{x}}_j = [\hat{x}_{j1}, \hat{x}_{j2}]^\top$, where $\mathbf{T} \in \mathbb{R}^{2 \times 2}$, a and b are the parameters of the mapping.

$$\mathbf{x}_j = \mathbf{T}\hat{\mathbf{x}}_j + \begin{bmatrix} a \\ b \end{bmatrix}, \quad (5.2)$$

that maps the localized beacon locations to the true ones with least squared error using a shift specified by $[a, b]^\top$ and a rotation and reflection by the matrix \mathbf{T} . For the localization problem different nodes can act as anchors, depending on if knowledge about their absolute location is available or not. One possibility is to use some of the sensors itself. However, another approach that is followed in this chapter is to introduce additional beacons into the system. Those beacons are transmit-only-nodes and therefore simpler devices. They can potentially also be used for sensor node synchronization. A third option for anchoring is to use a mobile reference transmitter placed at exactly known locations during the system setup phase.

A practical real-world application that motivates anchoring by beacons, is the ATLAS system [24]. This is a wildlife tracking system in Hula Valley in northern Israel, an area that lies on an important bird-migration route. In the ATLAS project, birds are tagged with a transmitter and their movements can be observed in real-time. The system uses a number of base stations that perform time of arrival measurement of the bird tags. These arrival times are sent to a central fusion center that calculates the locations based on the resulting TDOAs. Locations of the sensor antennas, most of which are mounted on cellular network towers, can be erroneous. For example this can be due to the GPS antenna not placed next to the receive antenna or errors in the GPS position. The ATLAS system has some transmitting beacons in well known absolute locations. Section 5.5 explains how beacons at known locations can be used to anchor the solution of the self-localization.

5.4 Differential Multidimensional Scaling

In TDOA systems, the ability to perform ranging between sensors might not be available due to technical reasons. On the other hand, differential measurements between two receiving sensors and a third transmitting sensor are a natural operation and require insignificant changes in the system software. However, there is no known approach to solve the MDS problem from differential measurements. Therefore, in this chapter an iterative algorithm is introduced and studied that is able to derive the sensor locations from the full set of TDOA measurements between all combinations of sensors. For that, following along the lines of classical MDS, in order to find the sensor locations an objective function has to be defined. In the context of MDS this function has been called *Stress* [190] and the solution of the problem can be obtained by minimizing the function.

Consider the system of M sensor nodes with coordinates \mathbf{x}_j located in a two-dimensional euclidean space as defined above. The sensor locations are initially unknown. Additionally, a number of N beacons with known locations $\mathbf{x}_b = [x_{b1}, x_{b2}]^T, b \in \{1 \dots N\}$ are available as anchors. The beacons are constantly transmitting and are not able to receive whereas the sensors are able to receive as well as transmit signals. After deployment the system enters into a self-localization phase. In this phase, consecutively each sensor transmits a calibration signal while all the other sensors are listening and obtaining TOA measurements. The sensors are assumed to be perfectly time synchronized. Moreover, it is assumed that the signals emitted by the sensors are orthogonal to the beacon signals such that they do not interfere with the measurements.

Assuming free-space propagation, the TDOA measurements for a transmitting sensor at location \mathbf{x}_j and receiving sensors at locations \mathbf{x}_k and \mathbf{x}_l can be expressed as

$$\tau_{j,k,l} = \frac{1}{c} \|\mathbf{x}_j - \mathbf{x}_k\|_2 - \frac{1}{c} \|\mathbf{x}_j - \mathbf{x}_l\|_2 + \eta, \quad j, k, l \in \{1 \dots M\}, \quad j \neq k \neq l, \quad (5.3)$$

where c denotes the speed of the wave and η is a Gaussian distributed noise term. Note that this is essentially identical to what is given in Chapter 3, however in this case all of the participating nodes are sensors and none of the coordinates of the sensors are known.

Instead of working with the TDOA measurements one can equivalently define distance differences

$$\Delta_{j,k,l} = c * \tau_{j,k,l}. \quad (5.4)$$

The full set of $\Delta_{j,k,l}$ contains $M(M-1)(M-2)$ measurements, the problem is symmetric in the sense that $\Delta_{j,k,l} = -\Delta_{j,l,k}$, this can potentially be exploited to further speed up the algorithm described in the following. To measure $\Delta_{j,k,l}$ it is only necessary to have M transmission, each sensor has to transmit once while all the others are listening.

After obtaining the full set of differential measurements the relative locations of the sensors shall be estimated. In the context of MDS these relative locations are called a *configuration*. Clearly, if the locations of the sensors are rigidly translated, rotated, and reflected, the pairwise distances and their differences will not change. Therefore, one can determine the relative sensor locations and subsequently perform a mapping to absolute coordinates if required by the application.

As mentioned before, MDS, as first introduced in [188], provides a well known solution to the problem at hand if the distance matrix D is known. Next an algorithm is introduced that can solve for a configuration even if only the differential distances $\Delta_{j,k,l}$ are known. This algorithm is denoted as Differential multidimensional scaling (DMDS). It is only possible for a set of more than three sensors. For three sensors a unique solution does not exist. Showing this ambiguity of a three sensor solution is easily possible by finding two sets of sensor locations for the same difference measurements. Therefore, a minimum of four sensors is required. The algorithm is inspired by the Shepard-Kruskal algorithm [189, 195, 190] that finds a configuration by defining an iterative rule, with iteration step i for moving the points $\hat{\mathbf{x}}^{(i)}$ to new points $\hat{\mathbf{x}}^{(i+1)}$.

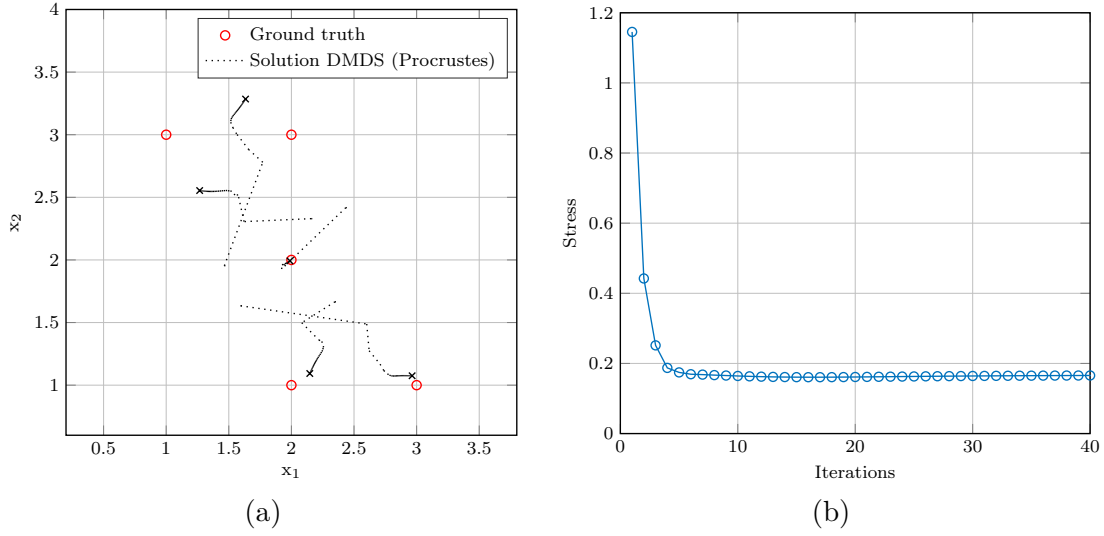


Figure 5.1: Example of the algorithm running into a local minimum (a) and the evolution of the Stress function (b), showing that it has converged but not to a the near-zero value that is expect for the ground truth configuration.

5.4.1 Stress Criteria for Differential MDS

In order to evaluate the fitness of the configuration, define the function

$$\hat{\Delta}_{j,k,l}^{(i)} = \|\hat{\mathbf{x}}_j^{(i)} - \hat{\mathbf{x}}_k^{(i)}\|_2 - \|\hat{\mathbf{x}}_j^{(i)} - \hat{\mathbf{x}}_l^{(i)}\|_2, \quad j \neq k \neq l. \quad (5.5)$$

Now define the cost function S , equivalent to the Stress function defined by Kruskal [190],

$$S(\hat{\mathbf{x}}_1^{(i)}, \dots, \hat{\mathbf{x}}_M^{(i)}) = \sqrt{\frac{\sum_{j,k,l} (\Delta_{j,k,l} - \hat{\Delta}_{j,k,l}^{(i)})^2}{\sum_{j,k,l} \Delta_{j,k,l}^2}}, \quad (5.6)$$

The Stress is a functional that maps $\mathbb{R}^{2 \times M}$ (M points in the plane) to \mathbb{R} . Now it is possible to define the iterative DMDS algorithm that obtains the sensor locations by minimizing the Stress.

5.4.2 Iterative Displacement of Points

As a starting point consider a uniformly-distributed random configuration with location vectors $\hat{\mathbf{x}}_j^{(0)}$, $j \in \{1 \dots M\}$. Ensuring $\hat{\mathbf{x}}_j^{(0)} \neq \hat{\mathbf{x}}_k^{(0)}$ for $j \neq k$, then seek to minimize S . The classical algorithm introduced by Sheppard intuitively achieves this by comparing all distances of tuples in the configuration to the measurements and then displacing the points accordingly, i.e., moving them slightly closer or further away from all other points of the configuration in each iteration. However, the present problem uses differential measurements, consisting of triples of points, i.e. all combinations of one transmitting

sensor and two receiving sensors. Therefore, it is not directly obvious how to displace points in order to achieve convergence to the minimum-Stress configuration. Based on empirical studies, we propose for each triple to displace one of the receiving sensors and to choose the direction of displacement as the direction from this receiver to the transmitter,

$$\mathbf{b}_{jk}^{(i)} = \frac{\hat{\mathbf{x}}_k^{(i)} - \hat{\mathbf{x}}_j^{(i)}}{\|\hat{\mathbf{x}}_k^{(i)} - \hat{\mathbf{x}}_j^{(i)}\|}. \quad (5.7)$$

The velocity of displacement is chosen based on the residual error between the current configuration and the measurement as

$$v_{jkl}^{(i)} = \Delta_{j,k,l} - \hat{\Delta}_{j,k,l}^{(i)}. \quad (5.8)$$

From this, the displacement vector of each point in each iteration is determined as

$$\mathbf{d}_j^{(i)} = \sum_{k,l} v_{j,k,l}^{(i)} \mathbf{b}_{j,k}^{(i)}. \quad (5.9)$$

Finally, the new location of each point is calculated

$$\tilde{\mathbf{x}}_j^{(i+1)} = \hat{\mathbf{x}}_j^{(i)} - \alpha \frac{1}{(M-1)(M-2)} \mathbf{d}_j^{(i)}, \quad (5.10)$$

where $(M-1)(M-2)$ is a normalization term and $\alpha \in \mathbb{R}$ is a step-size parameter that is chosen experimentally. After each iteration, the configuration is shifted so that its center of mass coincides with the origin,

$$\mathbf{o}^{(i+1)} = \frac{1}{M} \sum_j \tilde{\mathbf{x}}_j^{(i+1)}, \quad (5.11)$$

$$\hat{\mathbf{x}}_j^{(i+1)} = \tilde{\mathbf{x}}_j^{(i+1)} - \mathbf{o}^{(i+1)}. \quad (5.12)$$

The procedure is repeated until convergence. Criteria for convergence are discussed next.

5.4.3 Convergence and Stopping Criteria

A possible measure for convergence is the Stress function S . Defining a threshold ϵ , convergence can be assumed if $S < \epsilon$. Due to the general non-convex nature of the problem, the proposed MDS procedure is not always guaranteed to converge to the global optimum and might get stuck in a local minimum. Therefore, a second criteria is introduced to measure the change of S

$$R^{(i)} = S(\hat{\mathbf{x}}_1^{(i+1)}, \dots, \hat{\mathbf{x}}_M^{(i+1)}) - S(\hat{\mathbf{x}}_1^{(i)}, \dots, \hat{\mathbf{x}}_M^{(i)}) \quad (5.13)$$

If $R < \delta$ and $S > \epsilon$ the algorithm is assumed to have reached a local minima. A scenario where a local minimum has been reached is depicted in Figure 5.1. These thresholds need to be determined empirically, especially for the case of noisy measurements.

5.4.4 Overcoming Local Minima

The non-convexity of the problem makes it difficult to find a solution within a limited runtime. However, two ideas are offered to help cope with local minima. A simple practical solution to overcome the minima problem, that should always lead to success but is not bounded in terms of execution time, is to restart the algorithm with a new random configuration. In simulations with up to 100 nodes it has been found that the probability of running into local minima is so low that it has always been possible to find the global minima with only one or a very limited number of initializations. Another idea that works for some scenarios is to evaluate a Stress function for individual nodes and interchange the location of nodes that exhibit the strongest stress values.

5.4.5 Numerical Gradient Descent

At this point, an iterative algorithm that minimizes the Stress and thereby finds the locations of the sensors has been fully defined. For comparison purposes the problem will now be formulated in a way that enables one to perform a numerical gradient descent. This is possible with a slight reformulation. Rewriting the estimated TDOAs as a function

$$\hat{\Delta}_{j,k,l}(\hat{\mathbf{X}}) = \|\hat{\mathbf{x}}_j - \hat{\mathbf{x}}_k\|_2 - \|\hat{\mathbf{x}}_j - \hat{\mathbf{x}}_l\|_2, \quad j \neq k \neq l, \quad (5.14)$$

an equivalent formulation of the Stress function as a scalar functional is given by

$$f(\hat{\mathbf{X}}) = \sum_{j,k,l} \left(\Delta_{j,k,l} - \hat{\Delta}_{j,k,l}(\hat{\mathbf{X}}) \right)^2, \quad (5.15)$$

which depends on the vector $\hat{\mathbf{X}} = [\hat{x}_{11}, \hat{x}_{12}, \dots, \hat{x}_{M1}, \hat{x}_{M2}]^T$, $\hat{\mathbf{X}} \in \mathbb{R}^{2M}$ that specifies locations $\hat{\mathbf{x}}_j$ for all the sensors.

The minimizer of

$$\min_{\hat{x}_{11}, \hat{x}_{12}, \dots, \hat{x}_{M1}, \hat{x}_{M2}} f(\hat{\mathbf{X}}), \quad (5.16)$$

also solves the original self-localization problem. A common approach to minimize f is to iteratively perform a gradient descent step, moving in the opposite direction to the gradient

$$\nabla f(\hat{\mathbf{X}}) = \left[\frac{\partial f}{\partial \hat{x}_{11}}, \frac{\partial f}{\partial \hat{x}_{12}}, \dots, \frac{\partial f}{\partial \hat{x}_{1M}}, \frac{\partial f}{\partial \hat{x}_{2M}} \right]^T. \quad (5.17)$$

The gradient descent method starts with a random $\hat{\mathbf{X}}^{(0)}$ value as an initial position guess and iteratively calculates new values by the recursive formula

$$\hat{\mathbf{X}}^{(i+1)} = \hat{\mathbf{X}}^{(i)} - \alpha \frac{1}{(M-1)(M-2)} \nabla f(\hat{\mathbf{X}})|_{\hat{\mathbf{x}}=\hat{\mathbf{X}}^{(i)}}. \quad (5.18)$$

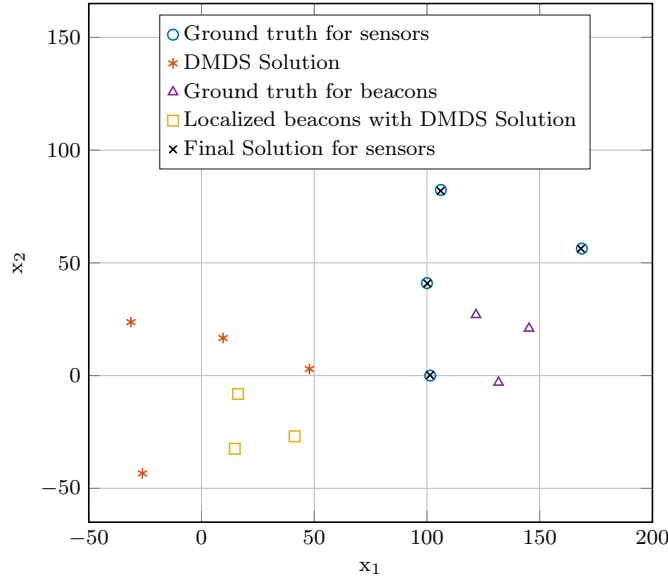


Figure 5.2: The steps of the self-localization and anchoring process visualized. The final solution is obtain using Procrustes analysis on the localized beacons.

As the analytical evaluation of the gradient (5.17) used in (5.18) is impractical for large a number of sensors, another way is to numerically evaluate it in a local region of size $2h$ around each variable $\hat{x}_{j\kappa}$ as

$$\frac{\partial f}{\partial \hat{x}_{j\kappa}} = \frac{f([\hat{x}_{11}, \dots, \hat{x}_{j\kappa} + h, \dots, \hat{x}_{M2}]) - f([\hat{x}_{11}, \dots, \hat{x}_{j\kappa} - h, \dots, \hat{x}_{M2}])}{2h}, \quad \kappa \in (1, 2). \quad (5.19)$$

Similar to the previous algorithm, α has to be determined experimentally and measures for overcoming local minima have to be taken.

5.5 Anchoring

After convergence of the DMDS, a configuration is obtained that exhibits the correct shape of the sensor network, but in general is shifted, rotated and reflected. Therefore, anchoring points at known locations need to be introduced. In practice these can be very inexpensive, constantly transmitting beacons, with no receive capability. They should be placed at a point that is accessible and can be localized with high accuracy using methods from land surveying. For example, in the ATLAS system [24], they are placed on the roof of a bird-watching shelter or in a tree top. For a two-dimensional solution, at least 3 beacons are required in order to find the true locations when using the following approach.

Based on the final configuration obtained from DMDS, the beacons coordinates are estimated as $\hat{\mathbf{x}}_b$ using a TDOA localization algorithm as described in [109]. Other TDOA localization algorithms from the literature might be used as well, which leads to similar results. Note that $\hat{\mathbf{x}}_b$ is relative to the DMDS solution and not to the ground truth. Therefore, in the next step Procrustes analysis is performed [194] to determine an absolute mapping using the approach from Section 5.3 This yields a linear transformation that maps the relative beacons locations $\hat{\mathbf{x}}_b$ to their ground truth \mathbf{x}_b . Finally, the same transformation is applied to the sensor locations in order to find the true locations of the sensors on the global map. Note that due to the dilution of precision problem [132], it is important to have beacons located in the center of the system, otherwise the accuracy of the solution might severely be affected. Each solution step of the process is shown in Figure 5.2. This concludes the self-localization phase; after that the system may enter into its operational state and localize target nodes.

5.6 Simultaneous Anchoring with Weighted Gradient Descend

The previously described anchoring approach that is based on beacon localization followed by Procrustes transformation suffers from the problem that the TDOA algorithms are quite sensitive with respect to erroneous sensor locations. Therefore a comparably small error in the relative solution of the self-localization can possibly result in large errors of the anchoring. An alternative approach is to combine the relative and absolute part of the self-localization by the means of a weighted gradient descend. To approach that, analog to (5.4) and (5.5) define the functions for the measurements between the sensors k, l and the beacons b as

$$\Lambda_{b,k,l} = c * \tau_{b,k,l}, \quad (5.20)$$

$$\hat{\Lambda}_{b,k,l}(\hat{\mathbf{X}}) = \|\hat{\mathbf{x}}_b - \hat{\mathbf{x}}_k\|_2 - \|\hat{\mathbf{x}}_b - \hat{\mathbf{x}}_l\|_2, \quad k \neq l. \quad (5.21)$$

Then a combined objective or Stress function can be defined as

$$f_a(\hat{\mathbf{X}}) = \sum_{b,j,k,l} \left((1 - \beta)(\Delta_{j,k,l} - \hat{\Delta}_{j,k,l}(\hat{\mathbf{X}})) + \beta(\Lambda_{b,k,l} - \hat{\Lambda}_{b,k,l}(\hat{\mathbf{X}})) \right)^2 \quad (5.22)$$

where $\beta \in \mathbb{R}$ is a weighting factor that determines the importance of the relative and absolute portion. The same gradient descend approach given by (5.17) and (5.18) can now be applied to minimize $f_a(\hat{\mathbf{X}})$ and obtain the absolute sensor locations. The weight β has to be chosen empirically and plays a crucial role for the probability of success of the gradient descend to find the global minimum. Intuitively, if β is chosen small, the solution of the relative self-localization problem is emphasized. In many cases this leads to the algorithm being stuck in a local minimum. Therefore, β should be chosen large, i.e., $\beta = 0.9$ to for the gradient descend to find a good absolute solution before converging to the relative locations.

5.7 Self-Localization in the Presence of Clock Offsets

Besides the anchoring issue, another problem in practice is the clock offset ϕ that each sensor's internal clock might experience. The resulting TDOAs are given as

$$\tau_{j,k,l} = \frac{1}{c} \|\mathbf{x}_j - \mathbf{x}_k\|_2 - \frac{1}{c} \|\mathbf{x}_j - \mathbf{x}_l\|_2 + \phi_k + \phi_l + \eta, \quad j \neq k \neq l. \quad (5.23)$$

Again, with the speed of the wave c this directly translates into distance differences. Furthermore, it is assumed that the clock offsets ϕ are constant during the course of the measurement. A solution to remove the offset is to apply the idea of DTDOA as mentioned in Section 3.8.1. For that it is necessary to introduce an additional beacon or references emitter with a known location into the system. One can then subtract the measurement of the reference transmission from each of the other measurements. In the following equations this beacon is denoted by "ref". Moreover, $\Delta, \hat{\Delta}$ and $\Lambda, \hat{\Lambda}$ need to be extended. For the intra-sensor measurements that yields

$$\Theta_{j,k,l} = c * \tau_{j,k,l} - c * \tau_{\text{ref},k,l}, \quad (5.24)$$

and for the sensor to beacon measurements

$$\Omega_{b,k,l} = c * \tau_{b,k,l} - c * \tau_{\text{ref},k,l}, \quad b \neq \text{ref}. \quad (5.25)$$

Analogously to (5.5) define

$$\begin{aligned} \hat{\Theta}_{j,k,l}(\hat{\mathbf{X}}) &= \|\hat{\mathbf{x}}_j - \hat{\mathbf{x}}_k\|_2 - \|\hat{\mathbf{x}}_j - \hat{\mathbf{x}}_l\|_2 \\ &\quad - \|\hat{\mathbf{x}}_{\text{ref}} - \hat{\mathbf{x}}_k\|_2 - \|\hat{\mathbf{x}}_{\text{ref}} - \hat{\mathbf{x}}_l\|_2, \quad j \neq k \neq l, \quad j \neq \text{ref}, \end{aligned} \quad (5.26)$$

$$\begin{aligned} \hat{\Omega}_{j,k,l}(\hat{\mathbf{X}}) &= \|\hat{\mathbf{x}}_b - \hat{\mathbf{x}}_k\|_2 - \|\hat{\mathbf{x}}_b - \hat{\mathbf{x}}_l\|_2 \\ &\quad - \|\hat{\mathbf{x}}_{\text{ref}} - \hat{\mathbf{x}}_k\|_2 - \|\hat{\mathbf{x}}_{\text{ref}} - \hat{\mathbf{x}}_l\|_2, \quad k \neq l, \quad b \neq \text{ref}. \end{aligned} \quad (5.27)$$

based on the configuration of estimated sensor coordinates. Note that the beacon used as a time reference does not simultaneously serve as an anchor for the self-localization. The objective function to be minimized for this case is

$$f_o(\hat{\mathbf{X}}) = \sum_{b,j,k,l} \left((1 - \beta)(\Theta_{j,k,l} - \hat{\Theta}_{j,k,l}(\hat{\mathbf{X}})) + \beta(\Omega_{b,k,l} - \hat{\Omega}_{b,k,l}(\hat{\mathbf{X}})) \right)^2. \quad (5.28)$$

As before β is chosen close to one to avoid a gradient descend approach running into local minima. Empirical numerical studies confirm that the algorithm converges even in this case with DTDOA measurements.

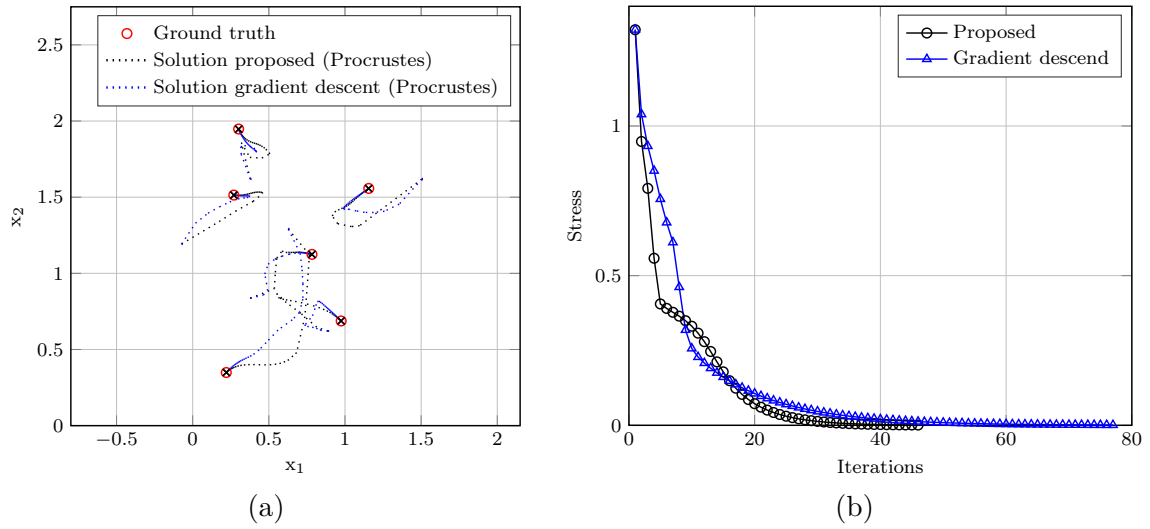


Figure 5.3: Trajectories of the sensor nodes during the iterations of the algorithm (a), together with the Stress functions (b).

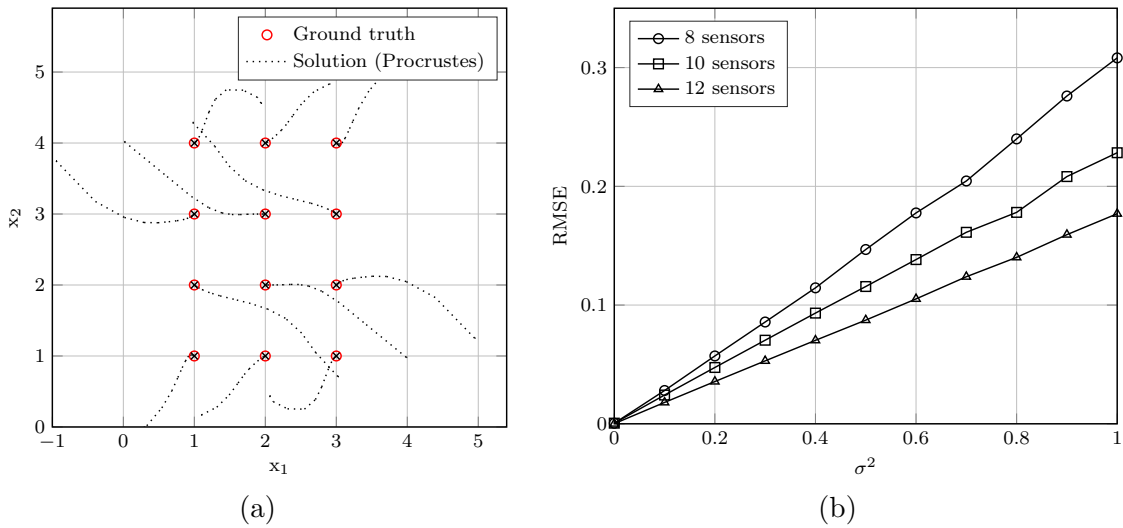


Figure 5.4: A simple scenario to study the behavior with noisy measurements (a). Adding more sensors and thereby more measurements, results in improved robustness of the self-localization against the measurement noise (b).

5.8 Results

After having proposed iterative algorithms for self-localization in TDOA sensor networks, this section presents numerical simulation results in order to investigate and visualize its performance. First a value for the thresholds that are needed to detect convergence of the algorithm has been experimentally determined. Values of $\epsilon = 0.001$ and $\delta = 0.001$ have been found to provide good results. Furthermore, good values for the step size, controlled by α have to be determined. Note that for high values of α , oscillation and divergence of the algorithm can occur. Whereas for very small values of α , the number of necessary iterations becomes large. For all presented results the value of α has been set to 1 in the DMDS and 0.1 in the gradient descend algorithm, which yields a good compromise between stability and speed of convergence.

Two types of experiments have been performed. First the proposed DMDS algorithm has been compared with the gradient descent. The same initial configuration has been used for both algorithms. Figure 5.3 shows an example for 6 sensor nodes and measurements not affected by noise. It can be observed that the trajectories of both algorithms follow a similar path. None of the algorithms has been observed to be always quicker. Repeating the experiment for many different random sensor locations, the convergence times of the two algorithms have been found to be comparable. Similarly, both of the algorithms might run into local minima. However, this doesn't necessarily occur jointly in both algorithms for a certain random instance of locations. In a second experiment the performance under noise conditions has been studied. For that, a regular grid of sensors as shown in Figure 5.4 has been used. The noise $\eta \sim \mathcal{N}(0, \sigma^2)$ on the measurements is increased step wise and the performance in terms of root-mean-square error (RMSE) is observed for different numbers of sensors. It is observed that the algorithm is stable as long as the noise term is reasonably low. Moreover, for the considered sensor placement an increased number of sensors increases the robustness of the system against noise. This can be intuitively explained by the increased number of available measurements.

6 | Experimental Evaluation using Software Defined Radio

For the experimental verification of this thesis, a real-time TDOA localization testbed utilizing a software defined radio framework and GPS based synchronization is presented in this chapter. A distributed software stack enables the localization of unknown signals by transporting the recorded baseband samples of several sensors over a backhaul network for centralized signal processing in a fusion center. To overcome the relatively large drifts of synchronization signals provided by standard GPS receivers, the system is permanently re-calibrated using a stationary reference beacon or alternatively a signal of opportunity. In a further step, the latest generation of low-cost GPS disciplined oscillators is introduced to simultaneously achieve single digit meter accuracy and high update rates necessary for target tracking. The tracking is performed using a KF running on the output of the localization algorithm. Therefore, the dilution of precision studied in Chapter 3 is applied to understand the system performance and improve the tracking. Finally outdoor measurements demonstrating the capabilities of the system are presented.

Parts of the following results have been presented in [9, 10].

6.1 Distributed Software Defined Radio Testbed

Implementation of wide area localization systems utilizing time measurements from electromagnetic waves has been notoriously challenging due to its extreme demands on the synchronization. Nanosecond synchronization accuracy is necessary in order to obtain meter to sub-meter localization performance. The technical challenges and high costs involved in the implementation of such systems is one of the major reasons hindering the research community from experimental work in the area. Using a common clock connected to all distributed sensors results in highly stable synchronization for TDOA measurements. However, such a solution involves a tremendous amount of cabling, very long setup times and large costs for a permanent installation. In a research environment, especially the long setup times can lead to the infeasibility of various experiments, e.g. if there is a time limitation of a single day. Consequently, it is desirable to work towards self-contained wireless sensor units. One approach to achieve this is to use distributed

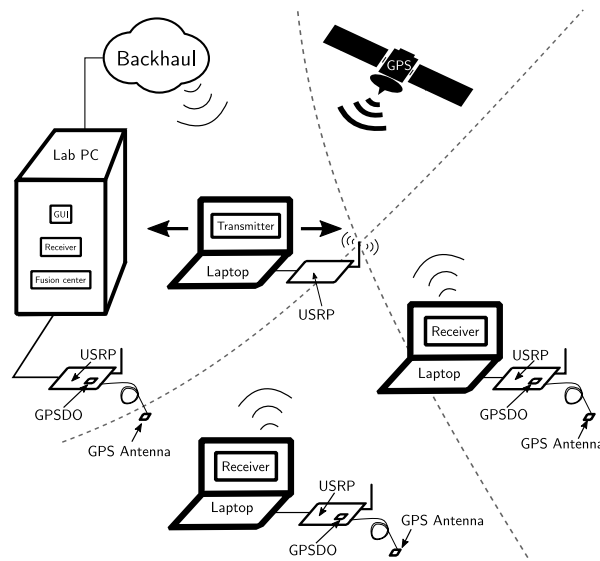


Figure 6.1: Exemplary setup of the testbed with WLAN backhauling. Receiver clocks are synchronized using GPS.

synchronization, e.g., based on GPS signals and a wireless backhaul solution. Another aspect in the design of a localization testbed is the choice of the underlying technology. The computer science community regularly follows the approach to use standardized technology such as the IEEE 802.11 WLAN family, sometimes with slight modifications to the device driver. While this approach leads to fast, reliable and cost effective results by abstracting away most of the physical layer signal processing from the researcher, it also sets very tight limits to the physical layer design space. Therefore, the electrical and communications engineering community often decides to utilize SDR, e.g., using GNU Radio [6], as the basis of system design. This allows for highly increased freedom in the design of RF waveforms for localization research. Figure 6.1 depicts the setup of a distributed localization testbed based on SDR.

In the literature, several systems have been presented [196, 197, 198, 199, 200]. These solutions either use a common clock or exhibit large errors caused by insufficient synchronization, often in the order of 100m or more. Further, some system are missing real-time capabilities and only support offline signal processing of recorded signals. One goal of this thesis is to show how recent developments in SDR and GPS synchronization technology enable the implementation of affordable real-time TDOA-based localization systems. The developed system is able to achieve single-digit meter accuracy without the use of a common clock. To achieve this goal, sensor synchronization in the order of ± 5 ns is necessary. Related to this, two types of GPSDOs with different performance have been studied. For the first type, additional beacon signals are necessary to achieve an acceptable performance. This approach is similar to the one in [24] developed at the same time. Using the second type GPSDO, currently a last generation state-of-the-art device, it is possible to obtain the same performance without the help of beacon signals. In [16], various related approaches for localization system synchronization are described;

however, it is based on proprietary technology not easily available to civil research. To further improve the results our system performs tracking of the emitter location using a KF.

6.2 System Architecture

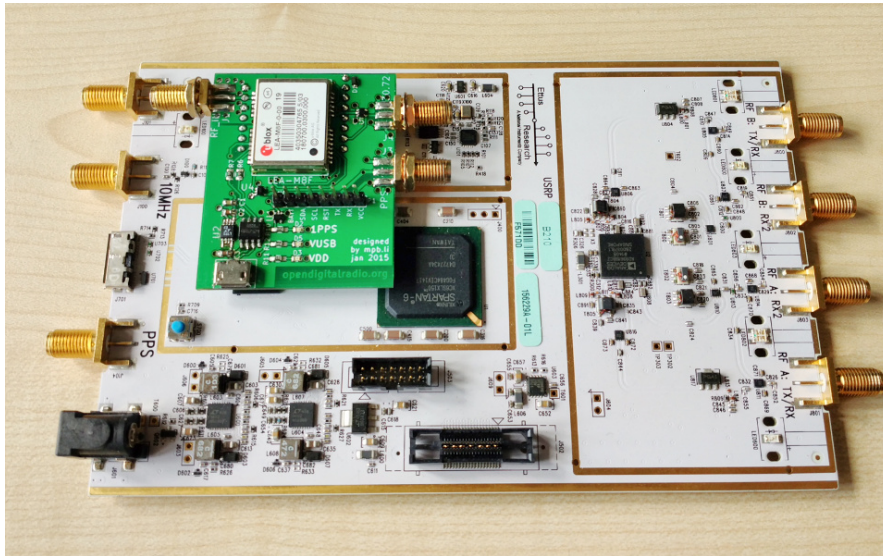
The presented localization system is implemented based on the SDR methodology. This includes hardware for basic radio frequency and baseband signal processing and software to perform the major part of the digital baseband signal processing.

6.2.1 Hardware

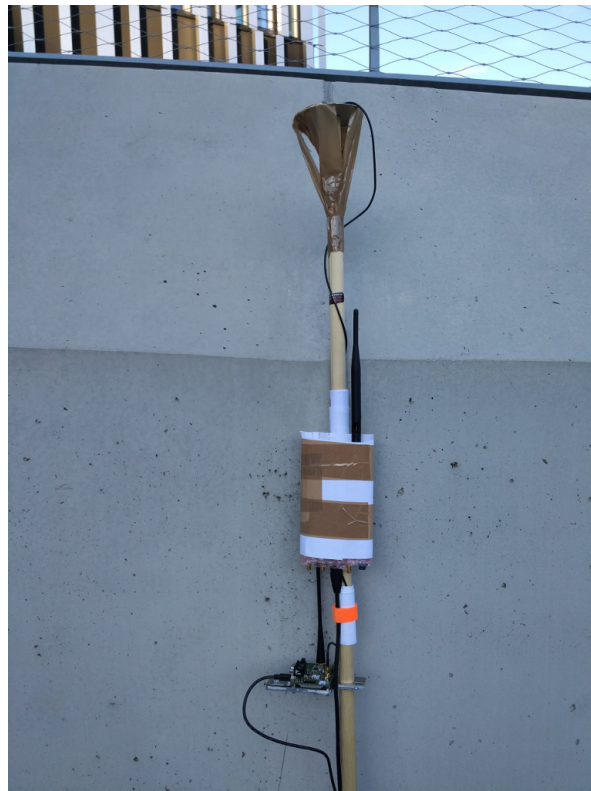
The baseline configuration of the system, as shown in Figure 6.1, uses three receiver nodes and one transmitting target node that shall be localized. Each node consists of a RF front-end and a computer running the SDR framework. The RF front-ends Ettus USRP B210, shown in Figure 6.2 (a), are able to deliver complex samples at a rate of up to 56 million samples per second. In order to enable time synchronization the receiver nodes additionally need a GPSDO that provides a clock signal for the front-end and a pulse per second (PPS) synchronization signal. Two devices have been evaluated, namely the LCXO manufactured by Jackson Labs Technologies and the u-blox LEA-M8F. Both can be plugged into the USRP B210 RF front-end. By default the USRP B210 is designed to receive a LCXO GPSDO, in order to mount the LEA-M8F a PCB specifically designed for that purpose [202] has been used. Note that the driver for the USRP B210 has to be patched in order to support the LEA-M8F. To improve mobility, laptop computers are used. With that is possible to power the RF front-end as well as the GPSDO through the laptop battery. Furthermore, the system needs a backhaul network in order to communicate the baseband samples of the receiver nodes. This is achieved either by Ethernet or IEEE 802.11 WLAN. When using WLAN, the nodes are completely self-contained and wireless, operation is only limited by the capacity of the laptop battery. To build the transmitting target object, that is to be localized, another USRP B210 is mounted on a long staff. Using SDR for transmission full flexibility in the choice of the transmitted signal is maintained.

6.2.2 Software

The software part of the localization system consists of four components: transmitter, receiver, FC and graphical user interface (GUI). A signal is created and transmitted by the transmitter component and several receiver components acquire the samples in a synchronized way. Those parts are implemented with the GNU Radio SDR framework [6]. For the transmitted signal BPSK as well as OFDM modulated signals are



(a)



(b)

Figure 6.2: (a) The RF front-end (Ettus USRP B210, white) with a last generation embedded GPSDO mounted (u-blox LEA-M8F, green) for time synchronization with other distributed nodes. (b) Staff used as target. GPS antenna for the RTK ground truth measurement on top, USRP B210 RF-frontend in the middle, GPS RTK receiver at the bottom.

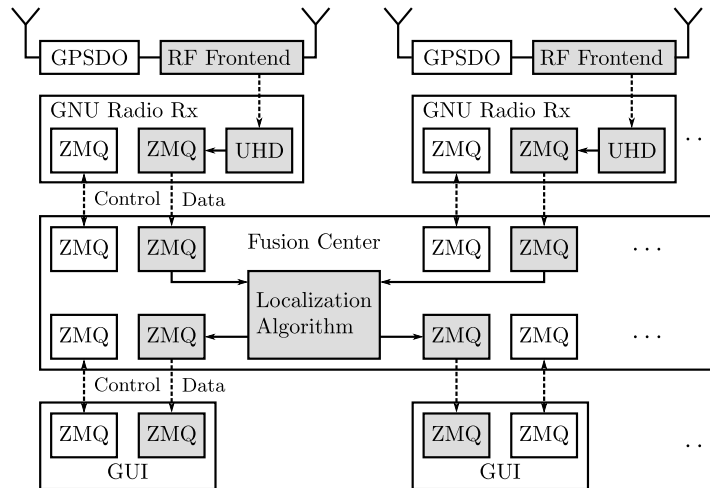


Figure 6.3: The distributed system architecture is based on GNU Radio [6] and ZeroMQ [201], the signal processing path is depicted in gray, the control path in white.

used. Baseband samples are then sent from the receivers to the FC using the ZeroMQ library [201]. Signal processing block supporting this messaging library have been integrated into the GNU Radio project. ZeroMQ is also used to communicate all necessary control commands from the GUI to the FC and from there to the distributed receiver nodes. For that purpose a remote procedure call (RPC) scheme has been implemented. Figure 6.3 gives an overview of the interconnections among the system components. The signal path is depicted in gray, it uses a streaming signal processing approach, the control path is depicted in white. The final result is sent back to the GUI and displayed to the user as shown in Figure 6.4.

System operation consists of two phases; initially all sensors have to be exactly synchronized to UTC as provided by the GPSDO. This is crucial, because for TDOA localization samples have to be acquired exactly at the same time. In the second phase, localization can be performed. For that, a start command is issued from the GUI. Subsequently, the FC orders all sensors to start continues reception of the target signal. As the system shall be able to localize unknown signals it is necessary to transport baseband samples to the FC. Due to capacity limitations in the backhaul each sensor takes snapshots, e.g., 1000 samples in each acquisition. The solution for the location is then calculated for each snapshot in the FC. Afterwards, all results are transmitted to one or more graphical user interfaces. Note that all software components can run independently on different computers in the network. In principle the number of receivers and GUIs is not limited.

With the LCXO GPSDO the update rate is limited by the necessary synchronization calibration process described in the next section. In that case the framework is able to obtain signal snapshots at a rate of 0.66 Hz. As explained later with the LEA-M8F GPSDO calibration requirements are relaxed, the update rate is 2 Hz and could be

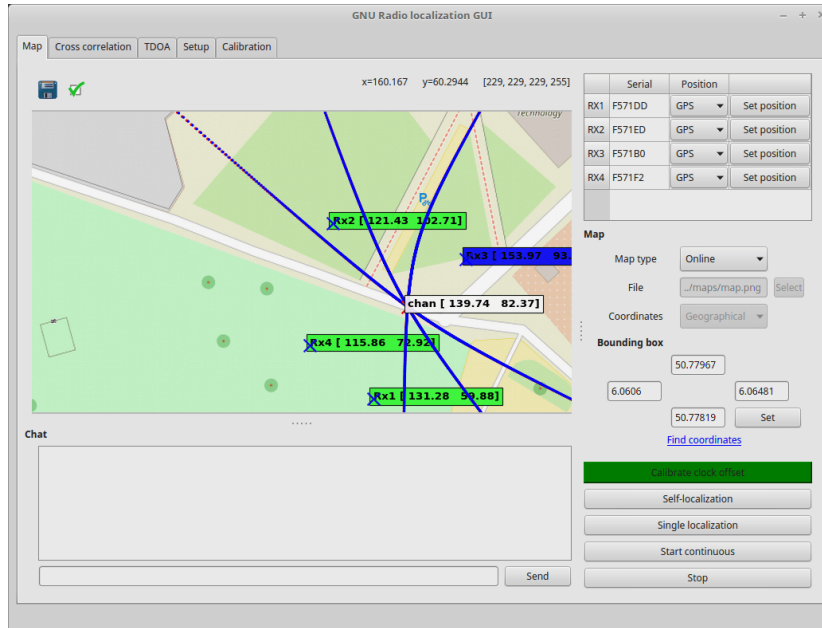


Figure 6.4: Graphical user interface of the localization testbed. Map data is obtained from OpenStreetMap [182]. Tracking performed using the algorithm of Chan [109] together with the KF described in Section 3.7.

increased further by optimizing the software of the FC and GUI components and the backhaul capacity.

6.2.3 Coordinate Systems

In order to display localization results in the framework, they need to be drawn on a map. Assuming that the region of interest is fairly small, internally, two dimensional Cartesian coordinates are used for calculation of the sensors and the target location. Smaller maps, for example building floor plans are often available in Cartesian coordinates and can therefore be used in a straightforward way as long as the scale and the offset between the internal coordinate system and the map is known. However, if common maps of the earth surface should be used, a global coordinate systems needs to be adopted. One prevalent system is World Geodetic System 1984 (WGS84), which is well known due to its usage in GPS. When working with the GPSDO or ground truth as described in Section 6.4.1, WGS84 is used. For displaying the map itself a projection of the three dimensional to two dimensional Cartesian coordinates is necessary, in this case from WGS84 to a transversal Mercator projection. To plot the results of the localization and the sensors the internal coordinate system is then aligned with the transversal Mercator projection of the map. In the framework the Matplotlib Basemap toolkit [203] has been used for this purpose while map data is obtained from the OpenStreetMap project [182].

6.3 Synchronization

Synchronization plays a major role in time-based localization. In fact in passive TDOA localization it is arguably the single most difficult problem in practice if no common clock approach based on wires is used. If each sensor is primarily using its own local clock, synchronization has to be carefully implemented to approach the physical possible limits. Besides the issues of the local oscillator, in wireless synchronization, signals are affected by external influences such as RF interference and multipath propagation effects. With some COTS sensor hardware, synchronization can be suboptimal due to limited access to the clock configuration parameters or timestamps. Exact timestamps for the signal samples with nanosecond accuracy are necessary if global systems synchronization is desired. Assuming a good synchronization scheme, e.g., as described in Section 3.8, the performance of the localization system is limited by the quality of the oscillators. Therefore, an understanding of clock characterization is necessary for a good system design.

6.3.1 Receiver Clock Characterization and Allan Deviation

Most electronic RF hardware uses one of three types of clocks

- **Temperature compensated crystal oscillator (TCXO):** the most critical issue for oscillators is their dependency on temperature, therefore this type of oscillator internally contains a voltage controlled crystal oscillator (VCXO) and compensates its temperature induced frequency change by adjusting the control voltage accordingly.
- **Oven controlled crystal oscillator (OCXO):** this type of oscillator is an improvement over the TCXO. With the oven it heats up the crystal oscillator to a higher temperature than the environment and then keeps the temperature constant using a control loop.
- **GPS disciplined oscillator (GPSDO):** this is a combination of a GPS receiver and either a TCXO or OCXO. It achieves short term stability from the local crystal oscillator and long term stability through the GPS time signal.

More stable oscillators such as Rubidium or atomic clocks are very uncommon in COTS hardware due to the high cost and large form factors. These types of oscillators are mostly limited to laboratory and measurement equipment. Due to basic physical limitations in the manufacturing process and additional aging effects, all clocks, even of the exact same type, exhibit errors in their nominal operating frequency that directly translate into time errors. This error is randomly Gaussian distributed with respect to different clocks. For typical clocks used in electronic circuits it is measured in parts per million (ppm), or for better clocks in parts per billion (ppb). TCXOs are usually available with an accuracy in the order of 0.5 to 20 ppm while an OCXO may achieve

20 ppb. Additionally, the clock frequency experiences a drift or wander of the frequency over time, e.g., due to temperature changes. The direct output of the oscillator also exhibits so called phase noise, in time domain called jitter. These are short term, usually Gaussian distributed, fluctuations of the oscillation around the nominal value.

As the receiver clocks play such an important role in the reception process underlying the TDOA measurements, it is important to have a tool to characterize them. The distribution of the time dependent error is non Gaussian, therefore simple variance estimation is insufficient to characterize the clock stability. For that reason, the Allan deviation and its extensions have been developed [204]. Given the time series of frequency error measurements of a clock

$$y_i = \frac{f(t) - f_0}{f_0}, \quad (6.1)$$

and its average

$$\bar{y}_j = \frac{1}{\tau} \sum_{i=0}^{M-1} y_i, \quad (6.2)$$

the Allan deviation is defined as

$$\sigma_{\text{AVAR}}(\tau) = \sqrt{\frac{1}{2(N-2)\tau^2} \sum_{j=1}^{N-2} (\bar{y}_{j+1} + \bar{y}_j)^2}. \quad (6.3)$$

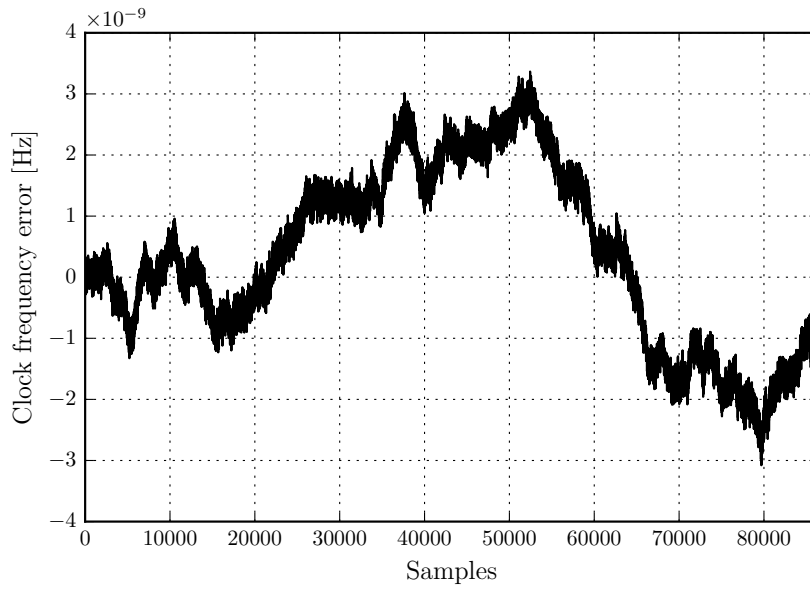
The frequency error can be modeled as a combination of a white noise process $w_i \sim \mathcal{N}(0, \sigma_w^2)$ and a random walk b_i , also known as brown noise

$$y_i = w_i + b_i. \quad (6.4)$$

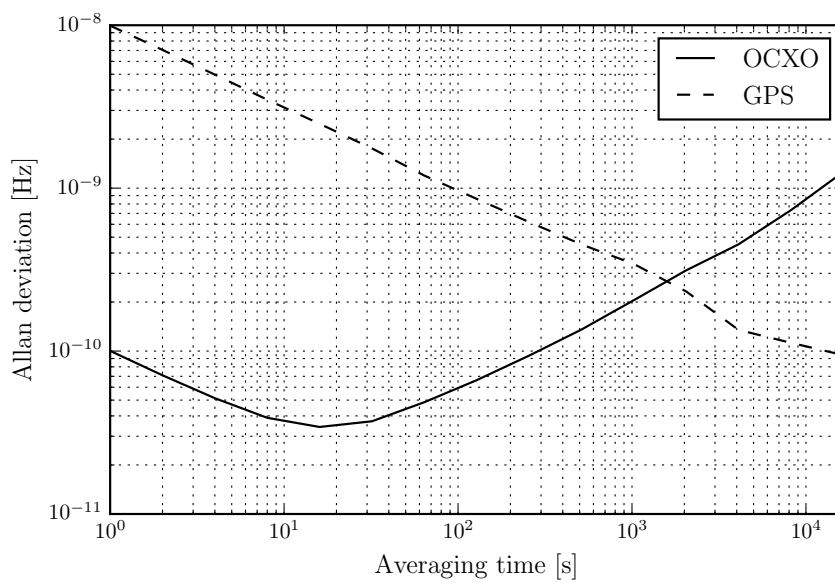
The brown noise can be iteratively derived from a second white noise process v_i as

$$b_i = b_{i-1} + v_i, \quad (6.5)$$

where $v_i \sim \mathcal{N}(0, \sigma_b^2)$ and $b_{-1} = 0$. Figure 6.5 shows the time frequency error series and the Allan deviation plot of a simulated typical 10 MHz OCXO. It can be seen that for averaging intervals below 10 seconds the deviation decreases; the clock frequency is relatively stable during such a short interval and dominated by the white noise process. Beyond that, for longer averaging times the wandering effect begins to dominate and the Allan deviation deteriorates. If such type of clocks are used in precise localization applications, clock error correction should be performed at a rate of less than the 10 seconds. If several updates are available during this interval, they might be averaged to improve the results. A way to improve the long term stability of the oscillator is to combine it with the GPS signal, which provides a relatively stable time for long averaging intervals. Hence, as explained in the following section, a combination of an OCXO with short term stability and the GPS signal with long term stability can provide a very accurate solution for distributed sensor synchronization.



(a)



(b)

Figure 6.5: Typical Allan deviation as expected from an OCXO and a GPS (b) with the corresponding frequency error measurements of the OCXO (simulated) over a course of one day (a).

In practice, the measurements that are necessary to calculate the Allan deviation are taken with respect to a reference clock that is usually of a higher quality than the clock under investigation. The outputs of both clocks are directly taken to obtain (6.1). Another way to characterize the clocks in a localization system is to record TOAs or TDOAs from a stationary transmitter. A comparison of different clocks based on this measurement setup is shown in Figure 6.6. One of the receivers uses a GPSDO and the second one uses the clock as specified above the plots. The nominal TDOA should be close to zero as the distance between the transmitter and the receiver is the same. Nevertheless, for all clock types a drift can be observed. Note that the GPS receiver used in this experiment does not support a timing mode. The differential plot shows the difference between consecutive TDOAs, this is useful to observe the error in the clock rate between the different clocks.

6.3.2 Synchronization Using GPS

In practice, when trying to achieve high accuracy in a TDOA-based localization system, two major challenges clearly stick out, synchronization and multipath propagation. Multipath propagation is out of the focus of the experimental part of this thesis but has been partially examined in Section 4.3.

Technically, difficulties in sensor node synchronization mainly arise due to their wide spatial separation. In this regard, aiming for a wireless synchronization method to avoid the logistic effort associated with a cabled common clock system, GPS based synchronization has been chosen in this thesis as one option. This is achieved by equipping each sensor with a GPSDO. The GPSDO disciplines the local oscillator using a PPS time pulse derived from the GPS signal. This can be achieved by a phase locked loop (PLL) and voltage control of the oscillator. In the PLL, the clock cycles of the local oscillator are divided or counted, then compared against the GPS time pulse and ultimately a control voltage is modified in order to increase or decrease the clock rate and bring the error of the comparator to zero. Additionally, it is necessary to filter and weight the local oscillator signal and the GPS time pulse based on their particular distribution. This differs for different types of oscillators and GPS receivers. A good approach for combining the GPS time pulses and the local oscillator signal is described in [205]. As the GPS timing signals are based on UTC, all the clocks in the sensor network can be globally synchronized in an absolute sense. Each GPSDO outputs a clock signal, e.g., 10 MHz and the PPS signal. The clock signal is used to drive the digital and analog circuits of the RF front-end, while the PPS signal is used to control the synchronized operation. In practice, a GPSDO is build from at least some discrete components as it is not possible to integrate a highly accurate oscillator into the digital signal processor (DSP) ICs. Figure 6.7 depicts the two latest generations of GPSDOs. Due to the proliferation of small cell base stations, there exists a rising demand for such devices. In order to enable mass production, the third generation therefore uses a cost effective, as much as possible integrated design. Fortunately, this

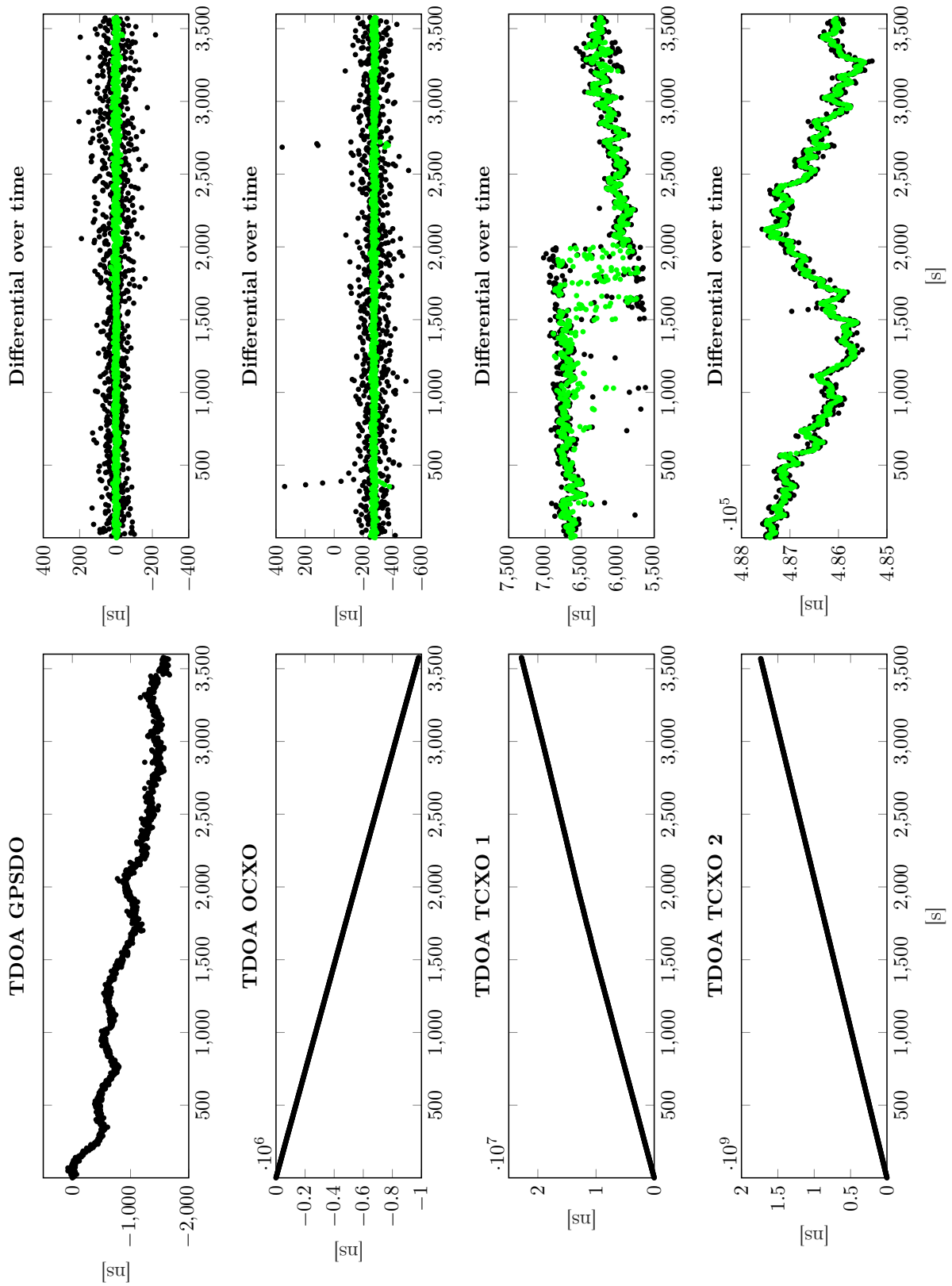


Figure 6.6: Comparison of different receiver clocks. Reference in one of the receivers is a GPSDO. Green values are averaged over 10 seconds.

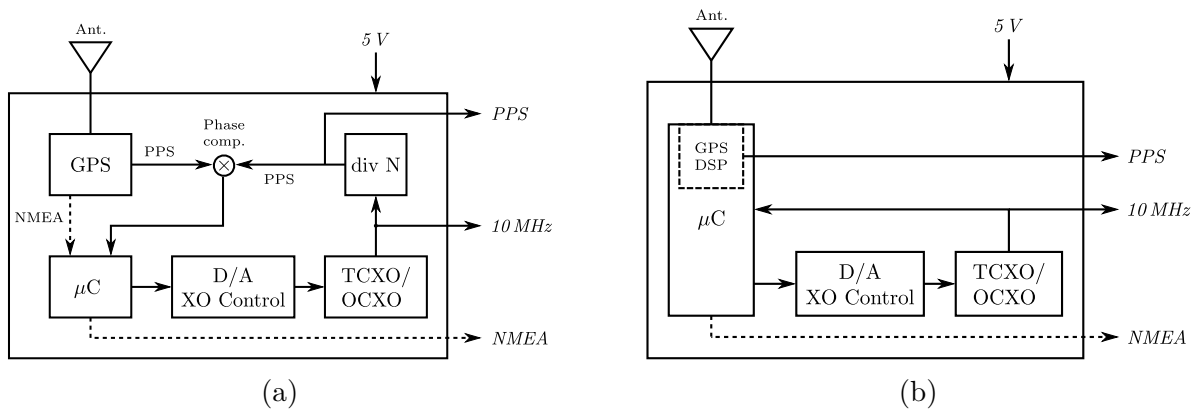
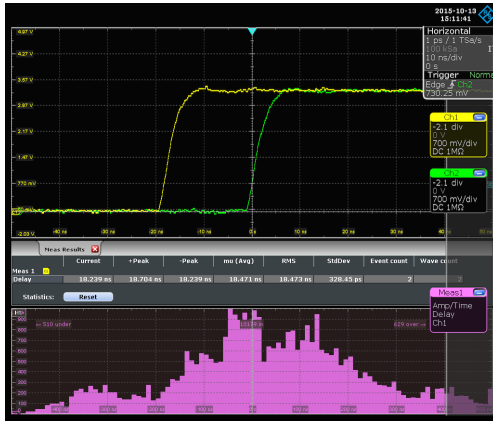


Figure 6.7: Different generations of GPSDOs [206]. (a) Second generation design as used by the LCXO. (b) Third generation design with integrated GPS DSP, micro-controller (μC) and PLL. This is used in the ublox LEA-M8F.

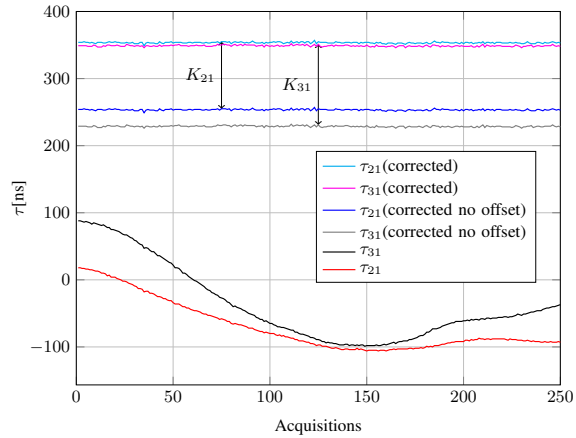
enables a joint configuration of the micro-controller and the GPS DSP which in the case of the ublox LEA-M8F enables the activation of the so-called time mode and a large number of further parameters such as the selection of supported satellites, supported constellations and an elevation mask.

To achieve synchronization in a SDR system typically two steps are necessary. First, the RF front-ends have to be synchronized to UTC on a hardware level. Note that due to latencies in the link between RF front-end and the host computer and the impact of the operating system, it is not feasible to perform the synchronization purely in software on the host side. Hardware level synchronization is indispensable to achieve synchronization in the order of nanoseconds. Second, once synchronization of the RF front-ends has been achieved, a command can be issued to all sensors to start the recording of baseband samples at an absolute point in time. Typical SDR frameworks such as GNU Radio [6] provide application programming interfaces (APIs) for both steps. Timestamps associated with the recorded samples enable the FC to check for consistent synchronization over the course of the system operation time. Assuming a proper implementation of the synchronization APIs, the performance for the TDOA localization is limited by the GPSDO performance as well as the signal-to-noise ratio of the transmitted signals. It is therefore important to study the synchronization problem on different levels.

First, one can directly measure at the PPS outputs of the GPSDOs. GPSDO performance has been studied in [207] and [208]. Under good conditions a standard deviation of 50 ns for the GPS time estimate can be expected for standard receivers like the one contained in the LCXO GPSDO. However, for TDOA it is necessary to take differential measurements between two synchronized receivers, which considerably increases the error. Accordingly, an oscilloscope connected to two different GPSDO PPS signals is used to plot the histogram of the difference. A measurement screenshot is shown in Figure 6.8(a). In this case the GPS antennas have been placed on the window shelf of



(a)



(b)

Figure 6.8: Drift of GPS based synchronization used for the distributed receiver nodes, measured with (a) an oscilloscope and (b) with the TDOAs of a stationary target, sample rate 50 MS/s, interpolation factor 10, signal bandwidth 5 MHz.

the laboratory which clearly deteriorates the performance compared to a clear sky-view.

Second, the TDOAs are usually estimated by finding maxima of the cross-correlations of the different sensor outputs. In Figure 6.8(b) the effect of the GPSDO drift on the TDOA estimation is depicted. If a correction is applied as explained in the next section and the drift is corrected, a good measure for the noise induced error distribution of the TDOAs is a histogram as shown in Figure 6.10 which has been obtained under clear sky-view conditions.

Third, subsequently, an algorithm such as [109] is used to calculate the location. The blue track in Figure 6.9 shows how the drift in the synchronization translates into a drifting localization result of a non-moving object. The experiment involves 3 sensors and the resulting error is in the order of 50 meters.

6.3.3 Hybrid Synchronization with GPS and a Reference Emitter

In order to overcome the GPS synchronization issues two approaches are introduced. The first approach is to use an additional signal from a stationary source to permanently re-calibrate the system. This is a hybrid approach as it uses the time synchronization ability of the GPS signals, as well as the calibration or reference emitter signal. This calibration signal can be a beacon signal such as in [24] or alternatively a signal of opportunity from a local broadcasting station, e.g., Digital Audio Broadcasting (DAB), Digital Video Broadcasting - Terrestrial (DVB-T), which is commonly seen by all sensors. If the signal of the emitter to be localized is a known and a multiple access method

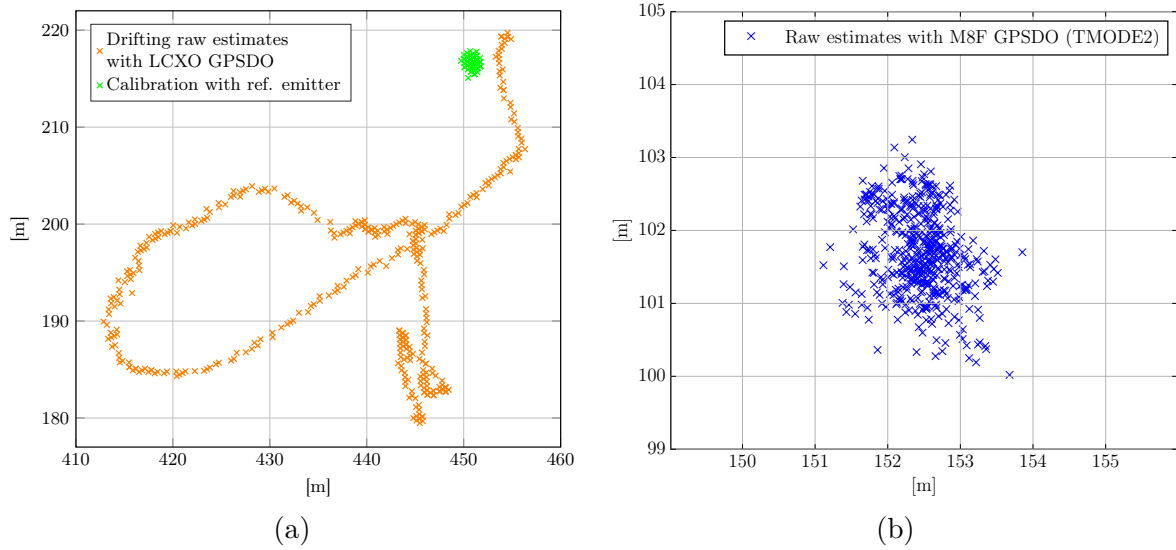


Figure 6.9: (a) Drift in the estimated location of a *stationary* object induced by drifting synchronization from LCXO GPSDOs (orange). Using automatic hybrid calibration with an additional beacon signal, the green result can be achieved. (b) When coordinates in the GPSDO are fixed and only time is estimated, synchronization results can be improved significantly. Results are slightly better than the hybrid approach.

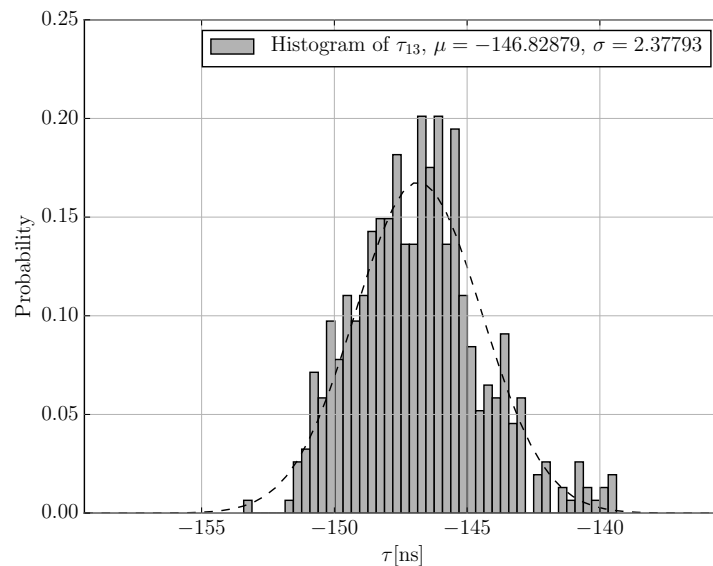


Figure 6.10: Histogram of the TDOA between two sensors with LEA-M8F GPSDO.

exists, the calibration signal can be transmitted in-band. This approach is followed by [24] for example. However, in the present case the no accurate knowledge about the target signal is assumed. This particularly means that controlled access to the channel is not possible. Therefore, it is necessary to use an out-of-band calibration signal and re-tune the sensors between the calibration and the target signal. Otherwise, the calibration signal might introduce unwanted interference on top of the target signal. Due to hardware limitations, this re-tuning leads to a limited acquisition and update rate of the system. The calibration procedure for TDOA can be described in the following way. The measured TDOAs $\hat{\tau}_{ij}$ are erroneous

$$\hat{\tau}_{ij} = \tau_{ij} + e, \quad (6.6)$$

where the error e contains a deterministic offset due to the synchronization error and a Gaussian noise component due to the measurement in the receiver. The deterministic part is estimated by comparing the TDOAs of the beacon calibration signal with its expected TDOA

$$e = \hat{\tau}_{ij}^b - \tilde{\tau}_{ij}^b \quad (6.7)$$

If the location of the calibration signal is erroneous, this results in a constant offset K_{ij}

$$\tilde{\tau}_{ij}^b = \tau_{ij}^b + K_{ij} \quad (6.8)$$

That means even if the location of the calibration emitter is unknown, the system can be calibrated by determining the constants K_{ij} using additional ground truth information. The GUI of our system includes a feature for that purpose. To perform this calibration it is necessary to take measurements with the target emitter placed at a known location. In Figure 6.9, it can be seen (green plotted points) that the calibration algorithm is able to keep the synchronization error within about ± 2 samples of the expected values and the corresponding localization error within a few meters.

A second approach, that works without calibration signals is to use a specific time mode available in certain GPS receivers. GPS receivers calculate a 3 dimensional position and the time using the signals of at least 4 satellites [2]. The largest error in this process arises from the propagation of the satellite signals through the ionosphere. This sets a natural limit to the performance of single frequency GPS receivers and thus to the accuracy of the emitted time pulse and causes the drift in the measurements as described above. An effective solution to this problem is to exclude the GPS receiver position from the equations. Obviously, this is only possible in timing applications such as the described localization system, where the GPS receivers are stationary and the position is very well known. When the time mode is used it can be observed that the standard deviation of the time pulse can be decreased up to one order of magnitude. The results in section 6.4 have been obtained with the LEA-M8F and the time mode enabled.

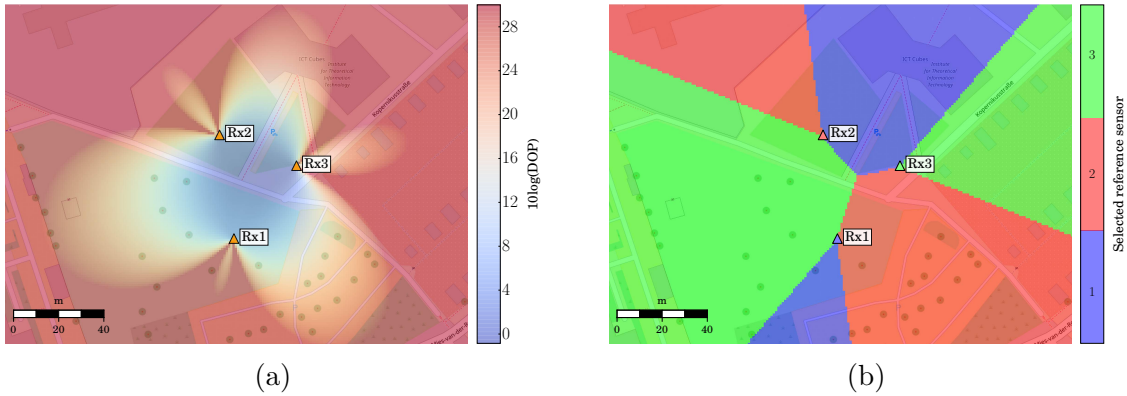


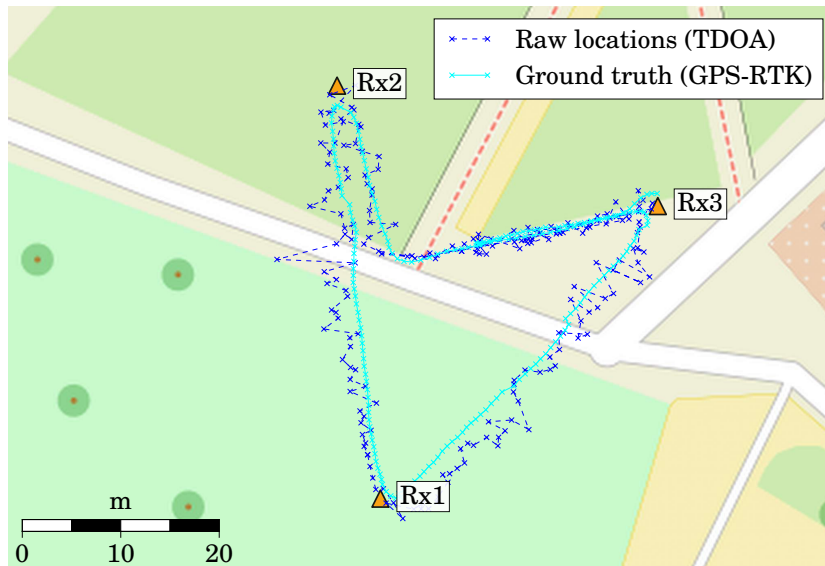
Figure 6.11: DOP analysis of the sensor setup used in the experiment with reference receiver selection (a). Optimum reference receiver selection (b), depending on the target location and based on the criteria in (3.57).

6.4 Measurement Results

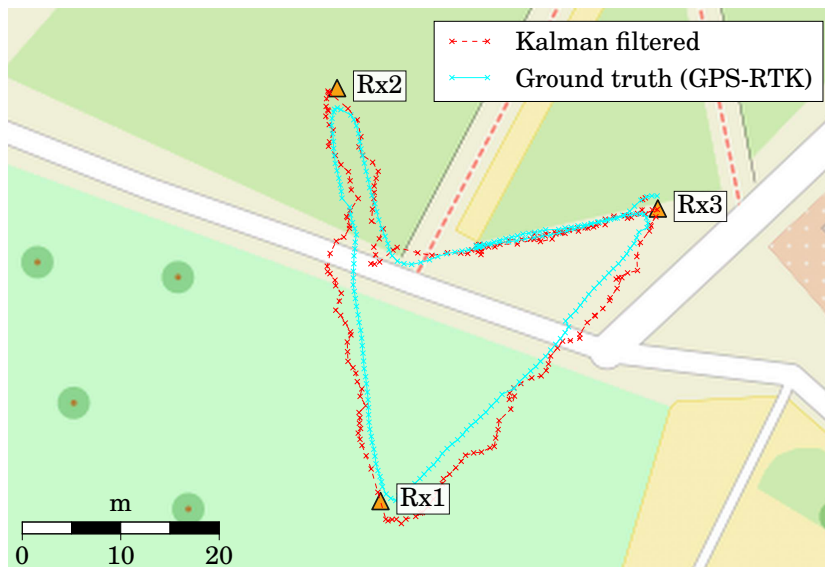
In the following Section, some selected measurement result are presented. The measurements have been obtained in an outdoor experiment series in a small park next to the university building of the author’s institute. Due to the large logistic effort, all experiments have been constraint to 3 and 4 sensor configurations.

6.4.1 Obtaining Ground Truth

The problem of obtaining highly accurate ground truth is solved using GPS Real Time Kinematic (RTK) technology [32]. RTK is a type of differential GPS that is based on carrier phase measurements. In good conditions, i.e., clear sky-view without multipath, it has an accuracy of $\pm(2-3)$ cm. A RTK system consists of two units, the base station and the rover. Both have to be connected to each other by a datalink to enable the calculation of the differential solution in the rover. The high achievable accuracy is based on the fact that the estimation of the carrier phase is possible with a very high accuracy. However, the carrier phase measurements are ambiguous, i.e., for a range estimate it is necessary to exactly know how many integer wavelength lie between the satellite and the receiver antenna. For RTK specific algorithms [209, 210] have been developed to efficiently resolve this integer ambiguity. Nevertheless, this is a difficult, combinatorial problem and in practice a single frequency GPS requires several minutes in order to resolve the ambiguities and obtain a fix. A library and set of tools called *RTKLIB* [33] provided initial affordable access for research to RTK and is regularly used. Though, for the presented results, primarily the very recently released u-blox C94-M8P has been used. This is an affordable fully embedded solution including a base station, rover and ultra high frequency (UHF) datalink. To obtain the absolute location of our RTK base station with centimeter accuracy, *SAPOS* [211] is used, the German



(a)



(b)

Figure 6.12: Localizing a walking pedestrian. The ground truth from the GPS-RTK is plotted in cyan. Raw localizations in (a) and the output of the KF in (b).

network RTK solution operated by the government. For this initial survey, SAPOS acts as a virtual RTK base station and one of our RTK capable receivers takes the role of the rover. This yields an exact absolute reference point. Afterwards, the RTK base station is placed on the surveyed point and the RTK rover together with the target emitter on the staff, such that the ground truth can always be accurately determined. In order to ensure proper working of the RTK rover, it is very important to have the GPS antenna mounted on a ground plate on top of the staff with unobstructed sky-view. The carrier phase measurements necessary for the RTK are highly susceptible to multipath reflections, a human body close to the antenna of base station or rover is sufficient to prevent the functioning of the system. The resulting setup is depicted in Figure 6.2 (b).

6.4.2 Pedestrian Tracking

With the ground truth recording problem solved, the system has been used to track the movement of a pedestrian. The measurement area has been about $50 \times 50 \text{ m}^2$ in size. A number of 3 sensors has been used, connected to the FC with a WLAN backhaul. The exact locations of the sensor antennas have been obtained with the RTK reference and the GPSDOs have been set to time mode. Signals transmitted by the target were binary phase shift keying signals with a bandwidth of 50MHz. The receiver bandwidth has been set to 50MHz with a subsequent lowpass filter. The received signals have been interpolated by a factor of 10. Finally the value for σ_τ , for the KF measurement noise has been measured as $3.16 \times 10^{-9} \text{ s}$ with a stationary target in the middle of the area. For pedestrian tracking, a good value for the KF process noise standard deviation σ_a has been determined experimentally to be 0.41 m/s^2 and the correlation coefficient $\rho = 0.15$. The measured tracks are shown in Figure 6.12. The root-mean-square error compared to the RTK solution is 2.27 m for the raw localizations and 1.64 m for the Kalman filtered result.

6.4.3 Sensor Self-localization

In this section the SDR implementation of the DMDS algorithm presented in Chapter 5 is discussed. The theoretical analysis of the algorithm assumes perfect synchronization between the sensors. In practice, this is often not given. Therefore an extension to asynchronous clocks and the use of a calibration receiver in the self-localization scenario, similar as in Section 5.7 is of interest but not within the scope of the experiments. Hence, during the self-localization experiment all sensors have been synchronized using the LEA-M8F GPSDO based on the surveyed locations from the RTK reference. This enables an exact comparison of the self-localization result with the ground truth. As opposed to target localization in two dimensions, the TDOA-based self-localization requires a minimum of four sensors. Additionally, three anchors with absolute coordinates need to be provided. Fortunately, the anchors do not have to transmit simultaneously

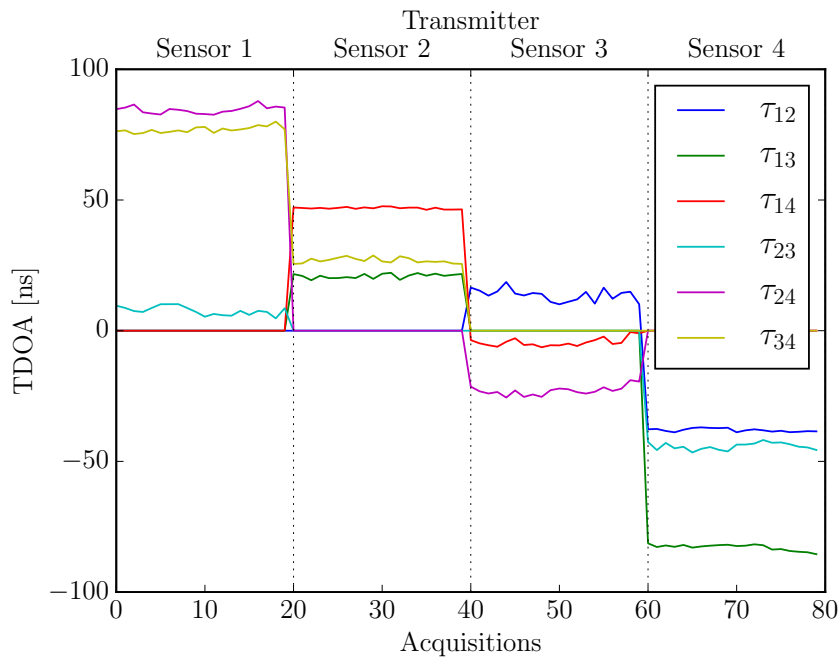


Figure 6.13: Measurements of the TDOAs between all triples of sensors. To obtain this, each sensor consecutively transmits a signal in a non-overlapping fashion.

and can therefore be emulated by a single mobile node. This also makes sense in commercial deployment of such a system because it is unnecessary to maintain three beacons after the self-localization procedure has been completed. In the described experiment, the role of the anchors has been taken by the target staff from the previous experiment. It carries the signal source as well as the RTK reference antenna needed for the determination of the anchor's global coordinates. Obviously the anchoring with a single transmitter has to be performed in a sequential fashion. A typical setup of the system consists of the following steps:

1. Place at least four sensors at arbitrary points in the region of interest.
2. Perform the measurements among the sensors, for this, each sensor has to transmit a signal in a round robin fashion.
3. Perform the measurements between anchors and sensors, this requires the anchor to be placed at three exactly surveyed coordinates.
4. Calculate the self-localization solution.
5. Switch to standard localization mode where the obtained sensor locations are used to localize targets.

For the self-localization TDOA measurements among all combinations of sensors are necessary. The transmission protocol used for this is a simple time division duplex approach. Controlled by the FC, one of the sensors, depending on its identification number, receives the command to begin a continuous transmission. Shortly after, all

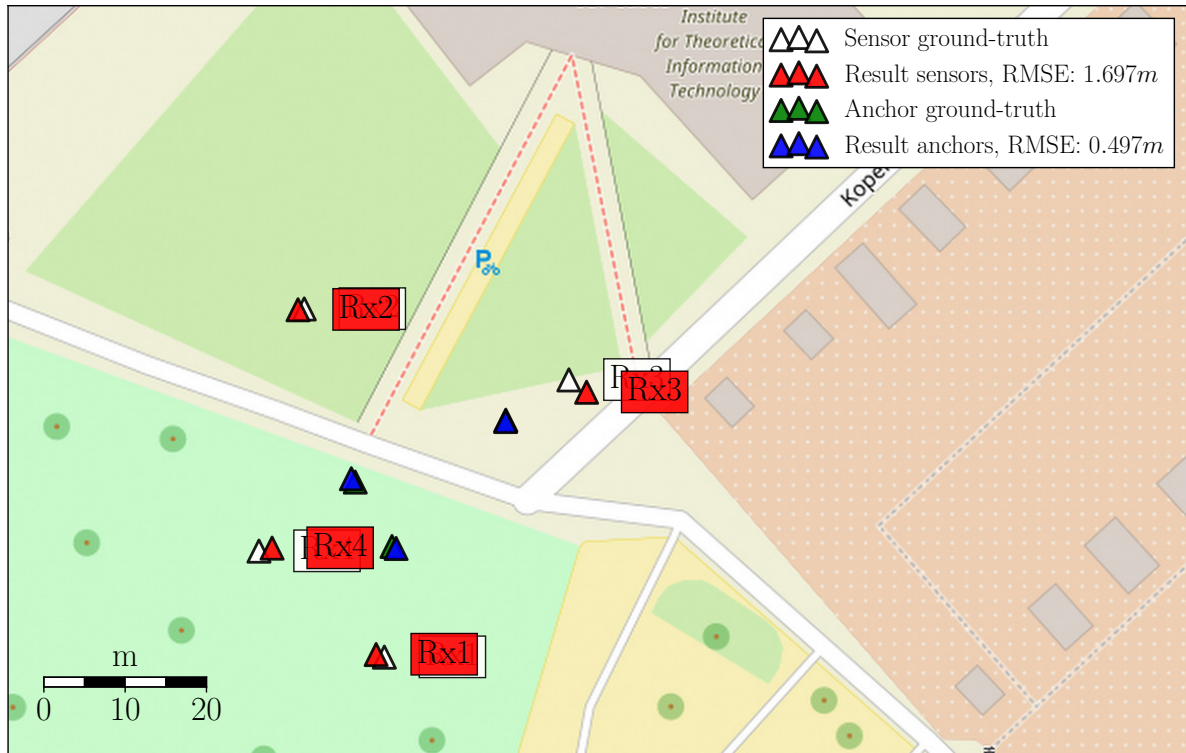


Figure 6.14: The result of the sensor self-localization compared to the ground truth. The known anchor locations are used to obtain the absolute solution in WGS84.

remaining sensors are then ordered to take a fixed number of measurements, i.e., snapshots of 1000 samples each. Subsequently, the process is repeated with each of the sensors. Note that in this scheme there is no two-way ranging necessary, this simplifies the protocol considerably and reduces the number of transmissions. In principle, each sensor only has to transmit once for the measurement and once to transport the measurements to the fusion center. Although, during the experiment, each individual snapshot has been send to the FC immediately, using the IEEE 802.11 WLAN backhaul link. For other sensor networks, where the backhaul channel uses the same band as the measurements a slightly more sophisticated media access control (MAC) layer protocol is necessary. The experiment has been performed at a carrier frequency of 2.4 GHz with a signal bandwidth of 20 MHz. All samples are collected in the FC, where TDOA measurements are calculated according to (5.3). A visualization of these measurement is shown in Figure 6.13. In this example each sensor has taken 20 snapshots.

After obtaining all necessary measurements and ground truth coordinates for the anchors, the FC performs the relative sensor self-localization algorithm according to Section 5.4.2. For the present application with stationary sensors the algorithm is not time critical, therefore the number of maximum iterations can be chosen rather high in the order of $10^3 - 10^4$. This also allows to recover from running into several local

minima. The evaluation of the algorithm yields the relative self-localization between the sensors. Anchoring to absolute coordinates is then performed using the approach from Section 5.5. The final result is depicted in Figure 6.14. It can be observed that the calculated sensor coordinates are slightly erroneous, with an RMSE of about 1.7 m. This error can be partially explained by the comparably low signal bandwidth and the influence of the multipath propagation that results in a slightly biased TDOA measurements in some instances. The other aspect, is the importance of the correct anchoring. An erroneous relative self-localization leads to errors in the localized anchors, hence the mapping to the anchor ground truth is inherently imperfect. Nevertheless, for applications such as wildlife tracking where an accuracy in the range of a few meters is sufficient the method is a good candidate for the simplification of the setup of the network. If necessary the accuracy could be considerably improved by increasing the bandwidth of the transmitted signals. Overall, the feasibility of the TDOA-based self-localization approach has been demonstrated.

7 | Conclusions

The ever increasing number of electronic devices and ongoing trend of automation driven by the digitalization of industry leads to an increased demand for localization solutions. The present thesis contributes to the theoretical foundations and advanced experimental research in the area of infrastructure assisted localization. Although satellite based navigation has become ubiquitous, for indoor navigation and certain outdoor applications such as wildlife tracking, ground based infrastructure supported methods are still relevant and often inevitable. Nevertheless, for indoor navigation and special applications such as wildlife tracking, ground based, infrastructure supported methods are still important and often inevitable. New extensions in recent releases of the LTE standard also show that network based localization remains important. Upcoming autonomous vehicles will have to make use of a whole collection of different localization sensors in order to provide ubiquitous awareness about themselves and nearby road users. Moreover, in the area of RF based technologies, software defined radio software defined radio (SDR) provides a very convenient tool for research that enables rapid prototyping not only for communication but for localization systems as well. Motivated by this, the experimental chapter of this thesis demonstrates how theoretical concepts from time difference of arrival (TDOA)-based localization can be deployed and experimentally verified in a straightforward way in an academic research environment.

7.1 Summary

In the following the main contents and contributions of the thesis are summarized.

Background and Theoretical Limits

The thesis begins with providing background information about RF based localization, presenting basic principles and a collection of examples. After that the focus is set on TDOA-based localization. The necessary principals and algorithms are given starting from the sampling of the physical signal and ending at the estimation of the location. A novel contribution in of this part is the examination of the modified Cramér-Rao lower bound (MCRLB) for TDOA localization with calibration emitters and imperfect

clocks. Experimental results on the synchronization of systems with calibration emitters are based on measurements from the ATLAS wildlife tracking system in northern Israel.

Sparsity-Based Algorithm and Multipath Propagation

In the next part some new ideas and results on localization, that exploits the underlying spatial sparsity are presented. The developed algorithm is based on principles from the area of compressed sensing (CS). Subsequently, the approach is extended for multipath and non-line-of-sight (NLOS) environments. This is achieved by adding additional knowledge about the environment gained from a ray tracing software package. The resulting data-driven algorithm is a member of the class of fingerprinting algorithms.

Self-localization

A common problem in sensor networks, for localization is the localization of the nodes itself. This occurs especially in ad-hoc sensor networks. It is desirable to provide only a minimum number of anchor points and obtain node localization through an automatic self-localization procedure. Often this problem is solved using pairwise distances between sensors obtained with two-way ranging and multidimensional scaling (MDS). A contribution of the thesis in that area is an algorithm working with TDOA measurements instead. The resulting algorithm is therefore termed Differential multidimensional scaling (DMDS). The complete method is split in two steps, where relative localization of the nodes is performed based on DMDS and afterwards anchoring to the absolute locations is achieved with a Procrustes transform.

Experimental Verification

The final part deals with results from the experimental work on an SDR localization framework that have been obtained during the cause of the thesis. Several of the previously described algorithms have been implemented and evaluated in the framework. In practice, the largest challenge in distributed sensor networks for time measurement based localization is synchronization. This is particularly important in the context of time of arrival TOA and TDOA measurements. System synchronization can be achieved using GPS, calibration emitters or a hybrid approach. Several implemented approaches and related aspects are discussed. Eventually, result of the self-localization of a small sensor network are presented.

7.2 Outlook

As an outlook for further research a few important open problems can be identified. First, the ray tracing based fingerprinting approach needs to be validated with experimental data. For that a deployed network of sensors in an urban area is necessary, alternatively measurement data from a cellular network could be used. Second, another interesting topic is to study and exploit the capabilities of OFDM waveforms, possibly also in combination with multi-antenna receivers. In the form of LTE this type of localization technology is expected to play a larger role in the near future. This point also includes research on carrier phased methods and super-resolution methods. Third, cooperative localization, i.e., performing cooperation between the mobile nodes, could turn out very beneficial in the expected automation of vehicular traffic in the coming decade. Therefore the presented framework should be extended with cooperative capabilities. Finally, from a technical point of view, further integration work is necessary to approach a fully embedded and mobile SDR sensor solution that is very easy to deploy and facilitates further experiments in different environments.

List of Acronyms

ADC	Analog-to-digital converter
ADS-B	Automatic dependent surveillance - broadcast
AIS-SART	Automatic identification system - search and rescue transponder
API	Application programming interface
APIT	Approximate point in triangle
ATLAS	Advanced tracking and localization of animals in real-life systems
BOC	Binary offset carrier
BPSK	Binary phase-shift keying
CDMA	Code-division multiple access
CoMP	Coordinated multi-point
COTS	Commercial off-the-shelf
CP	Cyclic prefix
CR	Cognitive radio
CRLB	Cramér-Rao lower bound
CS	Compressed sensing
CSI	Channel state information
DAB	Digital Audio Broadcasting
DMDS	Differential multidimensional scaling
DME	Distance measuring equipment
DOA	Direction of arrival
DOP	Dilution of precision
DSP	Digital signal processor
DTDOA	Differential time difference of arrival
DVB-T	Digital Video Broadcasting - Terrestrial

DV-Hop	Distance vector-hop
E112	Enhanced 1-1-2
E911	Enhanced 9-1-1
eNB	Evolved NodeB
EPIRB	Emergency position-indicating radio beacon
ESPRIT	Estimation of signal parameters via rotational invariance techniques
FCC	Federal Communications Commission
FC	Fusion center
FFT	Fast Fourier transform
FIM	Fisher information matrix
FSK	Frequency-shift keying
GCC	Generalized cross-correlation
GLONASS	Globalnaya navigatsionnaya sputnikovaya sistema
GNSS	Global navigation satellite system
GPSDO	GPS disciplined oscillator
GPS	Global Positioning System
GSM	Global System for Mobile Communications
GUI	Graphical user interface
IC	Integrated circuit
ILS	Instrument landing system
IMU	Inertial measurement unit
ISI	Inter symbol interference
ITU	International Telecommunication Union
KF	Kalman filter
LIDAR	Light detection and ranging
LTE	Long Term Evolution
MAC	Media access control
MCRLB	Modified Cramér-Rao lower bound
MDS	Multidimensional scaling

MFIM	Modified Fisher information matrix
MIMO	Multiple input multiple output
MUSIC	Multiple signal classification
NFER	Near-field electromagnetic ranging
NLOS	Non-line-of-sight
OCXO	Oven controlled crystal oscillator
OFDMA	Orthogonal frequency-division multiple access
OFDM	Orthogonal frequency-division multiplexing
OMP	Orthogonal matching pursuit
OSM	OpenStreetMap
OTDOA	Observed time difference of arrival
PLL	Phase locked loop
ppb	Parts per billion
ppm	Parts per million
PPS	Pulse per second
PRS	Positioning reference signals
PSR	Primary surveillance radar
QPSK	Quadrature phase-shift keying
RADAR	Radio detection and ranging
RF	Radio frequency
RMSE	Root-mean-square error
RPC	Remote procedure call
RSSI	Received signal strength indicator
RSS	Received signal strength
RTK	Real Time Kinematic
RTLS	Real-time locating system
SC-FDMA	Single-carrier frequency-division multiple access
SDR	Software defined radio
SLAM	Simultaneous localization and mapping

SNR	Signal-to-noise ratio
SRS	Sounding reference signal
SSR	Secondary surveillance radar
TCXO	Temperature compensated crystal oscillator
TDOA	Time difference of arrival
TOA	Time of arrival
TOF	Time of flight
UE	User equipment
UHF	Ultra high frequency
UMTS	Universal Mobile Telecommunications System
UTC	Coordinated Universal Time
UTDOA	Uplink time difference of arrival
UWB	Ultra-wideband
VCXO	Voltage controlled crystal oscillator
VOR	VHF omni directional radio range
WAM	Wide area multilateration
WGS84	World Geodetic System 1984
WLAN	Wireless local area network

List of Symbols and Notation

General Notation

\mathbb{N}	Set of natural numbers
\mathbb{R}	Set of real numbers
\mathbb{C}	Set of complex numbers
a	scalar
$\mathbf{a} \in \mathbb{C}^{N \times 1}$	Column vector of dimension N
$\mathbf{A} \in \mathbb{C}^{N \times K}$	Matrix of dimension N times K
\mathbf{a}^T	Vector transpose
\mathbf{A}^T	Matrix transpose
\mathbf{a}^H	Matrix Hermitian
\mathbf{a}^*	Component wise complex conjugate of vector
$[\cdot]_m$	Vector element m
$[\cdot]_{m,n}$	Matrix element, row m , column n
$\text{diag}(\mathbf{a})$	Diagonal Matrix with the elements of vector \mathbf{a} on the main diagonal
$\mathbf{1}_L$	Length L Vector of ones
$X \sim \mathcal{N}(\mu, \sigma^2)$	A Gaussian distributed random variable with mean μ and variance σ^2
$\text{var}(X)$	Variance of random variable X
$p(X)$	Probability density function of random variable X
$E\{\cdot\}$	Expected value
$\ \cdot\ _2$	Euclidean norm
$\ \cdot\ _1$	ℓ_1 -norm
$*$	Convolution operation
$\frac{\partial f}{\partial x_i}$	Partial derivative of $f(x_1, \dots, x_N)$
$\nabla f(x_1, \dots, x_N)$	Vector of partial derivatives of $f(x_1, \dots, x_N)$

Chapter 3

P	Number of transmitters
M	Number of receiving sensors
$s(t)$	Transmitted signal
$w_i(t)$	Additive noise at receiver i
$y_i(t)$	Received signal at receiver i
t_i	Time shift due to signal propagation seen at receiver i
h_i	Channel coefficient for receiver i
\mathbf{p}_k	Coordinates of the transmitter (2D)
\mathbf{r}_i	Coordinates of a receiver (2D)
$\tau_{i,j,k}$	Time difference of arrival TDOA between two receive antennas i and j and transmitter k
c	Propagation speed of the wave
$d_{i,k}$	Range, distance between transmitter k and receiver i
$\delta_{i,j,k}$	Distance difference, between transmitter k and receivers i and j
$g_{i,1}, g_{i,2}, K_i,$ $A, B, C, D,$ α, β, γ	Auxiliary variables
$\hat{\boldsymbol{\tau}}_k$	Vector of estimated TDOAs for transmitter k
$\boldsymbol{\tau}_k$	Vector of true TDOAs for transmitter k
$R_{y_i y_j}(\tau)$	Cross-correlation function between signals $y_i(t)$ and $y_j(t)$
T	Observation time for continuous cross-correlation function
T_s	Sampling interval
$\hat{R}_{y_i y_j}[\kappa]$	Discreet estimator for cross-correlation function
$Z_i[m]$	Discreet Fourier transform of signal $z_i[n]$
$B_{i,k}(x)$	Pieces of B-spline
$\zeta(x)_3$	Piece of cubic spline
ν_i	Weights of cubic spline
$x(t)$	Signals with waveform known to receiver such as OFDM signals
X_k	Message symbol transmitted over the k th subcarrier
N_{sym}	Number of OFDM subcarriers

N_{cp}	Number of cyclic prefix samples
T_{sym}	OFDM symbol duration
T_{cp}	OFDM cyclic prefix duration
Δf	Subcarrier spacing
$rect(t)$	Rectangular function
$P[n]$	Correlator function for OFDM time synchronization
\mathbf{H}^j	Jacobian matrix of TDOAs
DOP^j	Dilution of precision with reference sensor j
σ_w^2	Variance of additive noise
E	Signal energy
N_0	Noise power spectral density
\bar{F}^2	Mean square bandwidth
SNR	Signal-to-noise ratio
\mathbf{C}_p	Covariance matrix of location estimate
\mathbf{C}_τ	Covariance matrix of TDOA estimates
$\mathbf{I}(\boldsymbol{\tau})$	Fisher information matrix
σ_τ	Variance of TDOA estimates
$\boldsymbol{\pi}_\kappa$	Kalman filter state vector
$\boldsymbol{\Phi}$	Kalman filter motion model Matrix
\mathbf{M}	Kalman filter measurement matrix
\mathbf{Q}	Kalman filter model covariance matrix
\mathbf{R}_k	Kalman filter measurement covariance matrix in time step k
$\boldsymbol{\pi}_{\kappa \kappa-1}$	A-priori state estimate
$\boldsymbol{\pi}_{\kappa \kappa}$	A-posteriori state estimate
$\mathbf{P}_{\kappa \kappa-1}$	A-priori covariance matrix
$\mathbf{P}_{\kappa \kappa}$	A-posteriori covariance matrix
ϕ_i	Time offset of clock in receiver i
ϵ_i	Drift rate of clock in receiver i with respect to real time
$t_{i,k}^{(q)}$	TOA from transmitter k , signal transmitted at time instance q received at sensor i
$n_i^{(q)}$	Additive Gaussian noise of received signal transmitted at instance q at receiver i

List of Symbols and Notation

$\Delta\tau_{i,j,k,k}^{(q,r)}$	DTDOA of two received signals transmitted at time instances q and r from the same transmitter k
$\Delta\tau_{i,j,k,l}^{(q,r)}$	DTDOA of two received signals transmitted at time instances q and r from different transmitters k and l
β_j	Ratio between clock rate of receiver j and reference receiver clock
\mathbf{u}	Vector of estimation parameters for MCRLB analysis
\mathbf{v}	Vector of unwanted parameters for MCRLB analysis
$p(\boldsymbol{\tau}_k \mathbf{v}; \mathbf{u})$	Joint conditional probability density function
$\boldsymbol{\mu}$	Vector of expected values
\mathbf{C}	Covariance matrix
$\sigma_{\phi_i}^2$	Variance of clock offset ϕ
$\sigma_{\epsilon_i}^2$	Variance of clock rate ϵ

Chapter 4

R	Number of receivers
Q	Number of transmitters
$\mathbf{y}_r(\gamma)$	Vector of received signal of receiver r
$\bar{\mathbf{y}}_{ref}(\gamma)$	Normalized received signal vector of reference receiver
$\boldsymbol{\Psi}_r$	Matrix of time shifted reference receiver signals for receiver r
$\boldsymbol{\Phi}_r$	Random subsampling matrix for receiver r
N	Number of uncompressed signal samples
m	Number of compressed samples
\mathbf{A}_r	Fat matrix, multiplication of $\boldsymbol{\Phi}$ and $\boldsymbol{\Psi}$
\mathbf{b}_r	Sparse coefficient vector
\mathcal{G}	Grid of potential transmitter location bins
L_1	Number of location rows
L_2	Number of location columns
K	Number of location bins
\mathbf{x}_k	Cartesian coordinates of transmitter bin
\mathbf{z}_r	Cartesian coordinates of receiver bin
ε_r	Threshold for residual

\mathcal{P}	Set of location bins containing transmitters
β_r	Auxiliary variable for OMP type localization algorithm

Chapter 5

d_{jk}	Distance between sensor j and k
D	Matrix of pairwise sensor distances
$\Delta_{j,k,l}$	Distance differences of sensor triples
\mathbf{x}_j	True sensor location
$\hat{\mathbf{x}}_j$	Estimated relative sensor location
\mathbf{T}, a, b	Parameters of Procrustes transform
$\hat{\Delta}_{j,k,l}^{(i)}$	Distance differences of sensor triples in estimated configuration
$S(\hat{\mathbf{x}}_1^{(i)}, \dots, \hat{\mathbf{x}}_M^{(i)})$	Stress function
$\mathbf{b}_{j,k}^{(i)}, v_{j,k,l}^{(i)}, \mathbf{d}_j^{(i)}, \mathbf{o}^{(i+1)}$	Auxiliary variables for DMDS algorithm
α	Step size for iterative algorithm
$\hat{\mathbf{x}}_j^{(i)}$	Estimated sensor location in algorithm step i
$\tilde{\mathbf{x}}_j^{(i)}$	Estimated sensor location in algorithm step i with offset
$R^{(i)}$	Rate of change of Stress function
ϵ	Threshold for Stress
δ	Threshold for change of Stress
$\hat{\mathbf{X}}$	Vector of estimated sensor coordinates (configuration)
h	Coefficient for numerical gradient calculation
κ	Dimension of Cartesian sensor coordinates in numeric gradient calculation
$\Lambda_{b,k,l}$	Distance differences of sensor-beacon triples
$\hat{\Lambda}_{b,k,l}(\hat{\mathbf{X}})$	Distance differences of sensor-beacon triples in estimated configuration
β	Weighting factor for weighted gradient descend
$\Theta_{j,k,l}$	Differential Distance differences of sensor triples with respect to timing reference beacon
$\Omega_{b,k,l}$	Differential Distance differences of sensor-beacon triples with respect to timing reference beacon

List of Symbols and Notation

$\hat{\Theta}_{j,k,l}(\hat{\mathbf{X}})$	Differential Distance differences of sensor triples with respect to timing reference beacon in estimated configuration
$\hat{\Omega}_{b,k,l}(\hat{\mathbf{X}})$	Differential Distance differences of sensor-beacon triples with respect to timing reference beacon in estimated configuration

Chapter 6

f_0	Frequency of reference clock
$f(t)$	Frequency of device under test
y_i	Frequency error with respect to reference clock
\bar{y}_j	Average of frequency error
$\sigma_{\text{AVAR}}(\tau)$	Allan deviation
e	Error between expected TDOA and measurement
K_{ij}	Constant offset of TDOA measurement

Bibliography

- [1] F. P. Stockbridge, “How far off is that german gun? How 63 German guns were located by sound waves alone in a single day,” *Popular Science Monthly*, p. 39, December 1918.
- [2] E. Kaplan and C. Hegarty, *Understanding GPS: principles and applications*. Artech house, 2005.
- [3] A. H. Sayed, A. Tarighat, and N. Khajehnouri, “Network-based wireless location: challenges faced in developing techniques for accurate wireless location information,” *IEEE Signal Processing Magazine*, vol. 22, no. 4, pp. 24–40, 2005.
- [4] J. Mitola, “The software radio architecture,” *IEEE Communications Magazine*, vol. 33, no. 5, pp. 26–38, 1995.
- [5] F. K. Jondral, “Software-defined radio: basics and evolution to cognitive radio,” *EURASIP Journal on Wireless Communications and Networking*, vol. 2005, no. 3, pp. 275–283, 2005.
- [6] “GNU Radio - The free and open software radio ecosystem,” website: <http://gnuradio.org/>, accessed: February 16, 2018.
- [7] J. Schmitz, D. Dorsch, and R. Mathar, “Compressed time difference of arrival based emitter localization,” in *The 3rd International Workshop on Compressed Sensing Theory and its Applications to Radar, Sonar and Remote Sensing (CoSeRa 2015)*, Pisa, Italy, June 2015.
- [8] J. Schmitz, F. Schröder, and R. Mathar, “TDOA fingerprinting for localization in non-line-of-sight and multipath environments,” in *2015 International Symposium on Antennas and Propagation (ISAP)*, Hobart, Tasmania, Australia, November 2015, pp. 374–377.
- [9] J. Schmitz, M. Hernández, and R. Mathar, “Demonstration abstract: Real-time indoor localization with TDOA and distributed software defined radio,” in *15th ACM/IEEE International Conference on Information Processing in Sensor Networks (IPSN)*, Vienna, Austria, April 2016.
- [10] J. Schmitz, F. Bartsch, M. Hernández, and R. Mathar, “Distributed software defined radio testbed for real-time emitter localization and tracking,” in *IEEE ICC 2017 Workshop on Advances in Network Localization and Navigation (ANLN)*, Paris, France, 2017.

Bibliography

- [11] J. Schmitz, S. Shojaee, V. Radhakrishnan, R. Mathar, S. Toledo, and R. C. H. Reyes, "Differential multidimensional scaling for self-localization of TDOA sensor networks," in *2017 IEEE Wireless Communications and Networking Conference (WCNC)*, San Francisco, CA, USA, Mar 2017.
- [12] S. Shojaee, J. Schmitz, R. Mathar, and S. Toledo, "On the accuracy of passive hyperbolic localization in the presence of clock drift," in *submitted to IEEE PIMRC*, 2017.
- [13] E. Elnahrawy, X. Li, and R. P. Martin, "The limits of localization using signal strength: A comparative study," in *2004 First Annual IEEE Communications Society Conference on Sensor and Ad Hoc Communications and Networks, 2004. IEEE SECON 2004.* IEEE, 2004, pp. 406–414.
- [14] C. Fernandez-Prades, J. Arribas, P. Closas, C. Aviles, and L. Esteve, "GNSS-SDR: An open source tool for researchers and developers," in *Proceedings of the 24th International Technical Meeting of The Satellite Division of the Institute of Navigation (ION GNSS 2011)*, 2011, pp. 780–0.
- [15] J. Arribas, "GNSS array-based acquisition: Theory and implementation," Ph.D. dissertation, Universitat Politècnica de Catalunya, Barcelona, Spain, June 2012.
- [16] W. Neven, T. Quilter, R. Weedon, and R. Hogendoorn, "Wide area multilateration. report on EATMP TRS 131/04," 2005.
- [17] E. Lewis, R. Harvey, and J. Rasmussen, "Hyperbolic direction finding with sferics of transatlantic origin," *Journal of Geophysical Research*, vol. 65, no. 7, pp. 1879–1905, 1960.
- [18] W. J. Koshak, R. Blakeslee, and J. Bailey, "Data retrieval algorithms for validating the optical transient detector and the lightning imaging sensor," *Journal of Atmospheric and Oceanic Technology*, vol. 17, no. 3, pp. 279–297, 2000.
- [19] W. J. Koshak and R. Solakiewicz, "TOA lightning location retrieval on spherical and oblate spheroidal earth geometries," *Journal of Atmospheric and Oceanic Technology*, vol. 18, no. 2, pp. 187–199, 2001.
- [20] R. L. Dowden, J. B. Brundell, and C. J. Rodger, "VLF lightning location by time of group arrival (TOGA) at multiple sites," *Journal of Atmospheric and Solar-Terrestrial Physics*, vol. 64, no. 7, pp. 817–830, 2002.
- [21] E. Wanke, "Blitzortung.org – A low cost time of arrival lightning detection and lightning location network," *Universität Düsseldorf*, 2011. [Online]. Available: www.blitzortung.org/Documents/TOA_Blitzortung.pdf
- [22] R. Schmidt, "Multiple emitter location and signal parameter estimation," *IEEE Transactions on Antennas and Propagation*, vol. 34, no. 3, pp. 276–280, 1986.

- [23] R. Roy and T. Kailath, “ESPRIT-Estimation of signal parameters via rotational invariance techniques,” *IEEE Transactions on acoustics, speech, and signal processing*, vol. 37, no. 7, pp. 984–995, 1989.
- [24] A. W. Weiser, Y. Orchan, R. Nathan, M. Charter, A. J. Weiss, and S. Toledo, “Characterizing the accuracy of a self-synchronized reverse-GPS wildlife localization system,” in *2016 15th ACM/IEEE International Conference on Information Processing in Sensor Networks (IPSN)*. IEEE, 2016.
- [25] J. S. Jaffe, P. J. Franks, P. L. Roberts, D. Mirza, C. Schurgers, R. Kastner, and A. Boch, “A swarm of autonomous miniature underwater robot drifters for exploring submesoscale ocean dynamics,” *Nature Communications*, vol. 8, 2017.
- [26] F. Quitin, V. Govindaraj, X. Zhong, and W. P. Tay, “Virtual multi-antenna array for estimating the angle-of-arrival of a RF transmitter,” in *2016 IEEE 84th Vehicular Technology Conference (VTC Fall)*, 2016.
- [27] Y. Fu and Z. Tian, “Cramer-Rao bounds for hybrid TOA/DOA-based location estimation in sensor networks,” *IEEE Signal Processing Letters*, vol. 16, no. 8, pp. 655–658, 2009.
- [28] J. Wang, J. Chen, and D. Cabric, “Cramer-rao bounds for joint RSS/DoA-based primary-user localization in cognitive radio networks,” *IEEE Transactions on Wireless Communications*, vol. 12, no. 3, pp. 1363–1375, 2013.
- [29] K. Römer, “The lighthouse location system for smart dust,” in *Proceedings of the 1st international conference on Mobile systems, applications and services*. ACM, 2003, pp. 15–30.
- [30] S. Islam, B. Ionescu, C. Gadea, and D. Ionescu, “Indoor positional tracking using dual-axis rotating laser sweeps,” in *2016 IEEE International Instrumentation and Measurement Technology Conference Proceedings (I2MTC)*. IEEE, 2016.
- [31] A. Lédeczi, P. Volgyesi, J. Sallai, and R. Thibodeaux, “A novel RF ranging method,” in *2008 International Workshop on Intelligent Solutions in Embedded Systems*. IEEE, 2008.
- [32] R. B. Langley, “RTK GPS,” *GPS World*, vol. 9, no. 9, pp. 70–76, 1998.
- [33] T. Takasu and A. Yasuda, “Development of the low-cost RTK-GPS receiver with an open source program package RTKLIB,” in *International Symposium on GPS/GNSS*. International Convention Centre Jeju, Korea, 2009, pp. 4–6.
- [34] H. G. Schantz, “Near field propagation law & a novel fundamental limit to antenna gain versus size,” in *2005 IEEE Antennas and Propagation Society International Symposium*, vol. 3. IEEE, 2005, pp. 237–240.
- [35] ———, “Near field phase behavior,” in *2005 IEEE Antennas and Propagation Society International Symposium*, vol. 3. IEEE, 2005, pp. 134–137.

Bibliography

- [36] C. Kim, F. Chin, and H. K. Garg, "Multiple frequencies for accuracy improvement in near field electromagnetic ranging (NFER)," in *2006 IEEE 17th International Symposium on Personal, Indoor and Mobile Radio Communications*. IEEE, 2006.
- [37] H. G. Schantz, "A real-time location system using near-field electromagnetic ranging," in *2007 IEEE Antennas and Propagation Society International Symposium*. IEEE, 2007, pp. 3792–3795.
- [38] R. Reimann, A. Bestmann, and M. Ernst, "Distance measurement by means of radio waves comparison of classical and high-resolution spectral methods," 2013. [Online]. Available: <http://www.lambda4.com/easyPoint/>
- [39] R. Reimann, "Process for the determination of a position change or respectively resting and/or speed of an object," Patent, Jun. 6, 2013, WO Patent App. PCT/EP2012/050,159, Publication Number WO2013079224 A1.
- [40] D. Vasisht, S. Kumar, and D. Katabi, "Decimeter-level localization with a single wifi access point," 2016.
- [41] P. Bahl and V. N. Padmanabhan, "RADAR: An in-building RF-based user location and tracking system," in *Proceedings. IEEE INFOCOM 2000. Nineteenth Annual Joint Conference of the IEEE Computer and Communications Societies.*, vol. 2. Ieee, 2000, pp. 775–784.
- [42] M. A. Youssef, A. Agrawala, and A. U. Shankar, "Wlan location determination via clustering and probability distributions," in *Proceedings of the First IEEE International Conference on Pervasive Computing and Communications, 2003. (PerCom 2003)*. IEEE, 2003, pp. 143–150.
- [43] X. Wang, L. Gao, S. Mao, and S. Pandey, "CSI-based fingerprinting for indoor localization: A deep learning approach," *IEEE Transactions on Vehicular Technology*, vol. 66, no. 1, pp. 763–776, Mar 2016.
- [44] K. Kaemarungsi and P. Krishnamurthy, "Modeling of indoor positioning systems based on location fingerprinting," in *INFOCOM 2004. Twenty-third Annual Joint Conference of the IEEE Computer and Communications Societies*, vol. 2. IEEE, 2004, pp. 1012–1022.
- [45] K. Wu, J. Xiao, Y. Yi, D. Chen, X. Luo, and L. M. Ni, "CSI-based indoor localization," *IEEE Transactions on Parallel and Distributed Systems*, vol. 24, no. 7, pp. 1300–1309, 2013.
- [46] A. Tayebi, J. Gomez Perez, F. M. S. d. Adana Herrero, and O. Gutierrez, "The application of ray-tracing to mobile localization using the direction of arrival and received signal strength in multipath indoor environments," *Progress In Electromagnetics Research*, vol. 91, pp. 1–15, 2009.

- [47] K. Chintalapudi, A. Padmanabha Iyer, and V. N. Padmanabhan, “Indoor localization without the pain,” in *Proceedings of the sixteenth annual international conference on Mobile computing and networking*. ACM, 2010, pp. 173–184.
- [48] Z. Yang, C. Wu, and Y. Liu, “Locating in fingerprint space: wireless indoor localization with little human intervention,” in *Proceedings of the 18th annual international conference on Mobile computing and networking*. ACM, 2012, pp. 269–280.
- [49] A. Rai, K. K. Chintalapudi, V. N. Padmanabhan, and R. Sen, “Zee: Zero-effort crowdsourcing for indoor localization,” in *Proceedings of the 18th annual international conference on Mobile computing and networking*. ACM, 2012, pp. 293–304.
- [50] N. Bulusu, J. Heidemann, and D. Estrin, “Adaptive beacon placement,” in *21st International Conference On Distributed Computing Systems, 2001*. IEEE, 2001, pp. 489–498.
- [51] J. Blumenthal, R. Grossmann, F. Golatowski, and D. Timmermann, “Weighted centroid localization in zigbee-based sensor networks,” in *IEEE International Symposium on Intelligent Signal Processing, 2007. WISP 2007*. IEEE, 2007.
- [52] T. He, C. Huang, B. M. Blum, J. A. Stankovic, and T. Abdelzaher, “Range-free localization schemes for large scale sensor networks,” in *Proceedings of the 9th annual international conference on Mobile computing and networking*. ACM, 2003, pp. 81–95.
- [53] C. E. Shannon, “A mathematical theory of communication,” *The Bell System Technical Journal*, vol. 27, no. 3, pp. 379–423, 1948.
- [54] —, “Communication in the presence of noise,” *Proceedings of the IRE*, vol. 37, no. 1, pp. 10–21, 1949.
- [55] S. M. Kay, “Fundamentals of statistical signal processing: estimation theory,” 1993.
- [56] R. B. Langley *et al.*, “Dilution of precision,” *GPS World*, vol. 10, no. 5, pp. 52–59, 1999.
- [57] N. Patwari, J. N. Ash, S. Kyperountas, A. O. Hero, R. L. Moses, and N. S. Correal, “Locating the nodes: cooperative localization in wireless sensor networks,” *IEEE Signal Processing Magazine*, vol. 22, no. 4, pp. 54–69, 2005.
- [58] H. Wymeersch, J. Lien, and M. Z. Win, “Cooperative localization in wireless networks,” *Proceedings of the IEEE*, vol. 97, no. 2, pp. 427–450, 2009.
- [59] S. Čapkun, M. Hamdi, and J.-P. Hubaux, “GPS-free positioning in mobile ad hoc networks,” *Cluster Computing*, vol. 5, no. 2, pp. 157–167, 2002.

Bibliography

- [60] R. L. Moses, D. Krishnamurthy, and R. M. Patterson, “A self-localization method for wireless sensor networks,” *EURASIP Journal on Advances in Signal Processing*, vol. 2003, no. 4, pp. 348–358, 2003.
- [61] D. Mirza and C. Schurgers, “Motion-aware self-localization for underwater networks,” in *Proceedings of the third ACM international workshop on Underwater Networks*. ACM, 2008, pp. 51–58.
- [62] M. Hellebrandt, R. Mathar, and M. Scheibenbogen, “Estimating position and velocity of mobiles in a cellular radio network,” *IEEE Transactions on Vehicular Technology*, vol. 46, no. 1, pp. 65–71, 1997.
- [63] M. Hellebrandt and R. Mathar, “Location tracking of mobiles in cellular radio networks,” *IEEE Transactions on Vehicular Technology*, vol. 48, no. 5, pp. 1558–1562, 1999.
- [64] ETSI, “3GPP TS 22.071: Location services (LCS); functional description; stage 2,” *3rd Generation Partnership Project; Technical Specification Group Services and System Aspects*.
- [65] —, “3GPP TS 03.71: Stage 2 functional specification of user equipment (UE) positioning in UTRAN,” *3rd Generation Partnership Project; Technical Specification Group Radio Access Network*.
- [66] —, “3GPP TS 23.171: Functional stage 2 description of location services in UMTS,” *3rd Generation Partnership Project; Technical Specification Group Services and System Aspects*.
- [67] —, “3GPP TS 25.305: Stage 2 functional specification of user equipment (UE) positioning in UTRAN,” *3rd Generation Partnership Project; Technical Specification Group Radio Access Network*.
- [68] —, “3GPP TS 36.814: Further advancements for E-UTRA physical layer aspects,” *3rd Generation Partnership Project; Technical Specification Group Radio Access Network; Evolved Universal Terrestrial Radio Access (E-UTRA)*.
- [69] —, “3GPP 36.211: Evolved universal terrestrial radio access (e-utra); physical channels and modulation,” *3rd Generation Partnership Project; Technical Specification Group Radio Access Network; Evolved Universal Terrestrial Radio Access (E-UTRA)*.
- [70] T. A. H. Bressner, “Development and evaluation of UTDoA as a positioning method in LTE,” Master’s thesis, KTH Royal Institute of Technology, Stockholm, Sweden, 2015.
- [71] J. A. del Peral-Rosado, J. A. López-Salcedo, F. Zanier, and M. Crisci, “Achievable localization accuracy of the positioning reference signal of 3GPP LTE,” in *2012 International Conference on Localization and GNSS (ICL-GNSS)*. IEEE, 2012.

- [72] J. A. del Peral-Rosado, J. A. López-Salcedo, G. Seco-Granados, F. Zanier, P. Crosta, R. Ioannides, and M. Crisci, “Software-defined radio LTE positioning receiver towards future hybrid localization systems,” in *31st AIAA International Communications Satellite Systems Conference*, 2013, p. 5610.
- [73] W. Xu, M. Huang, C. Zhu, and A. Dammann, “Maximum likelihood TOA and OTDOA estimation with first arriving path detection for 3gpp LTE system,” *Transactions on Emerging Telecommunications Technologies*, vol. 27, no. 3, pp. 339–356, 2016.
- [74] J. A. del Peral-Rosado, J. A. López-Salcedo, S. Kim, and G. Seco-Granados, “Feasibility study of 5g-based localization for assisted driving,” in *2016 International Conference on Localization and GNSS (ICL-GNSS)*. IEEE, 2016.
- [75] H. Liu, H. Darabi, P. Banerjee, and J. Liu, “Survey of wireless indoor positioning techniques and systems,” *IEEE Transactions on Systems, Man, and Cybernetics, Part C (Applications and Reviews)*, vol. 37, no. 6, pp. 1067–1080, 2007.
- [76] Y. Gu, A. Lo, and I. Niemegeers, “A survey of indoor positioning systems for wireless personal networks,” *IEEE Communications Surveys & Tutorials*, vol. 11, no. 1, pp. 13–32, 2009.
- [77] E. Bruns, B. Brombach, T. Zeidler, and O. Bimber, “Enabling mobile phones to support large-scale museum guidance,” *IEEE MultiMedia*, vol. 14, no. 2, pp. 16–25, 2007.
- [78] D. B. Jourdan, D. Dardari, and M. Z. Win, “Position error bound for UWB localization in dense cluttered environments,” *IEEE Transactions on Aerospace and Electronic Systems*, vol. 44, no. 2, pp. 613–628, 2008.
- [79] C. Rohrig and M. Muller, “Localization of sensor nodes in a wireless sensor network using the nanoloc TRX transceiver,” in *IEEE 69th Vehicular Technology Conference, 2009. VTC Spring 2009*. IEEE, 2009.
- [80] R. Reimann, A. Bestmann, and M. Ernst, “Locating technology for aal applications with direction finding and distance measurement by narrow bandwidth phase analysis,” in *International Competition on Evaluating AAL Systems through Competitive Benchmarking*. Springer, 2012, pp. 52–62.
- [81] G. Galati, M. Leonardi, P. Magarò, and V. Paciucci, “Wide area surveillance using SSR mode S multilateration: advantages and limitations,” in *European Radar Conference, 2005. EURAD 2005*. IEEE, 2005, pp. 225–229.
- [82] J. Johnson, H. Neufeldt, and J. Beyer, “Wide area multilateration and ADS-B proves resilient in afghanistan,” in *2012 Integrated Communications, Navigation and Surveillance Conference (ICNS)*. IEEE, 2012.

Bibliography

- [83] D. Van Willigen, R. Kellenbach, C. Dekker, and W. van Buuren, “eDLoran – Next generation of differential loran,” in *Proceedings of the European Navigation Conference*, 2014, pp. 15–17.
- [84] G. Offermans, A. Helwig, and D. Van Willigen, “Eurofix: test results of a cost-effective DGNSS augmentation system,” *Journal of Navigation*, vol. 50, no. 02, pp. 209–223, 1997.
- [85] J. Safar, F. Vejrazka, and P. Williams, “Assessing the limits of eloran positioning accuracy,” *TransNav: International Journal on Marine Navigation and Safety of Sea Transportation*, vol. 5, no. 1, pp. 93–101, 2011.
- [86] J. Safar, C. K. Lebekwe, and P. Williams, “Accuracy performance of eloran for maritime applicaations,” *Annual of Navigation*, pp. 109–121, 2010.
- [87] D. Roemmich, G. C. Johnson, S. C. Riser, R. E. Davis, J. Gilson, W. B. Owens, S. L. Garzoli, C. Schmid, and M. Ignaszewski, “The argo program: Observing the global ocean with profiling floats,” 2009.
- [88] J. Yi, D. Mirza, R. Kastner, C. Schurgers, P. Roberts, and J. Jaffe, “ToA-TS: Time of arrival based joint time synchronization and tracking for mobile underwater systems,” *Ad Hoc Networks*, vol. 34, pp. 211–223, 2015.
- [89] ITU-R, “Handbook on national spectrum management,” *Radiocommunication Sector of International Telecommunication Union (ITU)*, 2005.
- [90] —, “Spectrum monitoring handbook,” *Radiocommunication Sector of International Telecommunication Union (ITU)*, 2011.
- [91] —, “Recommendation ITU-R SM.1050-2 - Tasks of a monitoring service,” *Radiocommunication Sector of International Telecommunication Union (ITU)*, 2004.
- [92] —, “Recommendation ITU-R SM.854-3 - Direction finding and location determination at monitoring stations,” *Radiocommunication Sector of International Telecommunication Union (ITU)*, 2011.
- [93] —, “Recommendation ITU-R SM.1598 - Methods of radio direction finding and location on time division multiple access and code division multiple access signals,” *Radiocommunication Sector of International Telecommunication Union (ITU)*, 2002.
- [94] —, “Recommendation ITU-R SM.2060-0 - Test procedure for measuring direction finder accuracy,” *Radiocommunication Sector of International Telecommunication Union (ITU)*, 2014.
- [95] —, “Recommendation ITU-R SM.2080-0 - Precision of time information in output data of monitoring receivers,” *Radiocommunication Sector of International Telecommunication Union (ITU)*, 2015.

- [96] R. Rose, C. Meier, S. Zorn, A. Goetz, and R. Weigel, “A GSM-network for mobile phone localization in disaster scenarios,” in *2011 German Microwave Conference (GeMIC)*. IEEE, 2011.
- [97] A. Goetz, S. Zorn, R. Rose, G. Fischer, and R. Weigel, “A time difference of arrival system architecture for GSM mobile phone localization in search and rescue scenarios,” in *2011 8th Workshop on Positioning Navigation and Communication (WPNC)*. IEEE, 2011, pp. 24–27.
- [98] S. Zorn, G. Bozsik, R. Rose, A. Goetz, R. Weigel, and A. Koelpin, “A power sensor unit for the localization of GSM mobile phones for search and rescue applications,” in *2011 IEEE SENSORS Proceedings*. IEEE, 2011, pp. 1301–1304.
- [99] R. E. Kenward, *A manual for wildlife radio tagging*. Academic Press, 2000.
- [100] G. C. White and R. A. Garrott, *Analysis of wildlife radio-tracking data*. Elsevier, 2012.
- [101] M. Hierold, S. Ripperger, D. Josic, F. Mayer, R. Weigel, and A. Koelpin, “Low-weight wireless sensor network for encounter detection of bats,” in *2015 IEEE Topical Conference on Wireless Sensors and Sensor Networks (WiSNet)*. IEEE, 2015, pp. 11–13.
- [102] M. Hartmann, T. Nowak, O. Pfandenbauer, J. Thielecke, and A. Heuberger, “A grid-based filter for tracking bats applying field strength measurements,” in *2016 12th Annual Conference on Wireless On-demand Network Systems and Services (WONS)*. IEEE, 2016.
- [103] M. Aatique, “Evaluation of TDOA techniques for position location in CDMA systems,” Master’s thesis, Virginia Polytechnic Institute and State University, 1997.
- [104] N. El Gemayel, “Smart passive localization using time difference of arrival,” Ph.D. dissertation, Karlsruhe, Karlsruher Institut für Technologie (KIT), 2016.
- [105] G. Shen, R. Zetik, and R. S. Thoma, “Performance comparison of TOA and TDOA based location estimation algorithms in LOS environment,” in *5th Workshop on Positioning, Navigation and Communication, 2008. WPNC 2008*. IEEE, 2008, pp. 71–78.
- [106] B. Yang and J. Scheuing, “A theoretical analysis of 2D sensor arrays for TDOA based localization,” in *2006 IEEE International Conference on Acoustics Speech and Signal Processing Proceedings*, vol. 4. IEEE, 2006.
- [107] H. C. So, Y. T. Chan, and F. K. W. Chan, “Closed-form formulae for time-difference-of-arrival estimation,” *IEEE Transactions on Signal Processing*, vol. 56, no. 6, pp. 2614–2620, 2008.

Bibliography

- [108] H. Schau and A. Robinson, "Passive source localization employing intersecting spherical surfaces from time-of-arrival differences," *IEEE Transactions on Acoustics, Speech, and Signal Processing*, vol. 35, no. 8, pp. 1223–1225, 1987.
- [109] Y. T. Chan and K. Ho, "A simple and efficient estimator for hyperbolic location," *IEEE Transactions on Signal Processing*, vol. 42, no. 8, pp. 1905–1915, 1994.
- [110] M. Compagnoni and R. Notari, "TDOA-based localization in two dimensions: the bifurcation curve," *Fundamenta Informaticae*, vol. 135, no. 1-2, pp. 199–210, 2014.
- [111] M. Compagnoni, R. Notari, F. Antonacci, and A. Sarti, "A comprehensive analysis of the geometry of TDOA maps in localization problems," *Inverse Problems*, vol. 30, no. 3, 2014.
- [112] W. H. Foy, "Position-location solutions by Taylor-series estimation," *IEEE Transactions on Aerospace and Electronic Systems*, no. 2, pp. 187–194, 1976.
- [113] D. J. Torrieri, "Statistical theory of passive location systems," *IEEE Transactions on Aerospace and Electronic Systems*, no. 2, pp. 183–198, 1984.
- [114] B. Friedlander, "A passive localization algorithm and its accuracy analysis," *IEEE Journal of Oceanic engineering*, vol. 12, no. 1, pp. 234–245, 1987.
- [115] B. T. Fang, "Simple solutions for hyperbolic and related position fixes," *IEEE Transactions on Aerospace and Electronic Systems*, vol. 26, no. 5, pp. 748–753, 1990.
- [116] J. Smith and J. Abel, "The spherical interpolation method of source localization," *IEEE Journal of Oceanic Engineering*, vol. 12, no. 1, pp. 246–252, 1987.
- [117] ———, "Closed-form least-squares source location estimation from range-difference measurements," *IEEE Transactions on Acoustics, Speech, and Signal Processing*, vol. 35, no. 12, pp. 1661–1669, 1987.
- [118] Y. Huang, J. Benesty, G. W. Elko, and R. M. Mersereau, "Real-time passive source localization: A practical linear-correction least-squares approach," *IEEE Transactions on Speech and Audio Processing*, vol. 9, no. 8, pp. 943–956, 2001.
- [119] K. Ho, "Bias reduction for an explicit solution of source localization using TDOA," *IEEE Transactions on Signal Processing*, vol. 60, no. 5, pp. 2101–2114, 2012.
- [120] H.-W. Wei, R. Peng, Q. Wan, Z.-X. Chen, and S.-F. Ye, "Multidimensional scaling analysis for passive moving target localization with TDOA and FDOA measurements," *IEEE Transactions on Signal Processing*, vol. 58, no. 3, pp. 1677–1688, 2010.
- [121] C. Knapp and G. Carter, "The generalized correlation method for estimation of time delay," *IEEE Transactions on Acoustics, Speech, and Signal Processing*, vol. 24, no. 4, pp. 320–327, 1976.

- [122] M. Azaria and D. Hertz, “Time delay estimation by generalized cross correlation methods,” *IEEE Transactions on Acoustics, Speech, and Signal Processing*, vol. 32, no. 2, pp. 280–285, 1984.
- [123] J. O. Smith, *Mathematics of the discrete Fourier transform (DFT): with audio applications - Second Edition*. W3K Publishing, 2007.
- [124] U. Meyer-Baese and U. Meyer-Baese, *Digital signal processing with field programmable gate arrays*. Springer, 2007, vol. 65.
- [125] E. Waring, “Problems concerning interpolations. by Edward Waring, MDFRS and of the institute of bononia, lucasian professor of mathematics in the university of cambridge,” *Philosophical Transactions of the Royal Society of London*, vol. 69, pp. 59–67, 1779.
- [126] C. De Boor, C. De Boor, E.-U. Mathématicien, C. De Boor, and C. De Boor, *A practical guide to splines*. Springer-Verlag New York, 1978, vol. 27.
- [127] P. Dierckx, *Curve and surface fitting with splines*. Oxford University Press, 1995.
- [128] R. H. Bartels, J. C. Beatty, and B. A. Barsky, *An introduction to splines for use in computer graphics and geometric modeling*. Morgan Kaufmann, 1995.
- [129] T. M. Schmidl and D. C. Cox, “Robust frequency and timing synchronization for OFDM,” *IEEE Transactions on Communications*, vol. 45, no. 12, pp. 1613–1621, 1997.
- [130] J.-J. Van de Beek, M. Sandell, and P. O. Borjesson, “ML estimation of time and frequency offset in OFDM systems,” *IEEE Transactions on Signal Processing*, vol. 45, no. 7, pp. 1800–1805, 1997.
- [131] R. K. Martin, C. Yan, H. H. Fan, and C. Rondeau, “Algorithms and bounds for distributed TDOA-based positioning using OFDM signals,” *IEEE Transactions on Signal Processing*, vol. 59, no. 3, pp. 1255–1268, 2011.
- [132] J. D. Bard and F. M. Ham, “Time difference of arrival dilution of precision and applications,” *IEEE Transactions on Signal Processing*, vol. 47, no. 2, pp. 521–523, Feb 1999.
- [133] R. Kaune, J. Hörst, and W. Koch, “Accuracy analysis for TDOA localization in sensor networks,” in *2011 Proceedings of the 14th International Conference on Information Fusion (FUSION)*. IEEE, 2011.
- [134] A. Weiss and E. Weinstein, “Fundamental limitations in passive time delay estimation—part I: narrow-band systems,” *IEEE Transactions on Acoustics, Speech, and Signal Processing*, vol. 31, no. 2, pp. 472–486, 1983.
- [135] E. Weinstein and A. Weiss, “Fundamental limitations in passive time-delay estimation—part II: Wide-band systems,” *IEEE Transactions on Acoustics, Speech, and Signal Processing*, vol. 32, no. 5, pp. 1064–1078, 1984.

Bibliography

- [136] B. M. Sadler and R. J. Kozick, “A survey of time delay estimation performance bounds,” in *Fourth IEEE Workshop on Sensor Array and Multichannel Processing, 2006*. IEEE, 2006, pp. 282–288.
- [137] W. Hahn and S. Tretter, “Optimum processing for delay-vector estimation in passive signal arrays,” *IEEE Transactions on Information Theory*, vol. 19, no. 5, pp. 608–614, 1973.
- [138] A. Quazi, “An overview on the time delay estimate in active and passive systems for target localization,” *IEEE Transactions on Acoustics, Speech, and Signal Processing*, vol. 29, no. 3, pp. 527–533, 1981.
- [139] G. C. Carter, “Coherence and time delay estimation,” *Proceedings of the IEEE*, vol. 75, no. 2, pp. 236–255, 1987.
- [140] Y.-T. Chan and K. Ho, “Joint time-scale and TDOA estimation: Analysis and fast approximation,” *IEEE Transactions on Signal Processing*, vol. 53, no. 8, pp. 2625–2634, 2005.
- [141] B. Yang and J. Scheuing, “Cramer-rao bound and optimum sensor array for source localization from time differences of arrival,” in *IEEE International Conference on Acoustics, Speech, and Signal Processing, 2005. Proceedings. (ICASSP’05).*, vol. 4. IEEE, 2005.
- [142] B. Yang, “Different sensor placement strategies for TDOA based localization,” in *IEEE International Conference on Acoustics, Speech and Signal Processing, 2007. ICASSP 2007.*, vol. 2. IEEE, 2007.
- [143] J. T. Isaacs, D. J. Klein, and J. P. Hespanha, “Optimal sensor placement for time difference of arrival localization,” in *Proceedings of the 48th IEEE Conference on Decision and Control, 2009 held jointly with the 2009 28th Chinese Control Conference. CDC/CCC 2009*. IEEE, 2009, pp. 7878–7884.
- [144] M. Grewal and A. Andrews, *Kalman Filtering: Theory and Practice Using MATLAB*. Wiley, 2011.
- [145] C. Yan and H. H. Fan, “Asynchronous self-localization of sensor networks with large clock drift,” in *Fourth Annual International Conference on Mobile and Ubiquitous Systems: Networking & Services, 2007. MobiQuitous 2007*. IEEE, 2007.
- [146] K. Ho and L. Yang, “On the use of a calibration emitter for source localization in the presence of sensor position uncertainty,” *IEEE Transactions on Signal Processing*, vol. 56, no. 12, pp. 5758–5772, 2008.
- [147] Y. Wang, X. Ma, and G. Leus, “Robust time-based localization for asynchronous networks,” *IEEE Transactions on Signal Processing*, vol. 59, no. 9, pp. 4397–4410, 2011.

- [148] M. R. Gholami, S. Gezici, and E. G. Strom, “TDOA based positioning in the presence of unknown clock skew,” *IEEE Transactions on Communications*, vol. 61, no. 6, pp. 2522–2534, 2013.
- [149] M. Leng, W. P. Tay, C. M. S. See, S. G. Razul, and M. Z. Win, “Modified CRLB for cooperative geolocation of two devices using signals of opportunity,” *IEEE Transactions on Wireless Communications*, vol. 13, no. 7, pp. 3636–3649, 2014.
- [150] A. N. D’Andrea, U. Mengali, and R. Reggiannini, “The modified Cramer-Rao bound and its application to synchronization problems,” *IEEE Transactions on Communications*, vol. 42, no. 234, pp. 1391–1399, 1994.
- [151] F. Gini, R. Reggiannini, and U. Mengali, “The modified Cramer-Rao bound in vector parameter estimation,” *IEEE Transactions on Communications*, vol. 46, no. 1, pp. 52–60, 1998.
- [152] M. Moeneclaey, “On the true and the modified cramer-rao bounds for the estimation of a scalar parameter in the presence of nuisance parameters,” *IEEE Transactions on Communications*, vol. 46, no. 11, pp. 1536–1544, 1998.
- [153] J. Tiemann, F. Eckermann, and C. Wietfeld, “Multi-user interference and wireless clock synchronization in TDOA-based UWB localization,” in *2016 International Conference on Indoor Positioning and Indoor Navigation (IPIN)*. IEEE, 2016.
- [154] Y.-C. Wu, Q. Chaudhari, and E. Serpedin, “Clock synchronization of wireless sensor networks,” *IEEE Signal Processing Magazine*, vol. 28, no. 1, pp. 124–138, 2011.
- [155] A. N. D’Andrea, U. Mengali, and R. Reggiannini, “The modified cramer-rao bound and its application to synchronization problems,” *IEEE Transactions on Communications*, vol. 42, no. 234, pp. 1391–1399, 1994.
- [156] E. J. Candès, J. Romberg, and T. Tao, “Robust uncertainty principles: Exact signal reconstruction from highly incomplete frequency information,” *IEEE Transactions on Information Theory*, vol. 52, no. 2, pp. 489–509, 2006.
- [157] D. L. Donoho, “Compressed sensing,” *IEEE Transactions on Information Theory*, vol. 52, no. 4, pp. 1289–1306, 2006.
- [158] E. J. Candes and T. Tao, “Decoding by linear programming,” *IEEE Transactions on Information Theory*, vol. 51, no. 12, pp. 4203–4215, 2005.
- [159] V. Cevher, M. Duarte, and R. G. Baraniuk, “Distributed target localization via spatial sparsity,” in *European Signal Processing Conference (EUSIPCO)*, 2008.
- [160] J. A. Bazerque and G. B. Giannakis, “Distributed spectrum sensing for cognitive radio networks by exploiting sparsity,” *IEEE Transactions on Signal Processing*, vol. 58, no. 3, pp. 1847–1862, 2010.

Bibliography

- [161] S. Nikitaki and P. Tsakalides, “Localization in wireless networks via spatial sparsity,” in *2010 Conference Record of the Forty Fourth Asilomar Conference on Signals, Systems and Computers (ASILOMAR)*, 2010, pp. 236–239.
- [162] C. R. Comsa, A. M. Haimovich, S. C. Schwartz, Y. H. Dobyms, and J. A. Dabin, “Time difference of arrival based source localization within a sparse representation framework,” in *2011 45th Annual Conference on Information Sciences and Systems (CISS)*. IEEE, 2011.
- [163] H. Jamali-Rad and G. Leus, “Sparsity-aware multi-source TDOA localization,” *IEEE Transactions on Signal Processing*, vol. 61, no. 19, pp. 4874–4887, Oct 2013.
- [164] M. Pourhomayoun, M. L. Fowler, and N. E. Wu, “Spatial sparsity based emitter localization,” in *2012 46th Annual Conference on Information Sciences and Systems (CISS)*, 2012.
- [165] D. J. Torrieri, *Statistical Theory of Passive Location Systems*, I. Cox and G. Wilfong, Eds. Springer New York, 1990.
- [166] A. C. Gürbüz, J. H. McClellan, and V. Cevher, “A compressive beamforming method,” in *IEEE International Conference on Acoustics, Speech and Signal Processing, 2008. ICASSP 2008.*, 2008, pp. 2617–2620.
- [167] C. R. Berger and J. M. F. Moura, “Noncoherent compressive sensing with application to distributed radar,” in *2011 45th Annual Conference on Information Sciences and Systems (CISS)*, 2011.
- [168] D. Baron, M. F. Duarte, M. B. Wakin, S. Sarvotham, and R. G. Baraniuk, “Distributed compressive sensing,” *arXiv preprint arXiv:0901.3403*, vol. abs/0901.3403, 2009. [Online]. Available: <http://arxiv.org/abs/0901.3403>
- [169] D. L. Donoho, “For most large underdetermined systems of linear equations the minimal ℓ_1 -norm solution is also the sparsest solution,” *Communications on Pure and Applied Mathematics*, vol. 59, no. 6, pp. 797–829, 2006.
- [170] Y. C. Pati, R. Rezaifar, and P. S. Krishnaprasad, “Orthogonal matching pursuit: Recursive function approximation with applications to wavelet decomposition,” in *1993 Conference Record of The Twenty-Seventh Asilomar Conference on Signals, Systems and Computers.*, 1993, pp. 40–44.
- [171] H. Rauhut, “Compressive sensing and structured random matrices,” in *Theoretical Foundations and Numerical Methods for Sparse Recovery*, ser. Radon Series Comp. Appl. Math., M. Fornasier, Ed. deGruyter, 2010, vol. 9, pp. 1–92.
- [172] Y. C. Eldar, P. Kuppinger, and H. Bölcskei, “Block-sparse signals: Uncertainty relations and efficient recovery,” *IEEE Transactions on Signal Processing*, vol. 58, no. 6, pp. 3042–3054, 2010.
- [173] A. Bourdeau, M. Sahnoudi, and J. Tourneret, “Tight integration of GNSS and a 3D city model for robust positioning in urban canyons,” in *ION GNSS*, 2012.

- [174] L. Wang, P. D. Groves, and M. K. Ziebart, “GNSS shadow matching: Improving urban positioning accuracy using a 3D city model with optimized visibility scoring scheme,” *Navigation*, vol. 60, no. 3, pp. 195–207, 2013.
- [175] M. P. Wylie and J. Holtzman, “The non-line of sight problem in mobile location estimation,” in *Proceedings of ICUPC - 5th International Conference on Universal Personal Communications*, vol. 2, 1996, pp. 827–831.
- [176] L. Cong and W. Zhuang, “Non-line-of-sight error mitigation in TDOA mobile location,” in *IEEE Global Telecommunications Conference, 2001. GLOBECOM’01.*, vol. 1, 2001, pp. 680–684.
- [177] J. Scheuing and B. Yang, “Disambiguation of TDOA estimation for multiple sources in reverberant environments,” *IEEE Transactions on Audio, Speech, and Language Processing*, vol. 16, no. 8, pp. 1479–1489, 2008.
- [178] S. Kitic, N. Bertin, and R. Gribonval, “Hearing behind walls: localizing sources in the room next door with cosparsity,” in *2014 IEEE International Conference on Acoustics, Speech and Signal Processing (ICASSP)*, 2014, pp. 3087–3091.
- [179] G. Wölfle, R. Hoppe, D. Zimmermann, and F. M. Landstorfer, “Enhanced localization technique within urban and indoor environments based on accurate and fast propagation models,” in *European Wireless*, 2002, pp. 25–28.
- [180] V. Algeier, B. Demissie, W. Koch, and R. Thomä, “State space initiation for blind mobile terminal position tracking,” *EURASIP Journal on Advances in Signal Processing*, vol. 2008, Jan 2008.
- [181] F. Schröder, M. Reyer, and R. Mathar, “Field strength prediction for environment aware MIMO channel models,” in *2012 6th European Conference on Antennas and Propagation (EUCAP)*, Prague, Czech, Mar. 2012.
- [182] “OpenStreetMap - The free wiki world map,” <http://www.openstreetmap.org/>, accessed: February 16, 2018.
- [183] J. Wendeborg, F. Höflinger, C. Schindelbauer, and L. Reindl, “Calibration-free TDOA self-localisation,” *Journal of Location Based Services*, vol. 7, no. 2, pp. 121–144, 2013.
- [184] L. Wang, T.-K. Hon, J. D. Reiss, and A. Cavallaro, “Self-localization of ad-hoc arrays using time difference of arrivals,” *IEEE Transactions on Signal Processing*, vol. 64, no. 4, pp. 1018–1033, 2016.
- [185] D. Moore, J. Leonard, D. Rus, and S. Teller, “Robust distributed network localization with noisy range measurements,” in *Proceedings of the 2nd international conference on Embedded networked sensor systems*. ACM, 2004, pp. 50–61.
- [186] X. Ji and H. Zha, “Sensor positioning in wireless ad-hoc sensor networks using multidimensional scaling,” in *IEEE INFOCOM 2004*, vol. 4. IEEE, 2004, pp. 2652–2661.

Bibliography

- [187] S. T. Birchfield and A. Subramanya, "Microphone array position calibration by basis-point classical multidimensional scaling," *IEEE Transactions on Speech and Audio Processing*, vol. 13, no. 5, pp. 1025–1034, 2005.
- [188] W. S. Torgerson, *Theory and methods of scaling*. Wiley, 1958.
- [189] R. N. Shepard, "The analysis of proximities: Multidimensional scaling with an unknown distance function. I." *Psychometrika*, vol. 27, no. 2, pp. 125–140, 1962.
- [190] J. B. Kruskal, "Multidimensional scaling by optimizing goodness of fit to a non-metric hypothesis," *Psychometrika*, vol. 29, no. 1, pp. 1–27, 1964.
- [191] R. Mathar, *Multidimensionale Skalierung: Mathematische Grundlagen und algorithmische Aspekte*. BG Teubner Stuttgart, 1997, vol. 738.
- [192] T. F. Cox and M. A. Cox, *Multidimensional scaling*. CRC press, 2000.
- [193] I. Borg and P. J. Groenen, *Modern multidimensional scaling: Theory and applications*. Springer Science & Business Media, 2005.
- [194] J. C. Gower, "Generalized procrustes analysis," *Psychometrika*, vol. 40, no. 1, pp. 33–51, 1975.
- [195] R. N. Shepard, "The analysis of proximities: Multidimensional scaling with an unknown distance function. II." *Psychometrika*, vol. 27, no. 3, pp. 219–246, 1962.
- [196] S. H. Cho, S. R. Yeo, H. H. Choi, C. Park, and S. J. Lee, "A design of synchronization method for TDOA-based positioning system," in *2012 12th International Conference on Control, Automation and Systems (ICCAS)*. IEEE, 2012, pp. 1373–1375.
- [197] J. Y. Yoon, J. W. Kim, W. Y. Lee, and D. S. Eom, "A TDoA-based localization using precise time-synchronization," in *2012 14th International Conference on Advanced Communication Technology (ICACT)*. IEEE, 2012, pp. 1266–1271.
- [198] N. El Gemayel, S. Koslowski, F. K. Jondral, and J. Tschan, "A low cost tdoa localization system: Setup, challenges and results," in *2013 10th Workshop on Positioning Navigation and Communication (WPNC)*. IEEE, 2013.
- [199] J. Wei, C. Yu *et al.*, "Performance analysis of TDOA based localization using SDRs," in *3rd Australian Control Conference: AUCC 2013*. Engineers Australia, 2013, p. 446.
- [200] A. Gaber, S. Prcanovic, and A. Omar, "High-resolution indoor positioning system using SDR modules," in *2015 IEEE Radio and Wireless Symposium (RWS)*. IEEE, 2015, pp. 209–211.
- [201] "ZeroMQ - Distributed messaging library," <http://zeromq.org/>, accessed: February 16, 2018.

- [202] Opendigitalradio, “ublox LEA-M8F PCB design for Ettus USRP B210,” <http://www.opendigitalradio.org/lea-m8f-gpsdo>, accessed: February 16, 2018.
- [203] “Matplotlib basemap toolkit,” <https://matplotlib.org/basemap/>, accessed: February 16, 2018.
- [204] D. A. Howe, D. Allan, and J. Barnes, “Properties of signal sources and measurement methods,” in *Thirty Fifth Annual Frequency Control Symposium*. IEEE, 1981, pp. 669–716.
- [205] L. Arceo-Miquel, Y. S. Shmaliy, and O. Ibarra-Manzano, “Optimal synchronization of local clocks by GPS 1PPS signals using predictive FIR filters,” *IEEE Transactions on Instrumentation and Measurement*, vol. 58, no. 6, pp. 1833–1840, 2009.
- [206] P. Kuykendall and P. V. W. Loomis, “In sync with GPS: GPS clocks for the wireless infrastructure,” *Trimble Navigation*, 2008, accessed: February 16, 2018. [Online]. Available: <http://www.4timing.com/SyncGPS.pdf>
- [207] V. Vigner, J. Roztočil, and B. Čemusová, “Evaluation of timing GPS receivers for industrial applications,” *12th IMEKO TC10 Workshop on New Perspectives in Measurements, Tools and Techniques for Industrial Applications*, 2013.
- [208] M. A. Lombardi, A. N. Novick, and V. S. Zhang, “Characterizing the performance of GPS disciplined oscillators with respect to UTC (NIST),” DTIC Document, Tech. Rep., 2005.
- [209] P. J. Teunissen, “The least-squares ambiguity decorrelation adjustment: a method for fast GPS integer ambiguity estimation,” *Journal of Geodesy*, vol. 70, no. 1, pp. 65–82, 1995.
- [210] P. De Jonge and C. Tiberius, “The LAMBDA method for integer ambiguity estimation: implementation aspects,” *Publications of the Delft Computing Centre, LGR-Series*, vol. 12, no. 12, pp. 1–47, 1996.
- [211] “SAPOS - Satellitenpositionierungsdienst der deutschen Landesvermessung,” <http://www.sapos.de/>, accessed: February 16, 2018.

Curriculum Vitæ

Johannes Heribert Theodor Schmitz

Sep. 15, 1984	Born in Krefeld, Germany
Sep. 1991 - Jul. 1995	Elementary school "kath. Grundschule an der Burg" Krefeld, Germany
Aug. 1995 - Jul. 2004	Academic high school "Marienschule", Krefeld, Germany
Jul. 2004	General qualification for university entrance (Abitur)
Aug. 2004 - Apr. 2005	Community service in retirement home "Marienheim", Krefeld, Germany
Mai. 2005 - Jun. 2005	Intern G. Siempelkamp GmbH & Co.KG, Krefeld, Germany
Oct. 2005 - Sep. 2011	Electrical Engineering and Information Technology Department of Electrical Engineering RWTH Aachen University, Aachen, Germany
Nov. 2007 - Feb. 2009	Student researcher Institute for Integrated Signal Processing Systems RWTH Aachen University, Aachen, Germany
Nov. 2009 - Feb. 2010	Student researcher Institute for Networked Systems RWTH Aachen University, Aachen, Germany
Jun. 2010 - Nov. 2010	Intern HelloSoft Pvt. Ltd., Hyderabad, India
Sep. 2011	Diploma degree Electrical Engineering and Information Technology RWTH Aachen University, Aachen, Germany
Since Nov. 2011	Research and Teaching Assistant Institute for Theoretical Information Technology RWTH Aachen University, Aachen, Germany